STUDIES OF TRAFFIC OSCILLATIONS: A BEHAVIORAL PERSPECTIVE

A Dissertation
Presented to
The Academic Faculty

By

Danjue Chen

In Partial Fulfillment
of the Requirements for the Degree
Doctor of Philosophy in the
School of Civil and Environmental Engineering

Georgia Institute of Technology
August 2012

STUDIES OF TRAFFIC OSCILLATIONS: A BEHAVIORAL PERSPECTIVE

Approved by:

Dr. Jorge A. Laval, Advisor
School of Civil and Environmental Engineering
Georgia Institute of Technology

Dr. John D. Leonard
School of Civil and Environmental Engineering
Georgia Institute of Technology

Dr. Randall L. Guensler
School of Civil and Environmental Engineering
Georgia Institute of Technology

Dr. Haomin Zhou
Mathematics
Georgia Institute of Technology

Dr. Michael O. Rodgers
School of Civil and Environmental Engineering
Georgia Institute of Technology

Date Approved: May 4, 2012

Dedicated To my parents
Xingguang Chen and Jingqing Zhu

ACKNOWLEDGEMENTS

I would like to thank all my committee members for their guidance and support in my Ph.D., consisting of Dr. Jorge Laval, Dr. Michael Rodgers, Dr. Randall Guensler, Dr. John Leonard, and Dr. Haomin Zhou. My special thanks go to Dr. Michael Rodgers. The first big challenge I had during the Ph.D. process was English communication, which almost stopped me from continuing the Ph.D., but Dr. Rodgers turned things around. Not only did he help me to take the weakness in a right way, but also point out my strengths. From the conversation with him I got the confidence, for the first time, that I can have my Ph.D. degree. Later in my Ph.D. journey, Dr. Rodgers gave me a hug whenever I progressed one step further, when I finished my proposal, when I got my first job offer, and when I passed my defense. I'm really grateful for having Dr. Rodgers in my committee.

My deepest gratitude goes to my advisor, Dr. Jorge Laval. Being his Ph.D. student, and the first Ph.D. student, is one of the best things that have happened to me in my life. Dr. Laval gave me all the possible flexibility, respect, and support that a student may have, which paved a productive and pleasant road for my Ph.D. I am most impressed by his patience and trust on me, which has been there for the past five years just like the air I breathed. I can't remember how many times Dr. Laval corrected my English pronunciation, revised my papers, and discussed research questions with me. He gave me every possible chance to learn, to grow, and to succeed, which has laid the foundation for my academic career. From Dr. Laval I have learned what makes a true scholar: original and creative research, simple but insightful results, and endless learning adventure. Meanwhile, I have learned from him that doing research could be that much exciting and enjoyable, and that it is possible to maintain a happy work-life balance. I am really fortunate to have such an outstanding advisor and mentor.

My gratitude also goes to all my friends. I can't imagine the life of Ph.D. without their support. To name a few, I would like to thank Yanzhi Xu and Yike Hu for their help and company at the very tough time of my PhD. Their friendship has made the tough time truly memorable. I would also like to thank my colleagues, Rama Chilukuri, Dwayne Henclewood, Wonho Suh, and Ming Ruan, for their help and support on study, research, career, and life. I'm very grateful and proud for having so many wonderful friends who bring so much joy to my PhD journey.

Finally, words cannot describe my gratitude to my parents. Wherever I go, whatever I do, their unconditional love is with me. Without that, I won't be who I am.

TABLE OF CONTENTS

LIST OF TABLES

LIST OF FIGURES

LIST OF SYMBOLS AND ABBREVIATIONS

AB1 Model	Asymmetric Behavioral 1-stage Model
AB2 Model	Asymmetric Behavioral 2-stage Model
CCW	Counter Clock-Wise
CW	Clock-Wise
NGSIM	Next Generation Simulation
OA	Originally Aggressive
ON	Originally Newell
OT	Originally Timid

SUMMARY

Traffic oscillations, or simply stop-and-go waves, are a common phenomenon arising in congested traffic but still not well understood. This phenomenon causes broad adverse impacts to safety risk, fuel efficiency and greenhouse emission. To eliminate or reduce those impacts, understanding the cause and propagation mechanism is essential. This dissertation studied driving behavior in traffic oscillations with the objective to uncover the formation and propagation mechanism of traffic oscillations.

This study establishes a behavioral car-following model, the Asymmetric Behavioral model, based on empirical trajectory data that is able to reproduce the spontaneous formation and ensuing propagation of traffic oscillations in congested traffic. By analyzing individual drivers' car-following behavior throughout oscillation cycles it is found that this behavior is consistent across drivers and can be captured by a simple model. The statistical analysis of the model's parameters reveals that driver' behavior during oscillation (i.e., reaction to oscillation) is strongly correlated with driver behavior before oscillations and it varies with the development stage of the oscillation. Simulation of the model shows that it is able to produce characteristics of traffic oscillations consistently with empirical observations.

This study also unveils the generation mechanism of the traffic hysteresis phenomenon arising in traffic oscillations using the Asymmetric Behavioral model. It is found that the occurrence of traffic hysteresis is closely correlated with driver behavior when experiencing traffic oscillations. In the growth and fully-developed stage of traffic oscillations, drivers behave differently, which results in different distribution of hysteresis patterns.

This research makes it possible to unveil new management and control strategies of traffic oscillations to improve traffic operation and to quantify the environmental and

safety impacts of traffic oscillations. For example, it can be used to estimate the increase of greenhouse emission and decrease of fuel efficiency imposed by traffic oscillations. It can also be used to study the increase of accident rate.

.

CHAPTER 1 INTRODUCTION

1.1 Background

Traffic congestion has become a prevailing problem in many cities around the world. In the United States, congestion has grown substantially over the last two decades. The 2011 Urban Mobility Report (Schrank, et al., 2011) states that congestion is a problem in 439 urban areas in the U.S. and that resulted in $101 billion cost in 2010 because of the travel delay and extra fuel consumption, five times the cost in 1982. In addition, statistics record indicates a trend of increasing cost.

Traffic oscillation, referred to as stop-and-go wave in the literature, is a common phenomenon associated with congested traffic. This phenomenon causes broad adverse impacts. For example, it increases safety risk (Bilbao-Ubillos, 2008; Herman et al., 1959; Zheng et al., 2010), reduces fuel efficiency, and increases greenhouse emission. In addition, the fluctuation in traffic flow affects travel time reliability and raises great challenges to travel time prediction and trip planning. From the traffic flow theory perspective, traffic oscillations are related to many important phenomena on the highway such as capacity drop (Leclercq et al., 2011; Yeo, 2008) and traffic hysteresis (Ahn et al., 2011). Every year, millions of dollars is spent to stabilize the traffic flow and therefore reduce the adverse impacts (Wilson, 2008).

To eliminate or reduce the impacts of traffic oscillations, understanding the cause and propagation mechanism is essential. Although traffic oscillations were first reported fifty year ago on the Lincoln tunnel (Edie and Foote, 1961), understandings are still limited. In the history of oscillation modeling, most studies analyzed the phenomenon out of physical or mathematical curiosity while the driving behavior received little

attention. The former perspective, however, provides very limited insights to understand driver behavior under traffic oscillations. A recent study (Laval and Leclercq, 2010) conjectured that the formation and propagation of traffic oscillations were due to aggressive or timid driver behavior. Simulations produced traffic oscillations with period and amplitude consistent with empirical observations. Although the conjecture is not validated empirically, it suggests a new and promising perspective to unveil the formation and propagation mechanism for traffic oscillations: the behavioral perspective, which explicitly traces the phenomenon to microscopic driver behavior, such as driver aggressiveness.

The behavioral perspective also allows for investigation of traffic hysteresis, a phenomenon associated with traffic oscillations, in a consistent context. Traffic hysteresis refers to the retarded recovery of speed in the deceleration-acceleration process (Ahn et al., 2011; Yeo, 2008) i.e., drivers behave differently in the acceleration and deceleration process. This phenomenon raises potential concerns in various aspects such as safety design, estimation of traffic flow transition, and capacity drop. However, it has been a long-term puzzle ever since it was reported in 1974 (Treiterer and Myers, 1974). For example, it is unclear whether traffic hysteresis exists generally and how it occurs. A few theories (Yeo and Skabardonis, 2009; Zhang, 1999; Zhang and Kim, 2005) were proposed to explain the cause, but no empirical validation was conducted. More importantly, to the best knowledge of the author, none of the studies has investigated traffic hysteresis from the behavioral perspective.

The behavioral perspective was not adopted in the previous studies is probably because detailed vehicle trajectory data were not available until very recent years. Fortunately, this becomes possible nowadays as high-resolution trajectory datasets (Hoogendoorn et al., 2003; NGSIM, 2006) emerge. These datasets allow for detailed examination of driving behavior at individual driver level. It is expected that this research will establish a traffic flow model to describe the formation and evolution

mechanism of traffic oscillations consistently with empirical observations. The model is also expected to explain the associated puzzling phenomena, such as traffic hysteresis, and enrich the understandings of the traffic flow fundamental. Furthermore, this model will serve as the base to study the negative impacts imposed by traffic oscillations, and thereafter design of control strategies.

1.2 Problem Definition

The problem this dissertation aims to address is the absence of a theory and a traffic flow model that is able to describe the formation and propagation mechanism of traffic oscillations from the perspective of driver behavior.

The research problem can be decomposed into several questions.

- *What is driver's behavior throughout traffic oscillations?* Apparently, how drivers follow other vehicles in congested traffic, referred to as driver's car-following behavior, when experiencing traffic oscillations is essential. This includes two critical issues: (a) how to measure driver behavior at the individual driver level? And (b) how to connect driver behavior in oscillatory and non-oscillatory conditions; i.e., before, during, and after traffic oscillations? A complete dynamic description of driver's car-following behavior is expected.

- *How to model driver behavior throughout traffic oscillations and then evaluate model performance?* A model will be established to describe driver behavior when experiencing traffic oscillations based on empirical observations. Two issues are particularly important: (1) how to keep the model as simple as possible without losing the important elements; and (2) how to evaluate the performance of the model?

- *What is the generation mechanism of traffic hysteresis? What is the relationship between traffic hysteresis and traffic oscillations?* It is well-known that traffic oscillations are characterized with traffic hysteresis. It is very likely that the driver behavior throughout traffic oscillations is related to the generation of traffic hysteresis. Hence, traffic hysteresis will be investigated in the same context with the studies of traffic oscillations. Particularly, this study will investigate why traffic hysteresis occurs and what is its connection with traffic oscillations.

1.3 Research Objectives

The primary objective of this study is to understand the evolution of traffic oscillations from the behavioral perspective and develop a comprehensive traffic flow model to predict the oscillation phenomenon. In particular, specific objectives are introduced as follows:

- *To understand the car-following behavior of individual drivers throughout traffic oscillations.*
- *To establish a behavioral model that is able to capture the formation and propagation of traffic oscillations.*
- *To understand the generation of traffic hysteresis from the behavioral perspective and investigate its connection with traffic oscillations.*

1.4 Research Contributions

The major contributions of this study are as follow:

(i) It provides a comprehensive dynamic description of driver's behavior profile when experiencing traffic oscillations;

(ii) It unveils the connection between driver's behavioral reaction to traffic oscillations and driver's characteristic before oscillations;

(iii) It develops a model to capture the formation and evolution of traffic oscillations;

(iv) It unveils the major generation mechanism of traffic hysteresis arising in traffic oscillations.

1.5 Dissertation Outline

The remaining of this dissertation is organized as follows. Chapter 2 provides an introduction on empirical findings of traffic oscillations and then reviews the modeling history of this phenomenon. Chapter 3 introduces the background of two models, which form the basic framework of the modeling efforts in this study. Chapter 4 presents the empirical data to be used in this study and then the methodology to measure driver behavior throughout traffic oscillations. Based on empirical measurement results, a model, Asymmetric Behavioral model, is proposed to describe driver's car-following behavior, which is introduced in the end of this chapter. In chapter 5, statistical analysis on model parameters is conducted based on empirical measurement and results are used to refine the Asymmetric behavioral model. After that, the model is tested by a rubbernecking experiment using simulations. In chapter 6, the Asymmetric Behavioral model is applied to explore the generation mechanism of traffic oscillation arising in traffic oscillations. Results from this traffic hysteresis study are used to further improve the Asymmetric Behavioral model. The performance of the improved model is tested by simulations and compared to the original model. This is conducted in chapter 7. Conclusions and future research work are introduced in chapter 8.

CHAPTER 2 LITERATURE REVIEW

This chapter reviews previous studies on traffic oscillations and traffic hysteresis. The purpose is to briefly introduce the progress and status of research on this subject, which serves as the starting point of this study. The first section describes the basic features of traffic oscillations that have been found empirically. Next, previous modeling efforts on traffic oscillations are introduced, which are categorized by the different research perspectives used. The third section presents the modeling perspective that is adopted in this study. In the fourth section, studies on traffic hysteresis are reviewed.

2.1 Features of Traffic Oscillations

Observations on traffic oscillations date back to the 1950s. A series of experiments carried on in the Holland and Lincoln tunnels in New York City (Edie and Foote, 1958, 1960, 1961; Forbes et al., 1958; Greenberg and Daou, 1960) revealed instabilities in dense traffic. In particular, these studies found that small disturbance from one vehicle would propagate upstream and the amplitude would grow, which may evolve to a complete stop. Similar phenomena were observed in Japan too (Koshi et al., 1983; Koshi et al., 1992).

In recent years, as traffic data become more extensive and accurate, significant progress has been achieved. Studies found that one cause of traffic oscillations is lane-changing maneuver (Ahn and Cassidy, 2006; Laval, 2006; Laval and Daganzo, 2006; Mauch and Cassidy, 2002; Zheng et al., 2011a; Zheng et al., 2011b). This was first explicitly shown by Ahn (Ahn, 2005) after examining vehicle trajectories extracted from video. It was found that the formation of traffic oscillations can be traced back to insertion that occurred under small spacing. The role of lane-changing has been confirmed in (Zheng et al., 2011a; Zheng et al., 2011b) based on analysis of NGSIM data (NGSIM, 2006). Meanwhile, it is evident that traffic oscillations can form away from

lane changes such as tunnels as the early experiments show or regular highway segments as in the NGSM sites. Interestingly, Zheng et al. (Zheng et al., 2011b) showed that traffic oscillations caused by lane-changing and car-following behaviors show similar features of oscillation propagations in terms of propagation speed, oscillation duration, and amplitude.

Studies on the propagation of traffic oscillations found that the oscillation amplitude may grow (i.e., vehicle speed inside the oscillation decreases) to certain extent as traffic oscillations propagate upstream and then become stable or start to decay (Li and Ouyang, 2011; Zheng et al., 2011b). However, interestingly traffic oscillation show regular periods in the propagation process, which vary from 2-15min (Ahn, 2005; Ahn et al., 2004; Kerner and Rehborn, 1996; Laval et al., 2009; Mauch and Cassidy, 2002). In the evolution process, the transition of traffic oscillations from the precursor (characterized by flat wave speed) to well-developed phases (characterized by oscillations propagating upstream) may be triggered by lane-changing behavior but that can also occur without lane-changing (Zheng et al., 2011b).

Although more and more features on the cause and propagation of traffic oscillations are uncovered, the mechanisms that induce oscillation amplitude growth and regular periods are still unknown, which generates urgent research needs. This dissertation aims to fill this gap. As the first step, the modeling history is reviewed, which is introduced in the following sections.

2.2 Existing Traffic Oscillation Models

According to the research perspective used, existing popular traffic oscillation models can be categorized into two major groups: unstable car-following models and fully-stochastic models. Since each group consists of numerous models, only some typical and popular ones are introduced.

2.2.1 Unstable car-following models

This group of models shares a common format: they describe the motion of vehicles through an acceleration (or speed) function, which may depend on speed, speed difference, and spacing. The function yields an equilibrium state in which a vehicle has the acceleration equal to zero. When a vehicle deviates from the equilibrium state, it accelerates or decelerates to recover, which may stimulate other vehicles to react. This process may cause traffic oscillations to form and propagate. In this sense, traffic oscillations are generated because the models are unstable.

From the view of physicists and mathematicians, traffic oscillation is a manifestation of system instability, either linear or non-linear (Gasser et al., 2004; Orosz et al., 2004; Scho¨nhof and Helbing, 2007; Ward and Wilson, 2011; Wilson, 2008; Wilson and Ward, 2011). This idea dates back to the early car-following models (e.g., (Gazis et al., 1961; Herman et al., 1959; Kometani and Sasaki, 1958).

Recent studies (Gasser et al., 2004; Orosz et al., 2004; Scho¨nhof and Helbing, 2007; Ward and Wilson, 2011; Wilson, 2008; Wilson and Ward, 2011) on car-following model linear instability suggest that these models can exhibit different types of linear instability: upstream (downstream) convective instability in which disturbance grows upstream (downstream) of the disturbance, and absolute instability in which disturbance blows up at all points spatially. But only upstream convective instability is reasonable for car-following models given the fact that traffic oscillations are observed to propagate upstream. The analytical criteria for different stability regions were also derived for a group of car-following models that describe vehicle motion through simple ordinary (or delay) differential equations; i.e., the vehicle acceleration is a function of spacing, speed, and speed difference. The stability regions depend on parameters and vary across models. While some models, such as OV model and the IDM, can show upstream convective instability within reasonable parameter regimes (Ward and Wilson, 2011) (Treiber and Kesting, 2011)), some cannot, such as Gipps's car-following model (Gipps, 1981), as pointed out by Wilson (Wilson, 2001).

In addition to the linear instability analysis, recent studies (Gasser et al., 2004; Helbing and Moussaid, 2009; Igarashi et al., 2001; Krauss et al., 1997; Lee et al., 1998; Li and Ouyang, 2011; Orosz and Stepan, 2006; Orosz et al., 2009; Safonov et al., 2002) analyzed the non-linearity of car-following models and tried to link that to the propagation of traffic oscillations. Li and Ouyang (Li and Ouyang, 2011) analytically examined the characteristics of traffic oscillations (such as period and amplitude) through their mathematical framework and found that non-linearity is critical in producing the bounded growth of oscillations while linear models yield unbounded growth. Their analytical prediction accords well with the numerical results.

These instability analyses, either linear or non-linear, help to understand system properties. As revealed, once a car-following model meets certain criteria, it can produce traffic oscillations and have them propagate if the parameters are well set. Consequence, it seems that the critical task is left for model parameter setting. These results indicate that the conventional perspective that describes vehicle motion through an acceleration (or speed) function and then parameterizes the model to produce traffic oscillations provides limited insights on driver behavior in oscillatory traffic. Particularly, it fails to establish an explicit connection between the instability and driver behavior that can be measured, validated, and calibrated in a clear physical sense. Neither does it consider the underlying root of driver behavior, which might be driver characteristics such as driver aggressiveness.

2.2.1.1 Early car-following models

The earliest investigation of traffic oscillations were inspired by the observations on traffic instabilities in 1950s (Edie and Foote, 1958, 1960, 1961; Forbes et al., 1958; Greenberg and Daou, 1960). Early modelers investigated the instabilities of car-following models (Chandler et al., 1958; Edie, 1961; Gazis et al., 1961; Herman et al., 1959; Kometani and Sasaki, 1958; Newell, 1961), which described the dynamics of

vehicles in dense traffic. These car-following models were usually written in the format of an acceleration function with the acceleration rate depending on speed, relative speed, and spacing. A general format is given in equation (2-1).

$$a(t+T) = \frac{-\lambda v^m (\Delta v)^n}{s^l}, \quad (2\text{-}1)$$

where T is the reaction time, λ is a coefficient, $v = v_f(t)$, the speed of the following vehicle, $\Delta v = v_f(t) - v_l(t)$, the relative speed, s is the spacing $s = x_f(t) - x_l(t) - l_l$, and m, n, and l are power coefficients.

In these car-following models, a driver would response to stimuli (either relative speed or spacing) with time lag,T. This delayed reaction might be too small or too big so that the following vehicle overreacts, which causes instability and has the instability amplified. Analyses of the instability focused on the coefficients to set stable and unstable zones.

The ideas of these early unstable car-following models in explaining traffic oscillations are straightforward and somewhat reasonable. However, they have been criticized for years mainly for two reasons: (1) the reaction time is at the order of several seconds and therefore the periods of traffic oscillations are expected to be of similar magnitude. However, the periods were found to be several minutes (Ahn and Cassidy, 2006; Kerner and Rehborn, 1996; Laval et al., 2009; Mauch and Cassidy, 2002; Newell, 1965). (2) They indicate that traffic oscillations will lead to crash (Newell, 1965; Treiber et al., 2000), which is not observed.

2.2.1.2 Models with optimal velocity functions

Different from the early car-following models that focus on acceleration, some models define vehicle motion through an optimal velocity function. The car-following model proposed by Newell (Newell, 1961) and the optimal velocity model proposed by Bando et al. (Bando et al., 1995) are two typical ones.

Newell's model ((Newell, 1961) defines a unique speed-spacing relationship. The main idea is that after reaction time, T, drivers will reach the optimal velocity $V(s)$, which depends on current spacing and desired speed. This model eliminates the possibility of collision, but the requirement that drivers reach the optimal velocity in reaction time T requires very high acceleration and deceleration rates, which is unrealistic. Additionally, since the reaction time is still at the magnitude of several seconds, this suffers the same problem with the early car-following models: very short oscillation period.

$$v(t+T) = V(s(t)) \qquad (2\text{-}2)$$

The spirit of Newell's model was incorporated later in the optimal velocity (OV) model (Bando et al., 1995) and ensuing modified OV models. The OV model also defines a optimal velocity function, which is shown by (2-3), but it replaces the reaction time with relaxation time τ, which could be of the order of 40s for highway traffic. However, to avoid crashes, this model requires the relaxation time τ to be of order of several seconds, which makes the model similar to Newell's model and thus suffer from the same problem of unrealistic high acceleration/deceleration rates (Treiber et al., 2000). Nevertheless, the OV model has been used widely by physicists or transportation scientists who study traffic oscillations from a mathematic perspective because this model is simple and allows for analytical investigation (Treiber et al., 2000).

$$a(t) = \frac{V(s) - v}{\tau} \qquad (2\text{-}3)$$

2.2.1.3 Models with optimal velocity functions

The Intelligent Driver Model (IDM) proposed by Treiber et al., (Treiber et al., 2000) shares the same methodology of defining an acceleration function but incorporating more variables:

$$\dot{v_\alpha} = a^{(\alpha)}\left[1 - \left(\frac{v_\alpha}{v_0^{(\alpha)}}\right)^{\delta} - \left(\frac{s^*(v_\alpha, \Delta v_\alpha)}{s_\alpha}\right)^2\right], \quad (2\text{-}4)$$

where the acceleration of vehicle α depends on acceleration rate $a^{(\alpha)}$, current speed v_α, desired speed $v_0^{(\alpha)}$, actual spacing s_α, and desired minimum gap s^*, which depends on speed and speed v_α and speed difference Δv_α. The power δ is a parameter. The desired minimum gap s^* has accounted the effect of safe time headway, maximum acceleration and deceleration, and jam distance between vehicles by incorporating them as the coefficients.

IDM is a typical representative of traffic oscillation modeling from the unstable car-following perspective, whose trend is to incorporate more factors in the vehicle motion function and conduct calibration to fit empirical data. Since this model has incorporated more factors that affect vehicle motion, it is not surprising that it can yield much better results than the models mentioned above. In fact, this model can produce traffic oscillations that are qualitatively consistent with empirical data at the macroscopic level if the parameters are carefully chosen (Treiber et al., 2000; Treiber and Kesting, 2011; Ward and Wilson, 2011). However, if the parameters are not well tuned, it can lead to unrealistic results, such as traffic oscillations that propagate downstream, which conflicts observations.

2.2.2 Fully stochastic models

Another group of car-following models that can produce oscillations are the fully stochastic models. Mainly the cellular automata (CA) models (Nagel and Schreckenberg, 1992) (Barlovic et al., 2002; Barlovic et al., 1998) and the gas-kinematic models (Helbing et al., 2001; Helbing and Treiber, 1998; Ngoduy, 2008; Ngoduy et al., 2006; Shvetsov and Helbing, 1999). These models employ random components to describe driver behaviors and produce traffic oscillations by using a braking probability, which is either a constant or a function of speed.

Newell (Newell, 1965) postulated that there exists different speed-spacing relations for acceleration and deceleration, i.e., an acceleration branch and a deceleration branch. However, he did not specify the path that connected the acceleration and deceleration branches.

del Castillo (del Castillo, 2001) took this conjecture and conducted a theoretical attempt to explain the evolution of traffic oscillations. In his theory, before perturbation drivers maintained a random spacing whose average was the value at full capacity, and after the perturbation they adopted spacing equal to the spacing at capacity. This interpretation suggests that drivers' reaction to perturbation is stochastic. So is the evolution of traffic oscillation, which could develop to full stoppage or dissipate. Additionally, it assumes that the distribution of spacing was stochastic in the deceleration process while deterministic in the acceleration. This theoretical effort yielded some useful insights. However, it expected the perturbation to be at most a few seconds, which could be much longer in the field (NGSIM, 2006).

Following the track of del Castillo (del Castillo, 2001), Kim and Zhang (Kim and Zhang, 2008) allowed both deceleration and acceleration branches to be stochastic. In their model, all drivers used the same speed but adopted random spacing, which led to stochastic wave speed. When the wave speed in acceleration exceeded (more negative) the value in deceleration, perturbation decayed. In contrast, if the deceleration wave traveled faster, perturbation amplified. Neither this model nor del Castillo's (del Castillo, 2001) explained the regular occurrence of traffic oscillations in several minutes.

It is probably true that the relation between speed and space contains randomness. However, whether the randomness is sufficient to explain the formation and evolution of traffic oscillation is questionable. More importantly, attributing randomness to be the impetus does not help to improve our understanding of driver behavior and may enclose the true mechanism of the formation and propagation of traffic oscillation.

2.3 Human Behavior Models

None of the three categories of models above explicitly linked traffic oscillations to the behavior of drivers. This is probably due to the lack of detailed vehicle trajectory data that allows for thorough examination of individual driver behavior. Recent findings (Ahn, 2005; Ahn and Cassidy, 2006; Zheng et al., 2011a; Zheng et al., 2011b) about the role of lane-changing maneuver in triggering traffic oscillations suggest that driver behavior may be responsible for traffic oscillations. Since then, a new class of traffic oscillations, human behavior model, emerges.

Newell (Newell, 1965) may be the first to associate traffic oscillation with driver behavior. He claimed that traffic oscillations might result from drivers' laziness or intentional failure to response to every stimulus rather than inherent reaction delay. When drivers accelerate, the following ones wait to check whether the acceleration trend will continue or not, which allows for excess spacing. If the trend continues, the following driver starts to accelerate. Otherwise, the follower might still stay with the large spacing for a long period of time if the leader did not make further change. From this perspective, Newell derived the idea of different acceleration and deceleration branches. In the context, the "laziness" is considered to be the special behavior in special states (acceleration or deceleration). Unfortunately, Newell's interpretation about the role of driver behavior did not receive sufficient attention.

Yeo and Skabardonis (Yeo and Skabardonis, 2009) examined vehicle trajectories in NGSIM datasets and speculated that the cause of oscillations may be human errors such as anticipation and overreaction, but no model was built. Shortly, Laval and Leclercq (Laval and Leclercq, 2010) conjectured that the formation and propagation of traffic oscillations were due to the aggressive or timid driver behavior. They built a model, referred to as the L-L model hereafter, based on Newell's (Newell, 2002) simplified car-following. They simulated drivers on a 3km single lane highway where a short uphill segment caused vehicles to slow down. The simulations produced regular

traffic oscillations with periods and amplitude consistent with field observations. This study suggests a promising future to explain the mechanism of formation and propagation for traffic oscillations from a new perspective: the behavioral perspective.

Notably, the behavioral perspective in the L-L model is only partial: it assumed that (1) drivers behave homogeneously and consistently (i.e., following the same speed-spacing relationship, or equivalently, the same fundamental diagram) before and after traffic oscillations; and (2) they randomly adopt aggressive or timid reaction during traffic oscillations. Apparently, the behavior of drivers before and after oscillations was not taken into account, nor was it related to the behavior during oscillations. It appears that drivers adopt the behavior during oscillations for no reason; i.e., the underlying root of adopting the behavior is missing. From this sense, the behavioral perspective is partial.

Nevertheless, the L-L model explicitly connects traffic oscillation to the physical behavior, which sheds lights on modeling the formation and propagation mechanism of traffic oscillation with explicit physical behavior insights. It is also promising because of its parsimoniousness and its capability in capturing the basic characteristics of traffic oscillation. Therefore, this study will base on the framework of the L-L model, but validate and extend it to meet the research needs.

Because the L-L model forms the base of this study, a more comprehensive introduction of the model will follow in the next chapter.

2.4 Studies on Traffic Hysteresis

Traffic hysteresis in freeway traffic was first reported in 1974 (Treiterer and Myers, 1974). It was found that the relationship between density and speed (and also volume) from a platoon of vehicles that underwent disturbances on a freeway exhibited obvious hysteresis loops. Similar hysteresis loops were found from transient traffic

conditions after incidents (Maes, 1979). Although traffic hysteresis has been observed over decades, understanding on its formation mechanism is still very limited.

Several theories and models have been proposed to explain traffic hysteresis. Newell (Newell, 1965) conjectured that hysteresis arise due to the asymmetry between acceleration and deceleration, which leads to two congested branches on a fundamental diagram. Zhang (Zhang, 1999) formulated the asymmetry mathematically. He used three traffic phases to describe traffic flow: acceleration, deceleration, and strong equilibrium phase, and showed that the transition of the speed-density relationship in different phases formed hysteresis loops. Some of the predictions from his theory accorded well with empirical data. Zhang and Kim (Zhang and Kim, 2005) proposed a car-following model in which the speed of a driver was determined by the traffic phase and the gap-time. When certain functions are used for the variable, gap-time, their model could produce traffic hysteresis, but the model has not been tested by empirical data. Yeo and Sakabardonis (Yeo and Skabardonis, 2009) divided traffic conditions into five states: free-flow, acceleration, deceleration, coasting and stationary, and argued that the acceleration and deceleration processes were asymmetric, which caused traffic hysteresis. However, according to their theory, counter clock-wise hysteresis loop will not be produced, which conflicts field observations (Ahn et al., 2011; Laval, 2010). These existing models/theories describe traffic hysteresis as a result of asymmetry in different traffic phases. However, the underlying root of asymmetry is unknown. Additionally, the effects of microscopic driver behavior, such as driver aggressiveness, on hysteresis have not been investigated.

Laval (Laval, 2010) and Ahn, et al. (Ahn et al., 2011)argued that the magnitude of hysteresis has been over-estimated in previous studies because of measurements taken during non-steady state conditions. All references in the previous paragraph may be subject to measurement bias. To overcome this problem, Laval (Laval, 2010) took measurements on regions of (near) steady states (i.e., stationary or stationary non-

equilibrium traffic states) from vehicle trajectory data using Edie's generalized definition of flow, density, and speed (Edie, 1961). Ahn et al. (Ahn et al., 2011) measured the evolution of speed-spacing relations as vehicles underwent stop-and-go oscillations. To account for the non-steady conditions, they measured the equilibrium spacing, rather than observed spacing. These studies found that the magnitude of hysteresis is not as significant as previously thought. Nevertheless, hysteresis was still present in the observations but in smaller frequency and magnitude. In addition, reverse (i.e., counter clock-wise) hysteresis loops were found in both studies (Laval, 2010), although its proportion was smaller (Ahn et al., 2011).

In most of the empirical and theoretical studies cited above, traffic hysteresis was not investigated with a behavioral perspective. In the few studies that mentioned driver behavior (Newell, 1965; Yeo and Skabardonis, 2009), the connection between traffic hysteresis and driver behavior was in a state of conjecture and was not investigated extensively. For example, in Newell' conjecture (Newell, 1965), the driving rules resulted in the asymmetry between the acceleration and deceleration branches. According to Yeo and Sakabardonis (Yeo and Skabardonis, 2009), human errors such as maneuvering errors and anticipation might be associated with the state transition and that causes the asymmetry, but the relationship between human errors and traffic hysteresis was not investigated. Nevertheless, the connection between hysteresis and driver behavior is still not clear. The human behavioral perspective reviewed in Section 2.3 is promising not only for studies on traffic oscillation but also for traffic hysteresis.

CHAPTER 3 MODEL BACKGROUND

This chapter will introduce the basic framework of the L-L model, which will be used in this study. But before that, the kinematic wave model and Newell's car-following model (Newell, 2002) embedded in the L-L model will be described.

3.1 The Kinematic Wave Model

The Kinematic wave (KW) model (Lighthill and Whitham, 1955; Richards, 1956), also referred to as the LWR model, is one of the simplest nonlinear scalar conservation law in engineering. It assumes that traffic flow q is a function of density $k(t,x)$. With that, for a homogenous road (with no exit or entrance), the conservation law is:

$$\frac{\partial k}{\partial t}+\frac{\partial q(k)}{\partial x}=0. \qquad (3\text{-}1)$$

Equation (3.1) is a first order nonlinear hyperbolic partial differential equation (PDE). The function $q(k)$ yields a fundamental diagram that gives the flow as a function of the density. The triangular shape fundamental diagram is widely used in the literature (e.g., Ahn et al., 2010; Laval, 2004; Laval and Daganzo, 2006) as experimental results (e.g., Cassidy, 1998b; Laval, 2004; Munoz and Daganzo, 2000b) suggest that a triangular shape is a good approximation; see Figure 3:1 for an example. The triangular fundamental diagram describes traffic states in two regimes:

free-flow, in which vehicles travel at a very high constant speed, u, with little interaction between each other, and congestion regime, in which vehicles are not able to travel at their desired speed and they are forced to follow vehicles ahead. These two regimes are described by the free-flow branch and congestion branch, respectively, see Figure 3:1 for an illustration where the three parameters, u, κ, and $-w$ denotes free-flow speed, jam density, and wave speed, respectively. Notice that the model predicts rarefaction fans associated with the acceleration processes if the flow function $q(k)$ is assumed concave, unless the triangular shape is assumed.

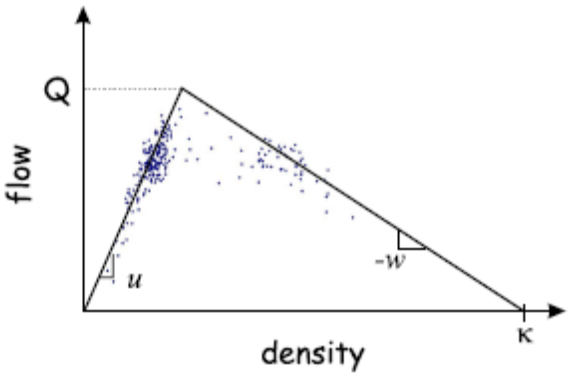

Figure 3:1 Triangular Fundamental Diagram

(3-min interval loop-detector data on I-80 @ University Avenue on 09/28/2002 from 6am to 9am, westbound) (Laval, 2004)

3.2 Newell's Car-following Model

Newell's car-following model (Newell, 2002) describes the movement of a vehicle in both the free flow and congested scenario. It gives the exact numerical solution of the kinematic wave model (Lighthill

and Whitham, 1955; Richards, 1956) with a triangular fundamental diagram. In free-flow vehicles always travel at the free-flow speed, while in congestion a vehicle trajectory is a translation in time and space of the leader's by τ and δ, respectively; see Figure 3:2(a).

$$x_{i+1}(t) = \min\{\underbrace{x_{i+1}(t-\tau) + u\tau}_{\text{free-flow}}, \underbrace{x_i(t-\tau) - \delta}_{\text{congestion}}\}, \quad (3\text{-}2)$$

where $x_{i+1}(t)$ represents the position of vehicle $i+1$ at time t and u is the free-flow speed. The time and space shift (τ, δ) is assumed constant for a given vehicle but may vary as a random walk across different vehicles. This model implies a linear speed-spacing relationship in congestion; see Figure 3:2 (b):

$$S(v) = \delta + \tau . v, \quad (3\text{-}3)$$

where v is vehicle speed and $S(v)$ is the corresponding equilibrium spacing. Notably, parameters τ and δ can be written using the wave speed$-w$, and jam density κ in the KW model, i.e.:

$$\tau = \frac{1}{w\kappa} \text{ and } = \frac{1}{\kappa}. \quad (3\text{-}4)$$

Therefore, δ can be interpreted as the jam spacing and τ as the wave trip time between two consecutive congested vehicles.

Newell's car-following model has been supported or verified by field observations (e.g.,Ahn et al., 2004; Windover, 1998; Windover and Cassidy, 2001). It is appealing for its simplicity and consistency with the KW model. However, in this model disturbances will never amplify or decay. Fortunately, this problem is solved in the L-L model.

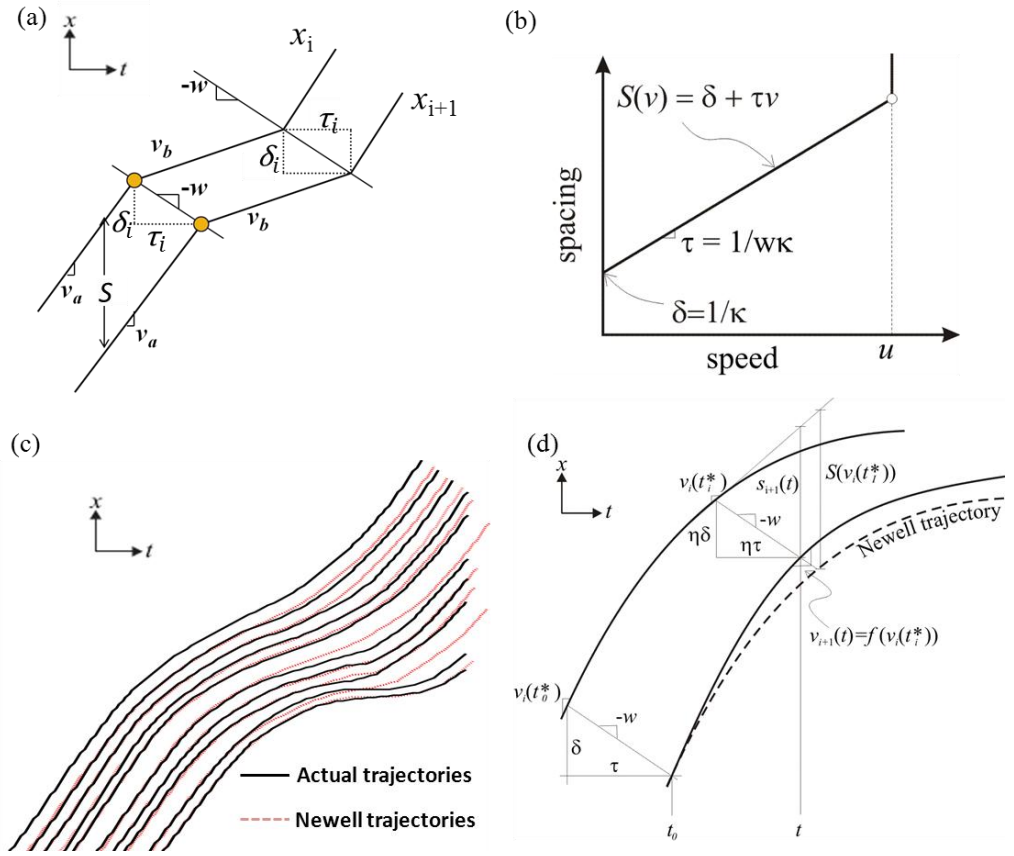

Figure 3:2 Newell's Car-following Model

3.3 The L-L Model

Laval and Leclercq (2010) observed that vehicle trajectories accord well with Newell' car-following model before they experience traffic oscillations. Namely, a follower's trajectory overlaps its leader's shifted by (τ, δ). In the sequel, this shifted trajectory is called a "Newell trajectory". However, deviations were significant during the oscillation; see Figure 3:2 (c). To capture these, the L-L model allows vehicle trajectories to deviate

from Newell trajectories by explicitly including a behavioral model via the term $\eta_i(t)$:

$$x_{i+1}(t) = \{\underbrace{x_{i+1}(t-\tau) + \min\{u\tau, \tilde{x}_{i+1}(t)\}}_{\text{free-flow}}, \underbrace{x_i(t - \eta_{i+1}(t)\tau) - \eta_{i+1}(t)\delta}_{\text{congestion}}\} \quad (3\text{-}5)$$

where $\tilde{x}_{i+1}(t)$ is the desired distance travelled during τ resulting from a vehicle kinematics model (FHWA, 2000) that limits accelerations:

$$a(v) = a_m(1 - {}^{v}/_{u}) - Gg\ , \quad (3\text{-}6)$$

where the acceleration $a(v)$ depends on the current speed v, maximum acceleration a_m, the gravitational acceleration $g = 9.8\ \mathrm{m/s^2}$, and the percent grade 100G%. By solving (3-6) analytically, one can obtain the expression for $\tilde{x}_{i+1}(t)$:

$$\begin{aligned}&\tilde{x}_{i+1}(t)\\ &= u\left(1 - \frac{gG}{a_m}\right)\tau\\ &\quad - \frac{\left(1 - e^{-\frac{\tau a_m}{u}}\right)\left(u\left(1 - \frac{gG}{a_m}\right) - v_{i+1}(t-\tau)\right)}{a_m/u}\end{aligned} \quad (3\text{-}7)$$

The term $\eta_{i+1}(t)$ captures the non-equilibrium behavior often observed in the dataset; i.e., deviations from Newell's model. It is defined as the ratio of the actual steady-state spacing and the equilibrium spacing; i.e.:
In congested traffic, $\eta_{i+1}(t)$ is used to capture the deviation, i.e., non-equilibrium behavior. It is defined as the ratio between the actual spacing of any vehicle and its equilibrium spacing, i.e.:

$$\eta_{i+1}(t) = s_{i+1}(t)/S(v_i(t_i^*)), \qquad (3\text{-}8)$$

where $s_{i+1}(t)$ is the steady-state spacing for vehicle $i+1$ at time t, $S(.)$ is the equilibrium spacing given by (3-3), and t_i^* is the time the characteristic line is emanated from the leader reaching the follower at time t; see Figure 3:2 (d). Notice that the steady-state spacing is measured by assuming that the leader is stationary and driving at $v_i(t_i^*)$ until time t, and $S(v_i(t_i^*))$ is obtained from (3-3) with v equal to $v_i(t_i^*)$ (see Figure 3:2 (d)). Clearly, when a driver is in equilibrium, $\eta_i(t) = 1$ and the follower's trajectory overlaps the Newell trajectory; otherwise, $\eta_i(t)$ deviates from 1. Non-equilibrium behavior in the follower is triggered in this model whenever the leader decelerates. The ensuing evolution of $\eta_i(t)$ is assumed to fall into one of three patterns, as illustrated in Figure 3:3: concave triangle, convex triangle, or constant. This gives rise to three user classes: timid, aggressive, and Newell drivers, respectively.

The physical meaning of the concave (convex) triangle pattern is that when drivers first perceive an oscillation they will tend to get farther (closer) to the leader -- relative to the equilibrium congested branch -- until some critical point where they will tend to come back to the equilibrium branch. The maximum degree of deviation from the equilibrium is denoted by α and the corresponding η_i-value, η_T. Namely, $\alpha = |\eta_T - 1|$. Clearly, the constant pattern implies that the driver will remain on their equilibrium branch throughout the oscillation. The rate $\varepsilon = \dot{\eta}_i(t)$ is assumed constant.

Notably, the driver behavior described by the L-L model was only a conjecture inspired from observations, and it has not been verified yet.

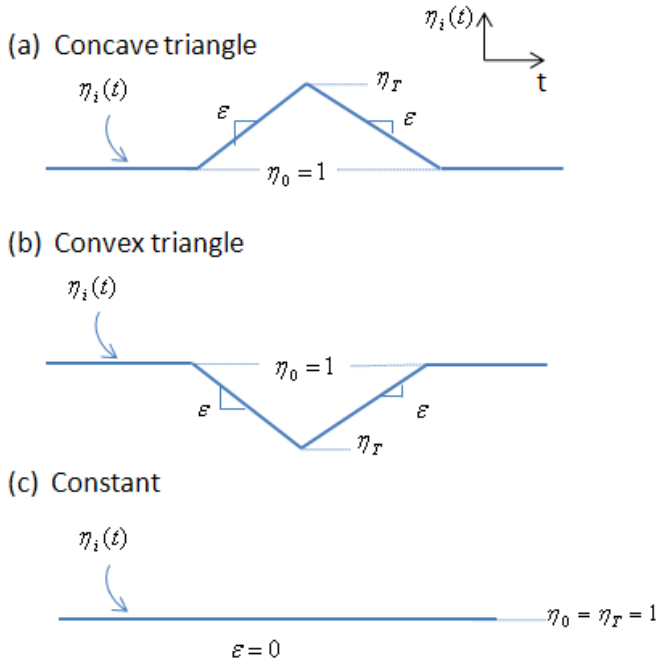

Figure 3:3 Behavior Patterns

CHAPTER 4 METHODOLOGY

This chapter introduces the trajectory data used and the method to measure the parameters of the L-L model. Measurement results are then used to formulate a new behavioral model, which will be present in the end of this chapter.

4.1 Data Description

The trajectory data used in this study are taken from the Next Generation Simulation (NGSIM) project(NGSIM, 2006); i.e., the 2100-foot southbound US-101 segment in Los Angeles, California from 7:50 a.m. to 8:35 a.m. on June 15, 2005. Figure 4:1 (a-b) shows the trajectories on the median lane from 7:50 a.m. to 8:20a.m.

Figure 4:1 (c) is a sketch of the study site. Notice that traffic oscillations spontaneously appear every 2-3 minutes in the first 15min (Figure 4:1(a)) but oscillations from downstream appear in the second 15min (Figure 4:1(b)). For the spontaneously formed oscillations, after thorough examination of the data, the possibility of lane-changing in triggering traffic oscillations is eliminated. Thorough examination of the freeway design elements and the video data suggests that the most likely cause for the traffic oscillations seems to be rubbernecking. During that time at the same location where traffic oscillations begin, clean-up work was being performed in the median; see Figure 4:1 (a) for a snapshot. Vehicles tend to slow down when they approached that spot. This thought about the cause will be tested and discussed in Chapter 5.

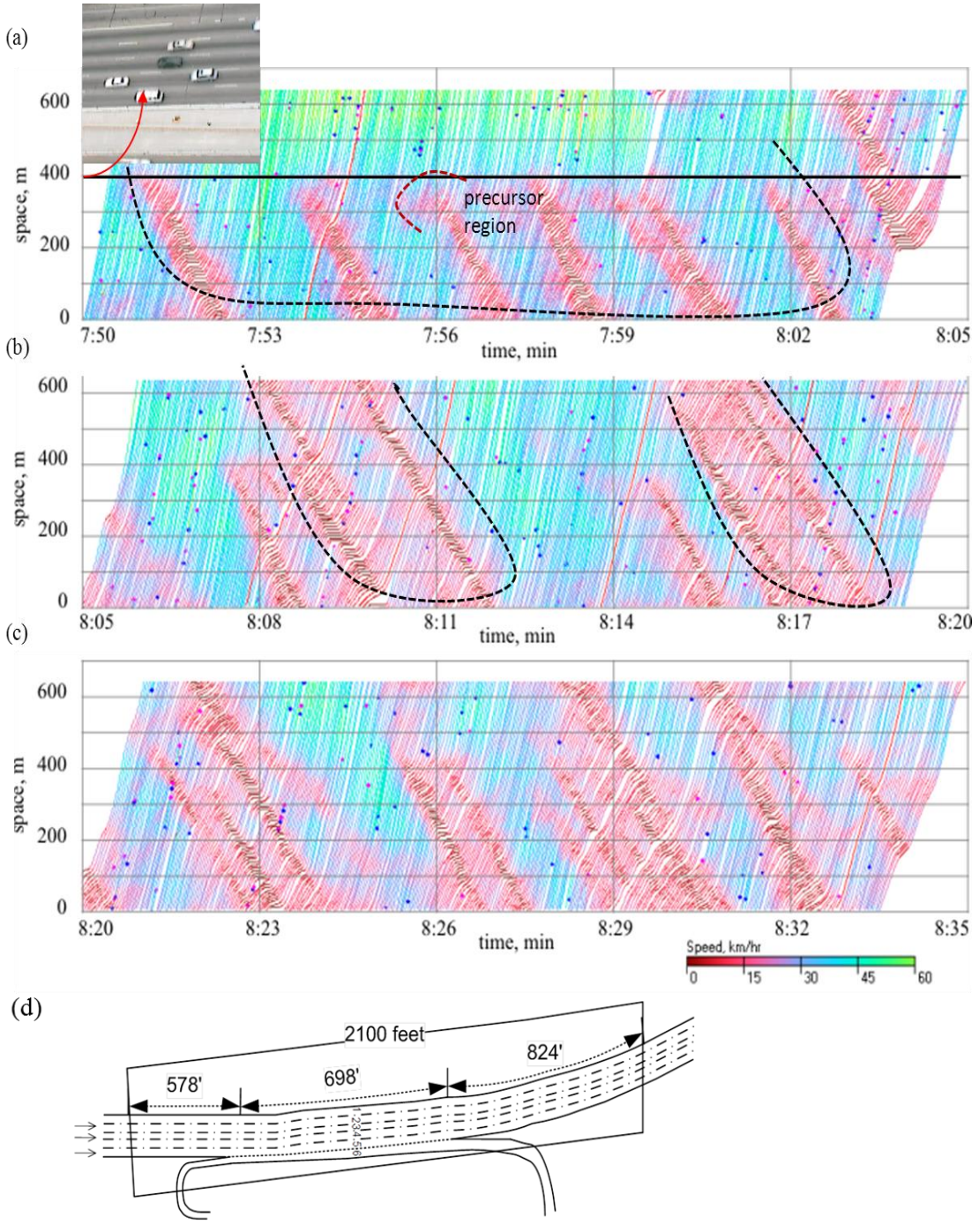

Figure 4:1 Illustration of Vehicle Trajectories and Study Site

(a-c) vehicle trajectory plot (lane 1 on US 101 study site); (d) schematic of the study site: southbound US-101 in Los Angeles, California.

4.2 Measurement

This section introduces the method to measure the parameters of the L-L model.

In the L-L model, all parameters can be obtained through the variable $\eta_i(t)$. Therefore, the key measurement is $\eta_i(t)$. The method is illustrated in Figure 4:2, where it can be seen that $\eta_i(t)$ can also be written as:

$$\eta_i(t) = \tau_i(t)/\tau, \qquad (4\text{-}1)$$

where $\tau_i(t)$ is the actual wave travel time and τ is the equilibrium value given by (3-4). It follows that the measurement of $\eta_i(t)$ boils down to measuring $\tau_i(t)$, which is much more convenient than measuring the steady-state spacing. To see this, recall that when the vehicle is accelerating/decelerating, its steady-state spacing is given by the term "$S(v_i(t_i^*))\eta_{i+1}(t)$" in Figure 4:2, which is not easy to observe from the data. By contrast, to measure $\tau_{i+1}(t)$, one only needs to launch a characteristic line from $(t, x_{i+1}(t))$ with the slope equal to wave speed $-w$. This line will intersect the leader's trajectory at $(t_i^*, x_i(t_i^*))$. The horizontal distance between the two points yields $\tau_{i+1}(t)$.

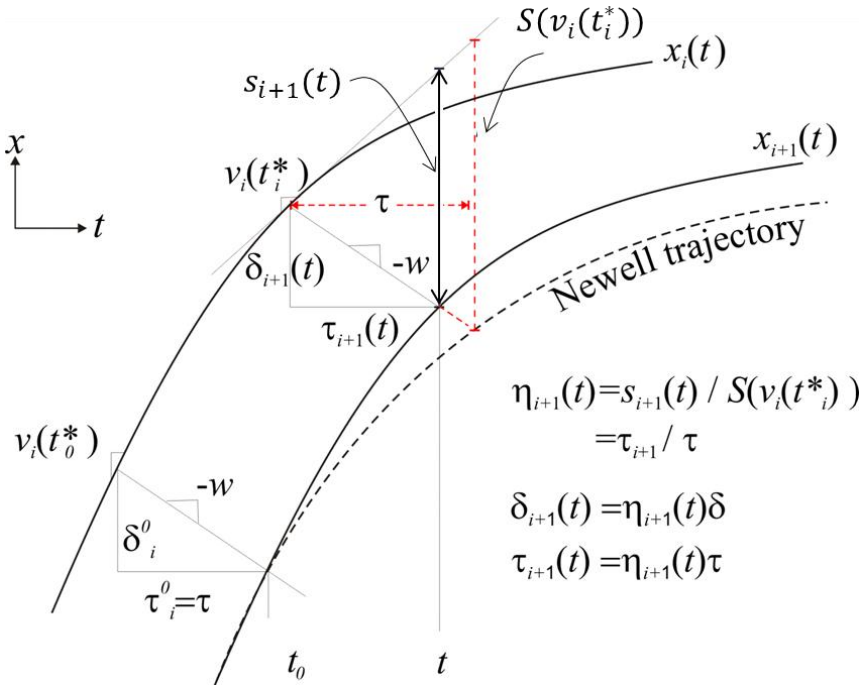

Figure 4:2 Measurement of $\eta_i(t)$

Notice that the value of $\eta_i(t)$ depends on the product $w\kappa$ by virtue of (3-4) and also on w alone since it defines the slope of characteristics, which is qualitatively illustrated in Figure 4:3. Let $-w_0$ and τ_0 represent the true wave speed and trip time and $-\overline{w}$ denote the value used. It follows that:

$$\overline{\tau}(v+\overline{w}) = \tau_0(v+w_0), \quad \overline{\tau} = (1+\frac{w_0-\overline{w}}{v+\overline{w}})\tau_0. \tag{4-2}$$

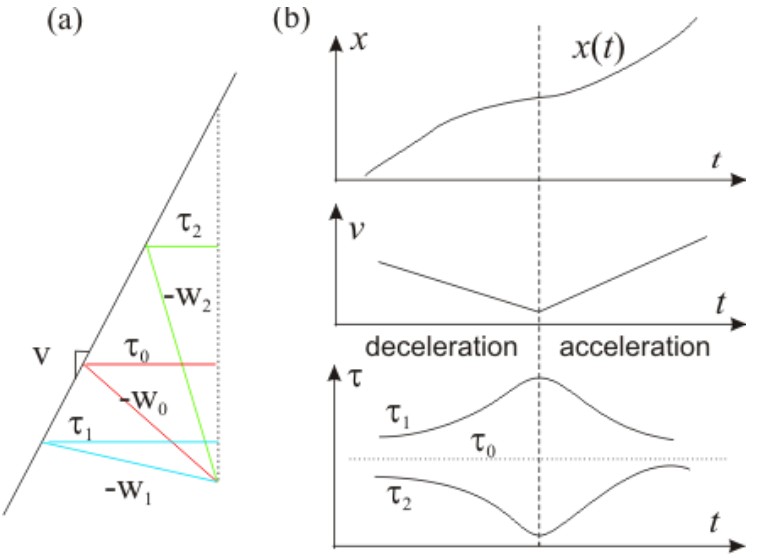

Figure 4:3 Impact of the Wave Speed

Apparently, the measured trip time $\overline{\tau}$ is a function of velocity v. When $\overline{w} < w_0$, $\overline{\tau}$ is greater than τ_0 and will increase and then decrease in a deceleration-acceleration cycle; see the case of w_1 and the corresponding concave τ_1 curve in Figure 4:3 (b). By contrast, when $\overline{w} > w_0$, $\overline{\tau}$ is smaller than τ_0 and the change of value shows the opposite trend; see the convex τ_2 curve. Hence, artificial error may be introduced by the wave speed used. Particularly, the shape of $\overline{\tau}$ curve will change from concave to convex if the wave speed used is varied from extreme low to extreme high value. Define the measurement error as $e = (\bar{\tau} - \tau_0)/\tau_0$. When $\overline{w}$ varies from $1.2w_0$ to $0.8w_0$, the maximum error ranges from -16.7% to 25%.

The literature suggests that wave speed might vary at microscopic level but remain stable at macroscopic level. According to Newell's car-following model (Newell, 2002), each vehicle has a pair of (τ_i, δ_i), which

"*varies as if they were sampled independently from some joint probability distribution*" but remain constant for a given vehicle. This suggests that the wave speed could be modeled as a random walk. This inference has been supported or verified by field observations (Ahn et al., 2004; Windover, 1998; Windover and Cassidy, 2001), which reveal that the wave speed of individual drivers is a random walk but macroscopically there is no wave focusing or acceleration fan outward. Indeed, the fact that acceleration and deceleration propagate upstream at a nearly constant speed without wave focusing or rarefaction fans has been widely reported (Ahn et al., 2004; Cassidy, 1998a; Cassidy and Windover, 1995; Chiabaut et al., 2009a; Chiabaut et al., 2009b.; Foster, 1962; Kerner and Rehborn, 1996; Munoz and Daganzo, 2000a). For example, Kerner and Rehborn (Kerner and Rehborn, 1996) traced the propagation of traffic oscillations for 13km and found that its shape was maintained along the way, which suggests constant wave speed in temporal and spatial dimension.

It is likely that the wave speed is random at the scale of a few seconds or closely located detectors. However, these random wave speeds fluctuate around a constant value, which turns out to be the nearly constant wave speed at macroscopic scale. Therefore, a triangular shape of fundamental diagram (i.e., constant wave speed) is assumed in the measurement, which has been supported by empirical studies (Banks, 1989; Hall et al., 1986; Hillegas et al., 1974) and has been recommended by traffic flow theorists (Daganzo, 2002; del Castillo, 2001; Newell, 1993). The triangular fundamental diagram is also adopted in the L-L model.

Measurement results also confirm that using the constant wave speed is reasonable. Measurement conducted on trajectory data shows that within a wide range of values of w (12-20km/h) and κ (120-200veh/km), the general shape of $\eta_i(t)$ is maintained across different measurements; see e.g. Figure 4:4. Therefore, it could be concluded that significant behavior changes occur during the traffic oscillations and the wave speed error does not dominate. Accordingly, in the following measurement, the wave speed w = 16 km/h is used, as the case in many studies that used NGSIM data (Durent et al., 2011; Laval and Leclercq, 2010), and τ is set to be the average of $\tau_i(t)$ in equilibrium before oscillations from all trajectories sampled.

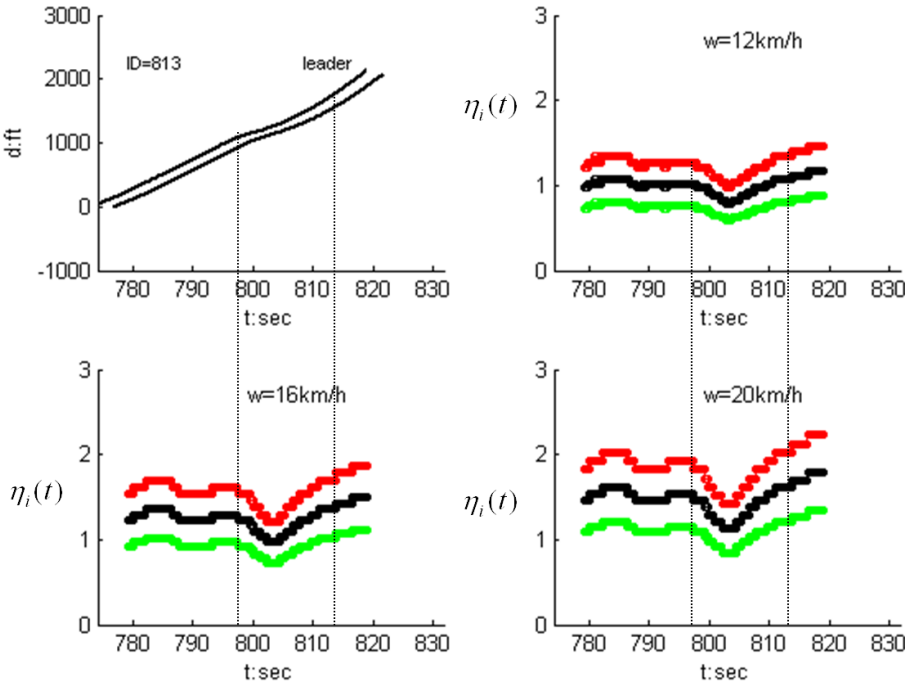

Figure 4:4 Effects of Model Parameters

4.3 Formulation of the Asymmetric Behavior Model

From empirical measurement, it is observed that driver behavior across traffic oscillations follows a very consistent pattern across the sample, i.e., see Figure 4:5 (a) for a typical example. Generally, drivers maintain a constant $\eta_i(t)$ before the oscillatory state. When the deceleration wave arrives, $\eta_i(t)$ deviates from the constant level, which implies that they enter the non-equilibrium mode. Interestingly, after the oscillation, $\eta_i(t)$ maintains a constant level again, although it is not necessarily the value before the non-equilibrium. Based on these observations, the "Asymmetric Behavior model" is proposed to describe a driver's car-following behavior in congestion: (i) drivers enter the non-equilibrium mode when an oscillation is triggered; (ii) the ensuing dynamics of $\eta_i(t)$ in non-equilibrium, called "reaction pattern", follow one of three categories: concave triangle, convex triangle, and constant; and (iii) before and after the non-equilibrium mode, drivers are in equilibrium. The model can be well described using the following parameters, as shown in Figure 4:5 (b):

η_i^0 is the stable value of $\eta_i(t)$ before the non-equilibrium behavior,

η_i^1 is the stable value of $\eta_i(t)$ after the vehicle has reached equilibrium,

η_i^T is the value of $\eta_i(t)$ when the vehicle has the maximum deviation from η_i^0,

ε_i^0 is the average slope of $\eta_i(t)$ between η_i^0 and η_i^T, and

ε_i^1 is the average slope of $\eta_i(t)$ between η_i^T and η_i^1.

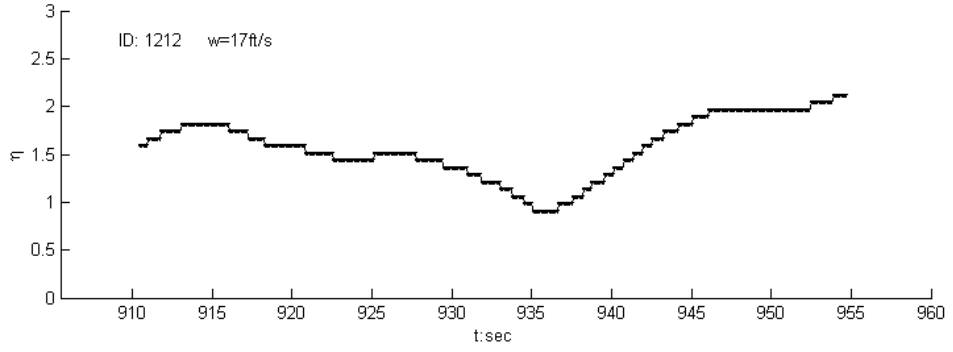

(a)

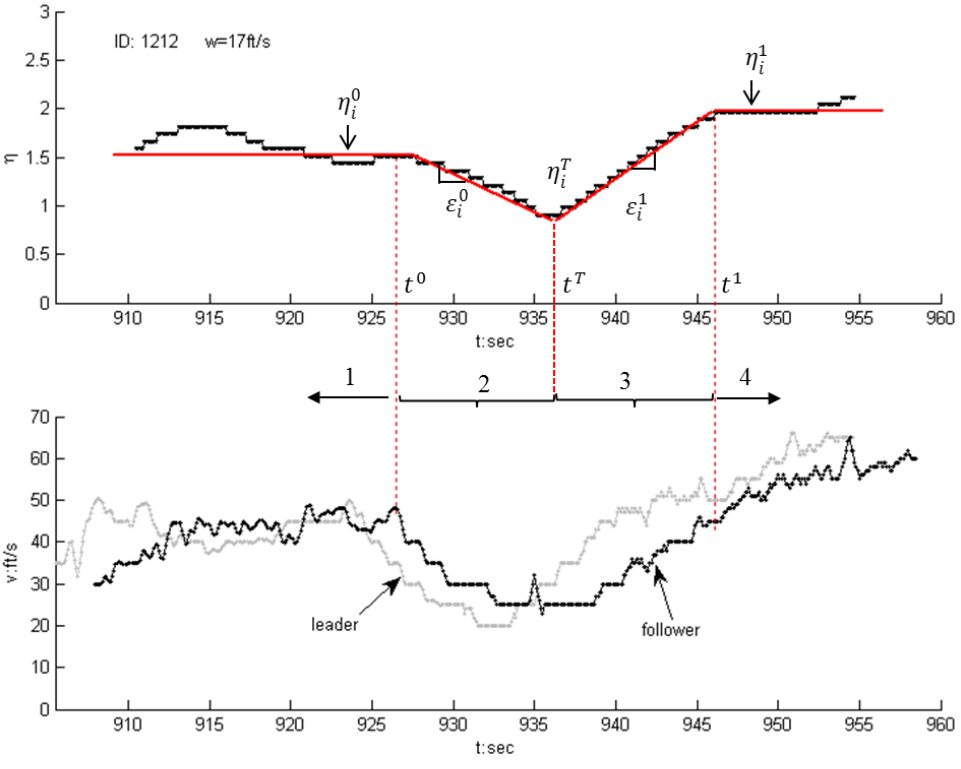

(b)

Figure 4:5 Behavior Profile of the Asymmetric Behavioral Model (a) empirical plot of $\eta(t)$; (b) illustration of asymmetric behavioral model.

The moment the non-equilibrium behavior starts is the last essential component of the model. Based on observations, in most cases the trigger

towards non-equilibrium is the initial deceleration wave emanated from the oscillation. Therefore, this model assumes that drivers in equilibrium will switch to non-equilibrium mode as soon as they are forced to decelerate. As an example, the dynamics of $\eta_i(t)$ for the concave triangle pattern can be written as:

Before non-equilibrium: $\eta_i(t) = \eta_i^0;$ (4-3)

During non-equilibrium $\begin{cases} \eta_i(t) = \eta_i^0 + \varepsilon_i^0 * (t - t^0), \eta_i(t) \le \eta_i^T; \\ \eta_i(t) = \eta_i^T - \varepsilon_i^1 * (t - t^T),\ \eta_i^1 \le \eta_i(t) \le \eta_i^T; \end{cases}$ (4-4)

After non-equilibrium: $\eta_i(t) = \eta_i^1;$ (4-5)

where t^0 denotes the starting point of non-equilibrium and t^T is the instance when η_i^T is achieved. The dynamics of convex pattern are identical except for the sign preceding $\varepsilon_i^0$and ε_i^1

Notice that in this model (i) drivers are heterogeneous and each driver has its own set of parameters [$\eta_i^0, \eta_i^1, \eta_i^T, \varepsilon_i^0, \varepsilon_i^1$], (ii) η_i^0 is not necessarily equal to 1, and it may change after the driver passes the oscillation to η_i^1, which means that each driver has a unique equilibrium congestion branch before traffic oscillations and does not necessarily come back to that branch after oscillations, and (iii) the reaction patterns (i.e., convex and concave triangles) are not necessarily isosceles; i.e., $\varepsilon_i^0 <> \varepsilon_i^1$.

The physical meaning of η_i^0 is clear. In the context of the KW model, different values of η_i^0 correspond to different congested branches in the fundamental diagram; see Figure 4:6. If $\eta_i^0 \ll 1 (\eta_i^0 \gg 1)$, the driver prefers to maintain a spacing smaller (larger) than the average level, referred to as “originally aggressive” (“originally timid”) driver,

abbreviated as OA (OT); see point "1" ("3"). If η_i^0 is close to 1 (i.e., $\eta_i^0 \sim 1$), the driver behaves at the average level, named as "originally Newell" driver, abbreviated as ON; see point '2'. Hence, the η_i^0-value captures the characteristics of a driver in equilibrium *before* traffic oscillations, and similarly the η_i^1-value captures the characteristics in equilibrium *after* traffic oscillations. Notice that driver categories are determined by their characteristics in equilibrium before traffic oscillations, and that every driver category can exhibit any of the three reaction patterns. In contrast, the original L-L model assumes that drivers are homogeneous and their reaction to oscillations is symmetric; i.e., $\eta_i^0 = \eta_i^1$ and $\varepsilon_i^0 = \varepsilon_i^1$. Additionally, driver categories are determined by the reaction pattern. Clearly, the original L-L model is only a special case of the asymmetric behavioral model. Table 4:1provides a summary of the asymmetric behavioral model and also the difference between this model and the original L-L model.

The parameters of the asymmetric behavioral model can be measured from the $\eta_i(t)$ plot obtained using the methodology introduced above. Particularly, the measured $\eta_i(t)$-function is approximated by a piecewise-linear function characterized by parameters $[\eta_i^0, \eta_i^1, \eta_i^T, \varepsilon_i^0, \varepsilon_i^1]$. This is illustrated in Figure 4:5 (b), which also shows the corresponding speed profile. Time t^0 corresponds to the beginning of the deceleration cycle (i.e., starting point of the non-equilibrium mode) and t^T is the instance when η_i^T, the maximum or minimum value of $\eta_i(t)$ during the oscillation, is achieved. Time t^1 is selected to minimize the variation of

linear regression on segment 3 and 4. The average level for segment 1 is η_i^0 and η_i^1 for segment 4. The slopes of segment 3 and 4 are ε_i^0 and ε_i^1, respectively.

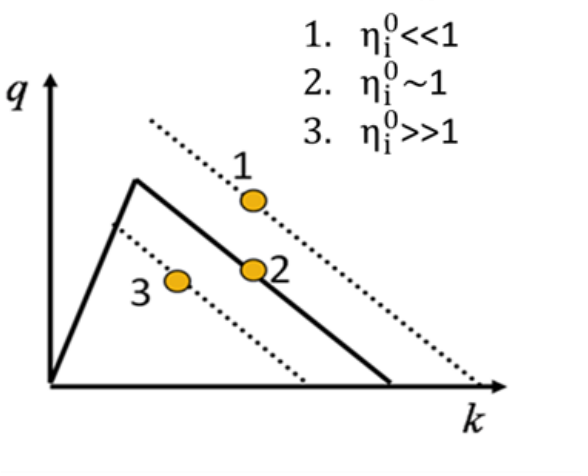

Figure 4:6 Physical Meaning of Driver Categories

Table 4:1 Difference between Two Models

	L-L Model	Asymmetric Behavioral Model
Vehicles	Identical. Share the same set of parameters.	Unique. Each vehicle has its own set of parameters
$\eta_i^0, \eta_i^1, \varepsilon_i^0, \varepsilon_i^1$	$\eta_i^0 = \eta_i^1 = 1$ $\varepsilon_i^0 = \varepsilon_i^1 = \varepsilon$	$\eta_i^0 <> \eta_i^1$ $\varepsilon_i^0 <> \varepsilon_i^1$
η_i^T	Identical within each driver category $\eta_i^T = 1 \pm \alpha$	Unique for each driver η_i^T
Driver categories in equilibrium	Homogenous $\eta_i^0 = 1$	$\eta_i^0 \ll 1$: originally aggressive $\eta_i^0 \gg 1$: originally timid $\eta_i^0 \sim 1$: originally Newell
Behavior patterns in non-equilibrium*	concave (aggressive) convex (timid) constant (Newell)	concave (OA, OT, or ON) convex (OA, OT, or ON) constant (OA, OT, or ON)

* With driver class in the parentheses.

CHAPTER 5 THE ASYMMETRIC BEHAVIOR CAR-FOLLOWING MODEL

In this chapter a statistical analysis is undertaken on the trajectory dataset. The main purposes are to (1) study the behavior characteristics of drives, and (2) examine the relationship between model parameters, which may help to further simplify the asymmetric behavioral model.

5.1 Trajectory Sample

As the first step to select the trajectory sample for study, the correlation among vehicle platoon is examined in order to determine the method for sampling. For this purpose, lane 1 was exhaustively sampled from 7:50a.m.-8:05a.m. to examine the correlation of driver characteristic (denoted by η_i^0) between successive drivers. Figure 5:1 shows the result from 123 trajectory pairs (with lane-changers excluded), where the horizontal and vertical axes are the η_i^0 value for the leaders and followers, respectively. The plot suggests no significant correlation between the value of η_i^0 for two successive drivers. The same analysis for the remaining parameters yields the same result. This implies that driver behavior is a "personality" characteristic, independent of other drivers. As a result, random sampling is used in the sequel to select trajectory pairs from other lanes/time periods for detailed investigation.

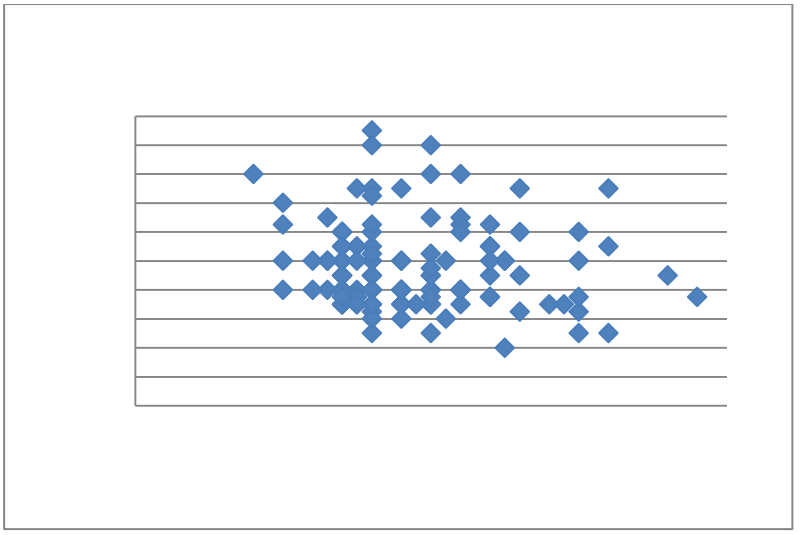

Figure 5:1 Correlation in Successive Drivers

The trajectory sample for detailed investigation was obtained by sampling trajectories from 7:50a.m.-8:20a.m. on lanes where traffic oscillations occurred, but excluding time period after 8:20a.m.because oscillations can hardly be distinguished thereafter; see Figure 4:1. The sample was split into two groups, period 1 and period 2 corresponding to the first and the second 15min. The reason for the splitting is that oscillations originating downstream of the study site appeared after about 8:03a.m.; see Figure 4:1 (a-b). In total 44 trajectories pairs from period 1 and 67 from period 2 were obtained. Particularly, trajectories in period 1 were from 7:50a.m.-8:05a.m. on lane 1, and trajectories in period 2 have 28 trajectory pairs from lane 1 and 39 pairs from lane 3. The oscillations sampled were circled by dashed lines on Figure 4:1 (a-b). Investigation was conducted on this sample.

5.2 Statistical Analysis on Model Parameters

5.2.1 Descriptive Results

Figure 5:2 is the histogram of η_i^0 for all 111 trajectory pairs. The threshold of ON drivers is set to be $0.9 \leq \eta_i^0 \leq 1.1$, and the lower (upper) regime corresponds to OA (OT) drivers. Notice from Figure 5:3 that the composition of driver categories is consistent in period 1 and period 2, and within period 2 the composition is consistent between sample from lane 1 and lane3; i.e., not significant at 95% confidence level from the statistical sense. This is compared using chi-square test for homogeneity of proportions (Greenwood and Nikulin, 1996), which is used to assess whether the distribution of a categorical variable (e.g., driver category) from different populations are significantly different at a given confidence level. Details of the chi-square test are provided in the Appendix A.1. Of course, the proportions may change if the threshold varies, but the magnitude should hold.

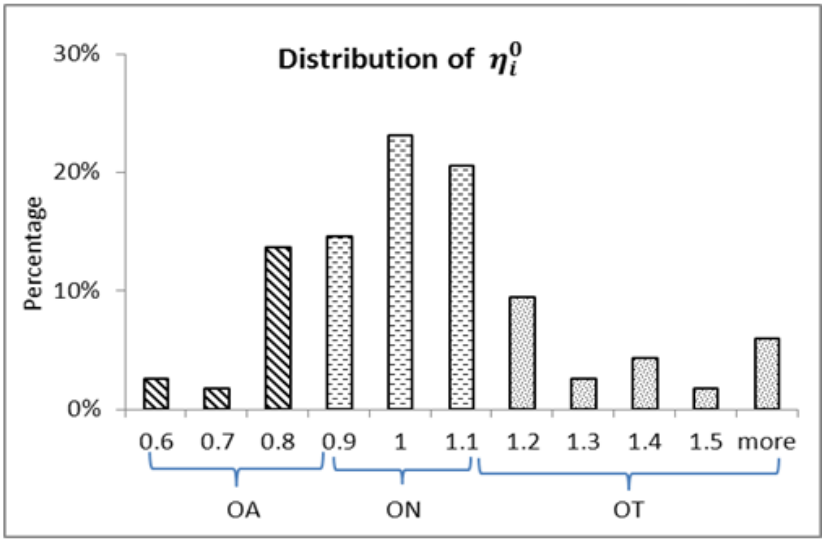

Figure 5:2 Histogram of η_i^0

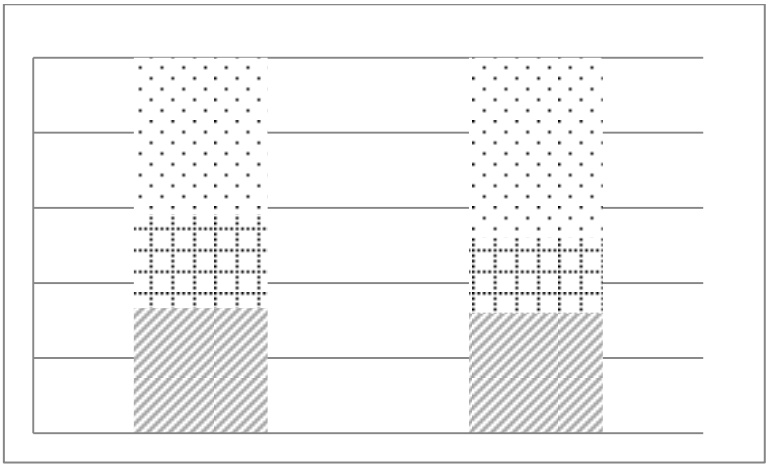

Figure 5:3 Vehicle Categories

A correlation between the driver category and the reaction pattern is found: (i) OA drivers tend to have the concave triangle pattern, and OT drivers the convex pattern; (ii) ON drivers are equally likely to have any of the three patterns in period 1 but prefer to concave triangle pattern in period 2; see statistics in Figure 5:4. Figure 5:5 illustrates some common and typical examples for the evolution of $\eta_i(t)$, which account for roughly 90%

of the sample. Result (i) is intuitive. OA drivers maintain a small spacing before the oscillation, and therefore, they have little room to further decrease the spacing in non-equilibrium. Consequently, they tend to increase the spacing to be safer during the oscillations. In contrast, OT drivers preserve more than enough room and may feel less pressure to react. In other words, OA drivers are less aggressive during oscillations and OT drivers are less timid. Result (ii), however, is surprising. Two reasons may contribute to this result: (1) Oscillations in period 1 spontaneously arose in the study site (at distance 400m, see Figure 4:1(a)) while originated from downstream in period 2 (see (b) on this figure); (2) in period 1 traffic was moderately congested with speeds of about 30mph before the oscillations and recovered to 40~50mph afterwards; while it was dense in period 2 with 20~30mph driving speed before the oscillations and below 30mph after. This can be seen in Figure 5:6. In dense traffic, the equilibrium spacing is much smaller, which forces ON drivers to adopt a relatively safe reaction pattern, in this case the concave triangle pattern. Under moderate congestion there is no particular reason to react in either way. Since the sample size is not large enough for hypothesis tests (e.g., chi-square test), it is unclear whether the difference of reaction pattern preference is statistically significant. This problem will be fully investigated in chapter 6 when a larger sample is available.

Figure 5:7 shows the histogram of all variables for the whole sample because no significant difference was observed between the distributions from periods 1 and 2. Table 5:1 shows the mean and coefficient of variation for all model parameters. The sample has been

broken down according to the reaction patterns to avoid spurious results. In both periods, the coefficients of variation for the η's are around 20 -- 35%, which indicates mild variability. A very high variability is observed in the case of the ε_i^0 and ε_i^1, which may be due to the large variation in the duration of the oscillations

(a)

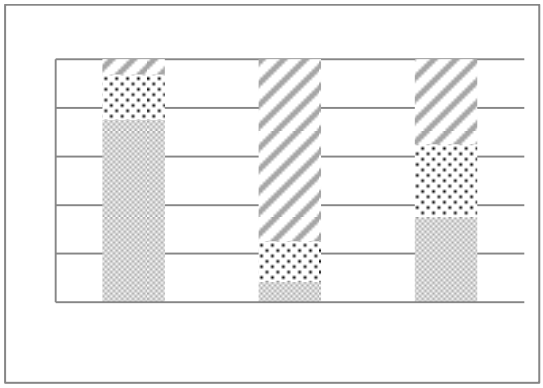

(b)

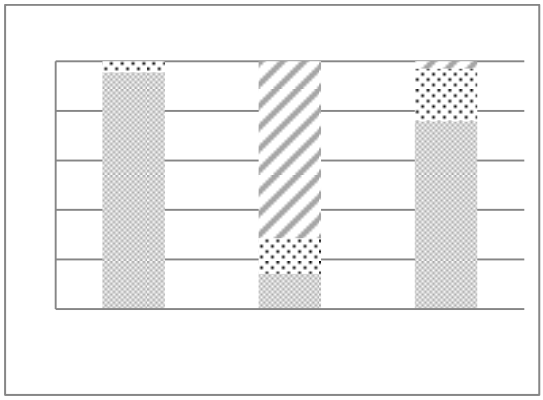

Figure 5:4 Behavior Pattern Statistics

(a) period 1; (b) period 2.

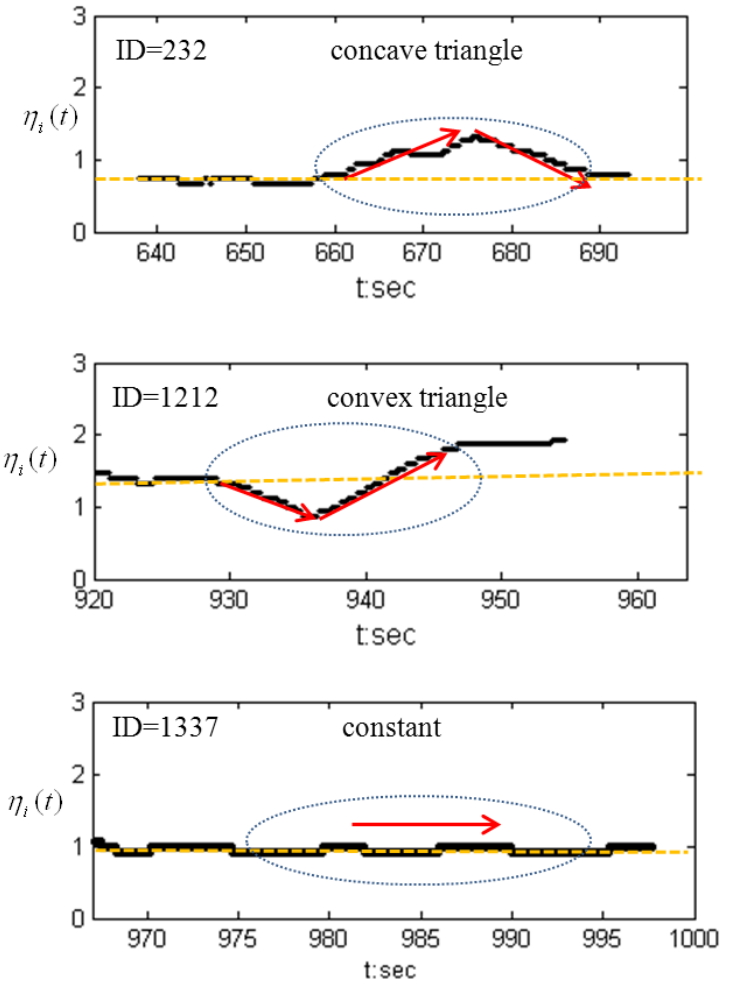

Figure 5:5 Examples of Behavior Patterns during Oscillations (circled in dashed line)

Top: originally aggressive driver; middle: originally timid driver; bottom:

originally Newell driver.

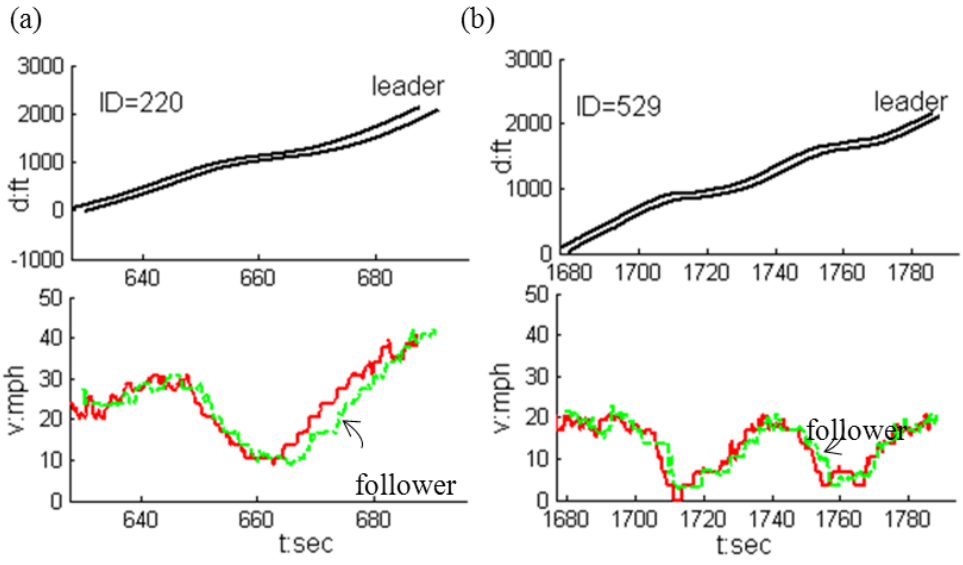

Figure 5:6 Examples of Trajectories in Different Periods
(a) Period 1; (b) Period 2.

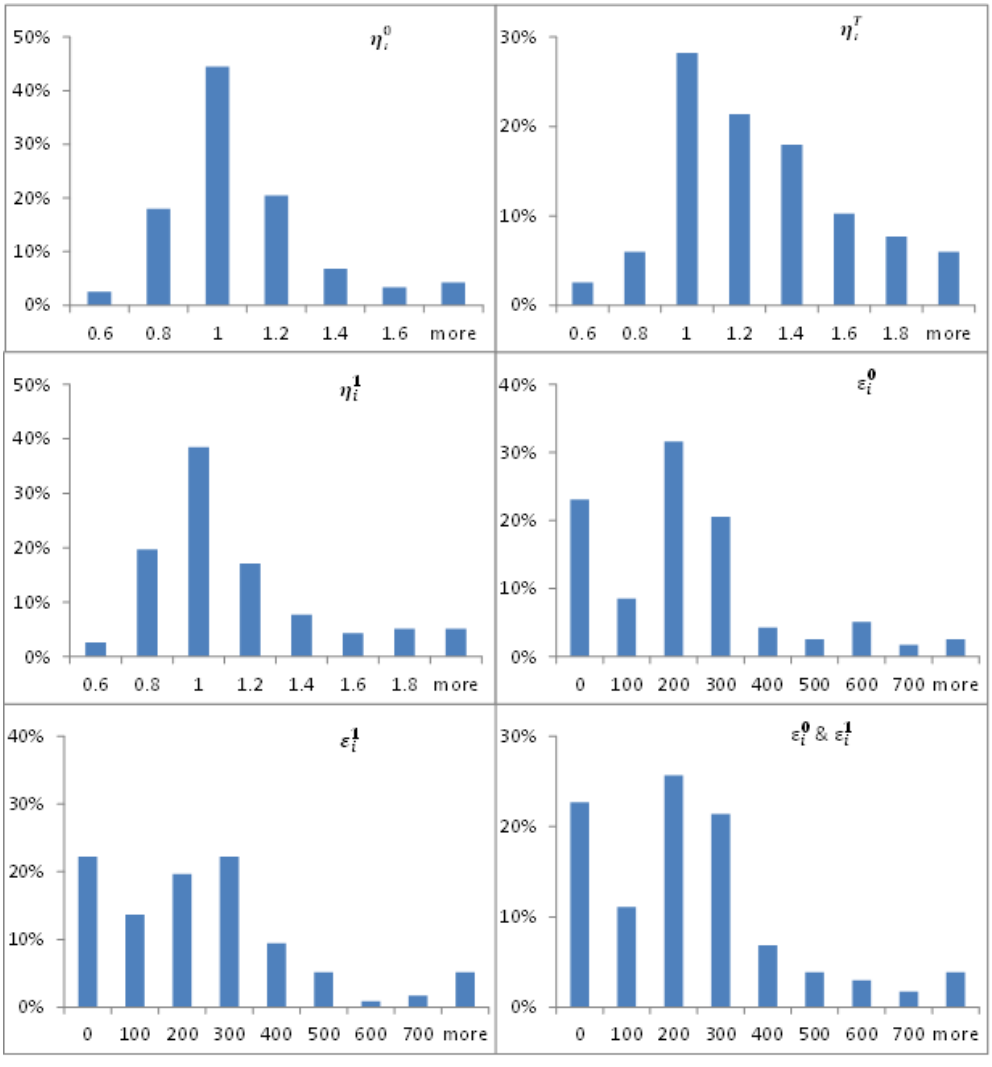

Figure 5:7 Histogram of All Variables

Table 5:1 Descriptive Statistics

		Period 1						Period 2					
Sample size		η^0	η^T	η^1	$\lvert\varepsilon^0\rvert$ veh/h	$\lvert\varepsilon^1\rvert$ veh/h	Sample size	η^0	η^T	η^1	$\lvert\varepsilon^0\rvert$ veh/h	$\lvert\varepsilon^1\rvert$ veh/h
Convex (16)	mean	1.14	0.88	1.46	215	272	Convex (11)	1.34	0.84	1.28	277	177
	cv	0.18	0.25	0.29	0.79	0.63		0.24	0.39	0.24	0.68	0.62
Concave (17)	mean	0.87	1.34	0.96	255	323	Concave (46)	0.90	1.39	0.91	198	201
	cv	0.25	0.24	0.29	0.48	0.60		0.16	0.26	0.19	0.72	0.76
Constant (11)	mean	0.99	0.99	0.99	0	0	Constant (10)	1.08	1.08	1.08	0	0
	cv	0.22	0.22	0.22	0.00	0.00		0.27	0.27	0.27	0	0
All(44)	mean	1.00	1.09	1.15	177	224	All (67)	1.00	1.25	1.00	184	170
	cv	0.24	0.31	0.35	0.93	0.91		0.26	0.32	0.26	0.87	0.89

*cv = coefficient of variation.

Table 5:2 Variable Correlation for Period 1

(t-statistics from least squares regression in lower diagonal and p-value from Wilcoxon signed-rank test in upper right, grey cells indicate significance at 5% significance level)

	Convex (sample size: 16)					**Concave (sample size: 17)**					**Combined (sample size: 33)**				
	η^0	η^T	η^1	$\lvert\varepsilon^0\rvert$	$\lvert\varepsilon^1\rvert$	η^0	η^T	η^1	$\lvert\varepsilon^0\rvert$	$\lvert\varepsilon^1\rvert$	η^0	η^T	η^1	$\lvert\varepsilon^0\rvert$	$\lvert\varepsilon^1\rvert$
η^0		0.002	0.004				0.002	0.281				0.174	0.002		
η^T	4.29		0.002			5.51		0.002			0.81		0.395		
η^1	3.90	2.71				4.84	3.58				7.77	-0.17			
$\lvert\varepsilon^0\rvert$	0.43	-1.93	-0.11		0.834	0.61	2.10	0.62		0.563	0.18	0.65	-0.32		0.597
$\lvert\varepsilon^1\rvert$	0.86	0.81	3.75	0.00		0.42	0.39	-0.44	0.66		0.31	1.12	1.04	0.53	

Table 5:3 Variable Correlation for Period 2

(t-statistics from least squares regression in lower diagonal and p-value from Wilcoxon signed-rank test in upper right, grey cells indicate significance at 5% significance level)

	Convex (sample size: 11)					**Concave (sample size: 46)**					**Combined (sample size: 57)**				
	η^0	η^T	η^1	$\lvert\varepsilon^0\rvert$	$\lvert\varepsilon^1\rvert$	η^0	η^T	η^1	$\lvert\varepsilon^0\rvert$	$\lvert\varepsilon^1\rvert$	η^0	η^T	η^1	$\lvert\varepsilon^0\rvert$	$\lvert\varepsilon^1\rvert$
η^0		0.006	0.584				0.000	0.943				0.000	0.728		
η^T	2.91		0.006			5.86		0.000			0.22		0.000		
η^1	5.25	2.66				7.16	5.57				13.07	0.89			
$\lvert\varepsilon^0\rvert$	0.61	-0.11	1.02		0.053	2.42	4.78	3.69		0.620	2.59	2.10	3.79		0.546
$\lvert\varepsilon^1\rvert$	-0.63	-1.09	0.04	2.41		2.40	3.20	1.60	3.21		0.53	2.54	0.70	3.55	

5.2.2 Hypothesis Test on Model Parameters

This section tests the correlation between model variables; i.e., all the five parameters are considered as random variables and the correlation of each pair is examined. Paired t-test is performed to see whether or not variables are significantly different. These are important because (i) the correlation will determine whether it is appropriate to assume independent distributions for the parameters in the model, and (ii) the significance of difference of paired differences will help to decide if parameters can be combined.

Table 5:2 and Table 5:3 show the t-statistic from least squares regression for all parameter combinations. The tables also show the p-values from the Wilcoxon signed-rank test (Kvam and Vidakovic, 2007), a non-parametric statistical hypothesis test used to compare two repeated measurements on a single sample to assess whether their population means differ. Notice that the sample size may be not large enough to estimate the distribution of a parameter. Therefore, non-parametric hypothesis tests were conducted, which did not require information about the variable distribution as the input. The main conclusions, at the 95% confidence level, are that in the two periods for both patterns (i)η_i^0, η_i^T, and η_i^1 are all correlated, and (ii) $\varepsilon_i^0$and ε_i^1 are not significantly different. Result (i) implies that all pairs among parameters η_i^0, η_i^T, and η_i^1, are correlated. Additionally, differences exist between samples from the two periods: (iii) ε_i^0 and ε_i^1 have no (or very week) correlation with each other and with the η's except for the concave pattern sample in period 2; and (iv) η_i^1 and η_i^0 are not significantly different in period 2 but the difference is significant for convex pattern sample and the combined sample in period 1.

The correlation among the model parameters was expected. It indicates that drivers behave differently and that these differences are consistent across drivers. Notice that the correlation may be obscured if samples of the two patterns are combined. For

example, the correlation between η_i^T and η_i^0 is significant for the separate samples, but not for the combined sample. Also expected was that $\varepsilon_i^0 = \varepsilon_i^1$ since there is no strong reason to believe that deviations to and from equilibrium should happen at different rates. But the finding about the distribution of η_i^1 and η_i^0 comes to a surprise. The result that $\eta_i^1 = \eta_i^0$ seems intuitive, because it implies that drivers stick to the same equilibrium branch before and after traffic oscillations, i.e., no change in drivers' behavior characteristics. However, that $\eta_i^1 \neq \eta_i^0$ indicates significant behavior changes imposed by traffic oscillations. Three potential explanations can be offered: (i) trajectories in period 1 are too short to capture the full recovery. Note that drivers experience long acceleration time after the oscillations in period 1 because the traffic state there is significantly less congested than before the oscillations; see Figure 5:6 (a). (ii) Lack of experience. It is found that in period 2 drivers experienced at least two consecutive oscillations; see Figure 5:6 (b). It is possible that drivers who experience oscillations for the first time, especially those react aggressively to oscillations (i.e., convex pattern), become more conservative after the oscillation passes; see the higher value of η_i^1 than η_i^0 for samples of period 1 in Table 5:2. As drivers gain more experiences, they react promptly and are able to recover to the original equilibrium branch. (iii) Oscillations in period 1 arise spontaneously while they are well developed in period 2, which allows drivers to anticipate the deceleration-acceleration process in the oscillation cycles and therefore maintain a consistent equilibrium branch. Nevertheless, it seems that $\eta_i^1 = \eta_i^0$ is more common. Otherwise, it means that every time drivers experience a traffic oscillation, they change their preferred equilibrium branches completely, in this sense that they come from a different distribution. A change in the distribution may be caused by extreme environmental changes, e.g. rain or sharp changes in geometric design, which are not observed in our case.

5.3 Simulation

In this section, simulation is conducted to evaluate the performance of the asymmetric behavior model and to compare its predictions with the L-L model. A simple model to capture the rubbernecking phenomenon is introduced in Section 5.3.1 and the corresponding simulation results are analyzed in Section 5.3.2. The comparison with the original L-L model follows in the end.

5.3.1 The Rubbernecking Model

Recall from Section 4.1 that there is strong indication that rubbernecking caused by the clean-up work on the median of US-101 may cause the oscillations in Figure 4:1 (a). In support of this conjecture, simulation was conducted for 32 minutes on a 1.25km flat one-lane roadway with a triangular fundamental diagram where u = 120 km/h, κ= 150 veh/km and w = 16 km/h. The rubbernecking zone is located at x $\in [1,1.05]$ km (see the red bar in Figure 5:8 (a)). When drivers enter this zone, they have a probability$r$ to rubberneck, which will cause their speed to drop by a factor of $(1-p)$. Rubbernecking will occur at most once in this zone, if any. The roadway is empty at $t = 0$ and the inflow demand is set to 80% of capacity. Drivers are assumed to travel at free-flow speed when there is no congestion, and follow the asymmetric behavioral model when traffic is congested. Several combinations of the parameters a_m, r, and p are tested in the simulations.

According to the previous section, in this simulation the asymmetric behavior model is reduced to three parameters per driver $[\eta_i^0, \eta_i^T, \varepsilon_i]$, in which $\varepsilon_i = \varepsilon_i^0 = \varepsilon_i^1$ and $\eta_i^1 = \eta_i^0$. Notice that some of the parameters are correlated and one should use their joint density function to generate the model parameters. However, as noted earlier, the sample size in this study may be not sufficient. Therefore, the sample enumeration method (Ben-Akiva and Lerman, 1985) is used. Namely, each trajectory pair measured yields a set of $[\eta_i^0, \eta_i^T, \varepsilon_i]$ from the original measurement of $[\eta_i^0, \eta_i^1, \eta_i^T, \varepsilon_i^0, \varepsilon_i^1]$, in which η_i^1 is dropped

and the value of ε_i is set to be the average of ε_i^0 and ε_i^1. In this way, the correlation, if any, among the three parameters of a parameter set $[\eta_i^0, \eta_i^T, \varepsilon_i]$ is preserved. The measurement of 111 pairs forms a parameter matrix. Each time a vehicle is generated, he/she will be assigned with a parameter set $[\eta_i^0, \eta_i^T, \varepsilon_i]$ randomly selected from the matrix. Notice that the matrix is a representation of the real measurement and no estimation of parameter distribution is required.

5.3.2 Results

The vehicle trajectories from a few simulation runs are shown in Figure 5:8 (b-d). Figure 5:8 (b) and (c) suggest that the asymmetric behavior model has produced traffic oscillations that are very consistent with the empirical oscillations in Figure 4:1 (a-b). Particularly, the oscillations produced have similar period (~3min), and they also exhibit precursor areas (circled by red dashed curves) that lead to fully grown oscillations, which are obvious in the empirical data. These two figures also illustrate how the period of oscillation is positively correlated with *p*. Notice that in both cases the precursor region is well reproduced and the amplitude grows similarly as in Figure 4:1 1(a). The detailed view in Figure 5:8 (d) make apparent the large white voids that appear in the traffic stream. Most of these voids are caused by OT drivers that prefer to maintain larger spacing.

Figure 5:9 shows the relationship between the period of oscillation and the parameters a_m, *r*, and *p*, predicted by the model. The period was measured using Fourier spectrum analysis (Li et al., 2009) to the speed time series collected at location $x = 500$ m. Each point in the figure represents the average for 5 simulation runs. Notice that the effect of maximum acceleration on the period is not very significant when the rubbernecker proportion is greater than 4%. Also notice how *r* is negatively correlated with the period and how *p* is positively correlated with it. This suggests that both the rubbernecker proportion and the speed reduction imposed by rubbernecking (denoted by

1-*p*) have negative impacts. Particularly, the relationship between period and *r* appear to be convex and rapidly approaching a stable value of about 2-3 min. The negative impact of *r* seems intuitive: the more rubberneckers, the more often (i.e., smaller interval) traffic oscillations may arise. Notice, however, that the period is not necessarily determined by the arrival of rubberneckers. The relationships are more complex. From Figure 5:8 (b) and (c) one can see that not every rubbernecker (denoted by a green trajectory) will lead to an oscillation. For example, in the precursor area labeled in Figure 5:8 (b) there are several rubberneckers that all contribute to the ensuing oscillation. More discussions on how the period of oscillation is determined will be provided in chapter 7.

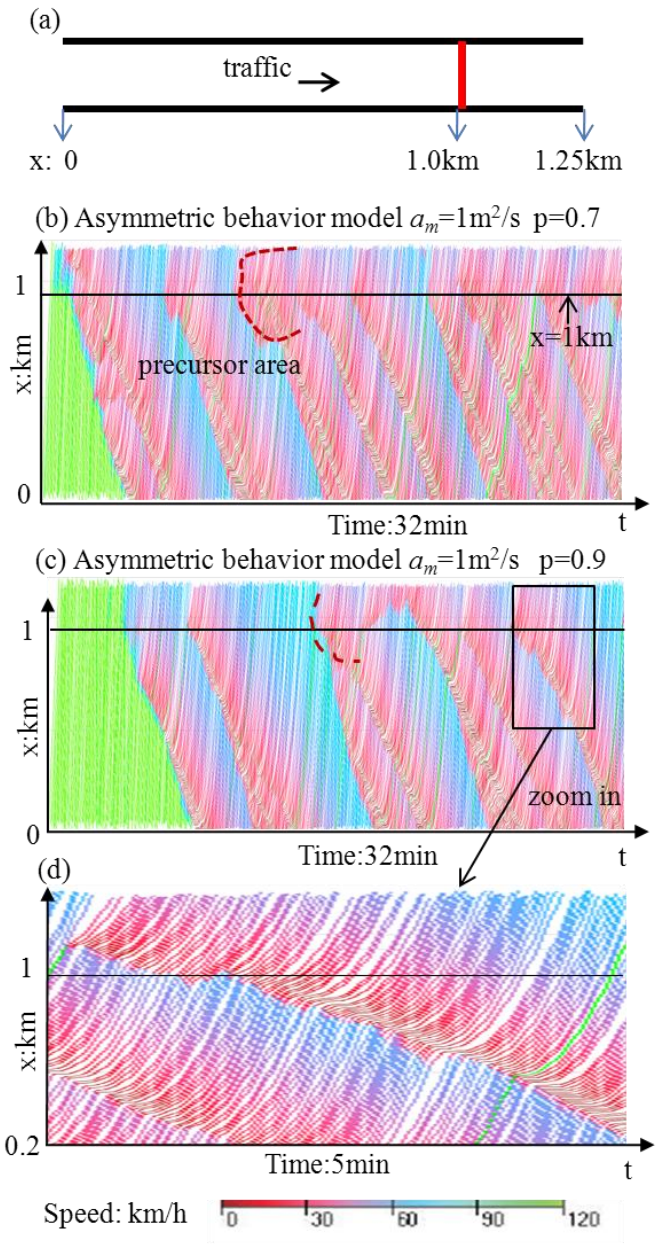

Figure 5:8 Trajectories from Simulations Using Asymmetric Behavioral Model

(a) sketch of the highway segment in simulations; (b-d) trajectories from simulations with $r = 4\%$ (green trajectories represent rubberneckers).

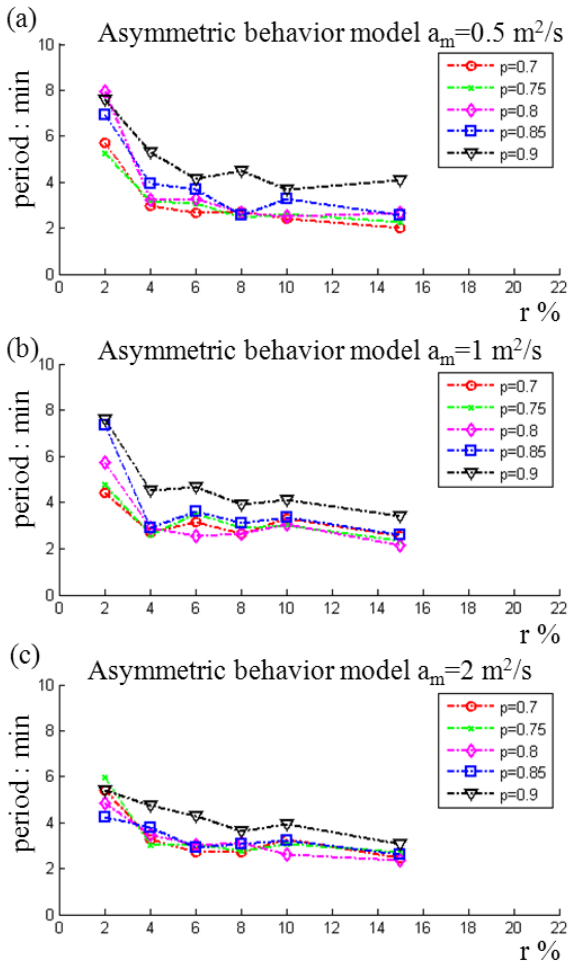

Figure 5:9 Oscillation Period vs. Rubbernecking Parameters in the Asymmetric Behavior Model.

5.3.3 Model Comparison

The same rubbernecking experiment was performed using the original L-L model. The parameters used in the L-L model correspond to sample averages; i.e., ε is set to be the mean of all ε_i, and α equals to the average of $|\eta_i^T - \eta_i^0|$. We have obtained ε=215veh/h, α=0.27. The proportion of different driver categories is taken from the whole sample: 33% of OA drivers, 22% of OT drivers, and 45% of ON drivers. Of course, η_i^0 and η_i^1 are set to be 1 as assumed in the model.

Figure 5:10 and Figure 5:11 present examples of trajectories from simulations and results of analysis, respectively. It is found that (1) the original L-L model has produced similar magnitude of period and the negative (positive) effects of *r* (*p*) on oscillation period. However, (2) there are more large white voids in trajectories from asymmetric behavior model as shown by Figure 5:8(c) and Figure 5:10 (c). Result (1) appears reasonable because the original L-L model can be considered as a representation of the *average* performance of drivers, which may result in some general features. Result (2) is probably caused by the different assumption of η_i^0-value in the two models. Recall that the original L-L model assumes that $\eta_i^0 = \eta_i^1 = 1$. Consequently, the white voids after traffic oscillations are due to the limited acceleration capability of drivers. By contrast, in the asymmetric behavior model, white voids can be created not only by limited acceleration capability but also by OT drivers (i.e., large η_i^0-value) because the model allows a wide range of $\eta_i^0(\eta_i^1)$.

The performance of the two models suggests that the asymmetric behavior model should be used in order to capture the important features of traffic oscillations and to understand why and how the features are generated.

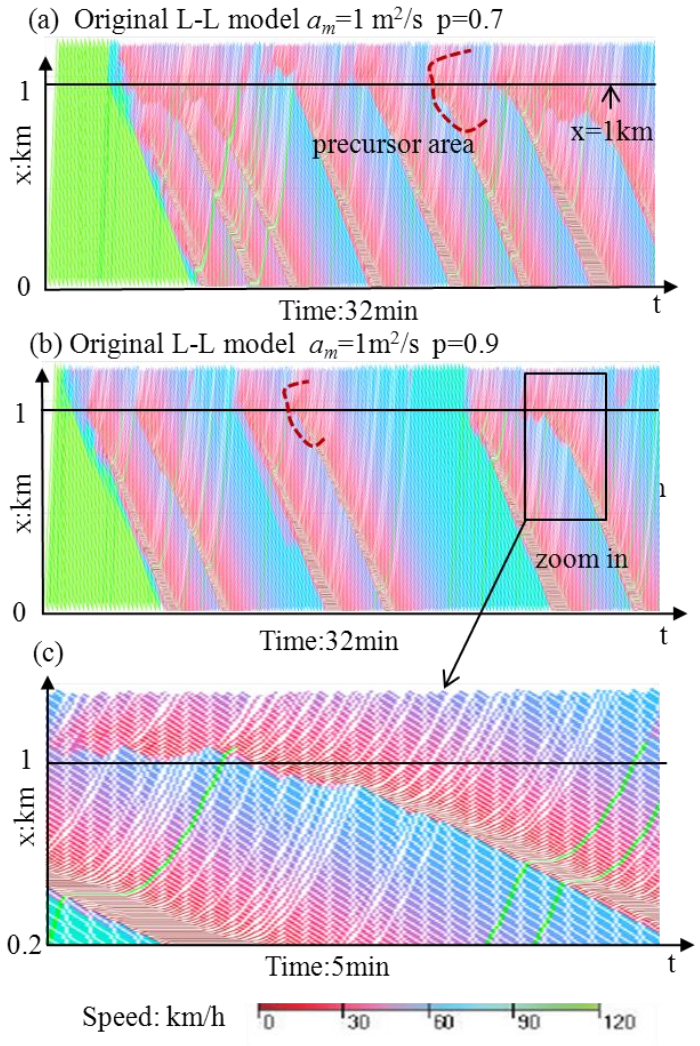

Figure 5:10 Trajectories from Simulations Using Original L-L Model

(r=4%, green trajectories represent rubberneckers)

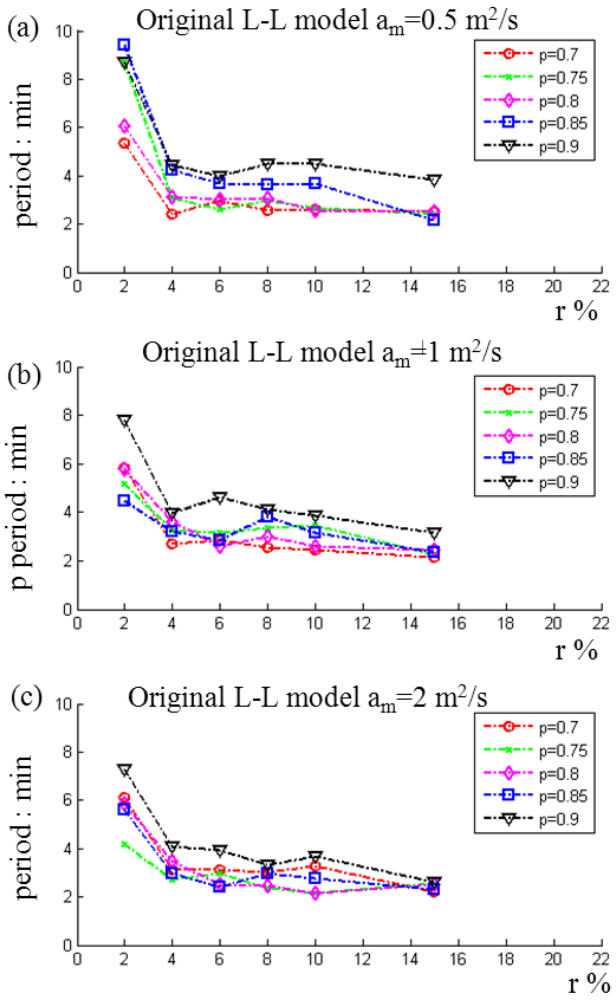

Figure 5:11 Oscillation Period vs. Rubbernecking Parameters in L-L model

5.4 Discussions

Using empirical trajectory data, Chapters 4 and 5 have unveiled the complete dynamic behavior profile of drivers experiencing traffic oscillations. This behavior can be described by the asymmetric behavior model with five parameters $[\eta_i^0, \eta_i^T, \ \eta_i^1, \varepsilon_i^0, \varepsilon_i^1]$ per driver, which could be drawn from a joint distribution function. It is found that drivers exhibit different characteristics in congestion, reflected by their unique equilibrium branches, and that these characteristics are correlated with their reaction to traffic oscillations. To some extent, drivers' characteristics in equilibrium determine their

response to traffic oscillations; i.e., it is the root of driver's behavior throughout traffic oscillations. In this sense, the driver heterogeneity causes traffic oscillation to form and propagate. Because the heterogeneity is inherent to drivers, the formation and propagation of traffic oscillations seem inevitable as long as triggering factors exist. This implies that triggering factors would be a primary concern in the control and management of traffic oscillations.

The statistical analysis and simulation results revealed that the model can be further reduced to three parameters per driver $[\eta_i^0, \eta_i^T, \varepsilon_i]$ if general macroscopic features are of interest. This is promising because it suggests that the simple asymmetric behavior model can serve as the basis of studies in traffic oscillations such as investigation of the formation and propagation mechanism and design of management policies that will help to reduce or mitigate the negative impacts of traffic oscillations. Of course, one should be cautious in transferring our results to different driver population, because the model parameters are correlated and may vary with driver populations. In applications, one may use the sample enumeration to generate the parameters as in this study if a large sample is not available or assume a joint distribution estimated from a large sample size.

Two controversial findings from the statistical analysis call for further investigation: (1) $\eta_i^1 \neq \eta_i^0$ in samples from period 1, and (2) the preferred reaction pattern of ON drivers differ s in period 1 and 2. Finding (1) is probably due to (a) the limited spatial extent of trajectories, or (b) lack of experience in traffic oscillations, or (c) different degree of development of oscillations. Finding (2) may be because of (c) or different congestion level. If the reasons (b) & (c) hold, they imply that traffic oscillations can significantly change driver behavior and one expects to see the changes of the distribution of η_i^0 occur quite often. These problems will be extensively explored in chapter 6.

The simulations seem to confirm the hypothesis that rubbernecking is the cause of the spontaneously formed oscillations observed on the study site. In particular,

simulation results show well-defined relationships between the percentages of rubberneckers (r), the speed reduction ($1-p$), and oscillation period. It is interesting to note that these relationships tend to approach a common lower bound of about 2-3 min, which is the same value as in the empirical data in Figure 4:1 (a-b), and as in the upgrade simulation experiments in Laval and Leclercq (Laval and Leclercq, 2010). This might be an indication that the minimum oscillation period that a bottleneck can create is within that range.

The original L-L model captures one ideal case of driver behavior but is far from sufficient to cover the general patterns unveiled in this study. Simulation results indicate that it is able to produce the general macroscopic features of oscillations, but it may disregard some important microscopic features such as the white voids. The L-L model, which is more parsimonious, may be satisfying for macroscopic interests. However, for microscopic studies such as individual driver behavior and impact evaluation, the asymmetric behavioral model should be used. In particular, to quantify the impacts of traffic oscillations on safety risk, fuel consumption, and greenhouse emission, the asymmetric behavioral model should be applied.

CHAPTER 6 HYSTERESIS IN TRAFFIC OSCILLATIONS

In this chapter, the asymmetric behavioral model is applied to study the phenomenon of traffic hysteresis that is often associated with traffic oscillations. The objective is to investigate this phenomenon from the behavioral perspective based on empirical data and uncover why it occurs in traffic oscillations.

6.1 Measurement

For this study on traffic hysteresis, COMPLETE traffic oscillations are selected; i.e., traffic oscillations that arise spontaneously and fully develop as they propagate upstream. This is because the generation of traffic hysteresis may vary across different development stages of an oscillation. If that exists, the difference can be captured through a complete traffic oscillation. Of course, oscillations that are short-lived are not included. These selection criteria are applied to the trajectory data described in Section 4.1 and five traffic oscillations that occurred on lane 1 from 7:50 a.m. to 8:05 a.m. are selected (shown in Figure 6:1). Measurements are conducted on leader-follower trajectory pairs. Trajectories in the vicinity of lane-changing maneuvers are excluded to avoid the compound effects of car-following and lane-changing.

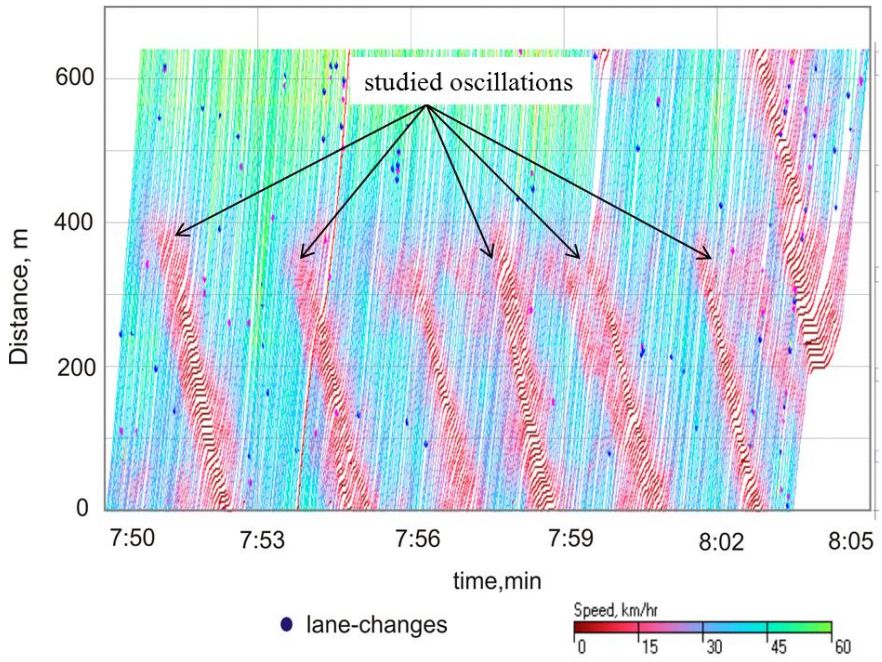

Figure 6:1 Trajectory Data (US 101 lane 1)

6.1.1 Measurement of Driver Behavior

Driver behavior throughout traffic oscillations is represented by the asymmetric behavioral model proposed in Section 4.3, and the measurement for model parameters is described by Section 4.2. Recall that they key measurement is the measurement of $\eta_i(t)$, which is boiled down to measure $\tau_i(t)$, and that $\tau_i(t)$ depends on the wave speed w. To capture the potential difference of wave speed across drivers, in this measurement the wave speed w is allowed to change within a range of -5ft/s~20ft/s as reported in the literature (Chen et al., 2012; Durent et al., 2011; Laval and Leclercq, 2010). The optimal w selected is the value that minimizes the variance of the $\tau_i(t)$ time series; i.e., that fits Newell's car-following model best. As a result, the wave speed used in the measurement is fixed for a given driver but it varies across drivers. With a given wave speed, the trip time $\tau_i(t)$ is measured along the follower's trajectory and that yields a time series of $\tau_i(t)$, which the same as the illustration in Figure 4:2. Similar to the measurement in Section 4.2, the equilibrium value τ is set to be the mean of $\tau_i(t)$ before oscillations from all trajectories sampled. .

The reaction patterns used in this study are: concave triangle, convex triangle, non-decreasing, and constant. Notice that the non-decreasing pattern is added to capture the case shown in Figure 6:2 (a-b), where $\eta_i(t)$ increases until reaching η_i^T but it has no obvious decrease thereafter; i.e., $\eta_i^1 <> \eta_i^T$. In most of the non-decreasing cases observed, $\eta_i(t)$ remains stable after reaching η_i^T as in the case of Figure 6:2(a), which appears similar to the concave pattern. However, later analyses find that it is necessary to distinguish these two patterns when explaining the formation of traffic hysteresis. This will be revisited later.

Similarly to chapter 5, the threshold is set to be $\eta_i^0 < 0.9$ for OA drivers, $\eta_i^0 > 1.1$ for OT drivers and $0.9 \leq \eta_i^0 \leq 1.1$ for ON drivers.

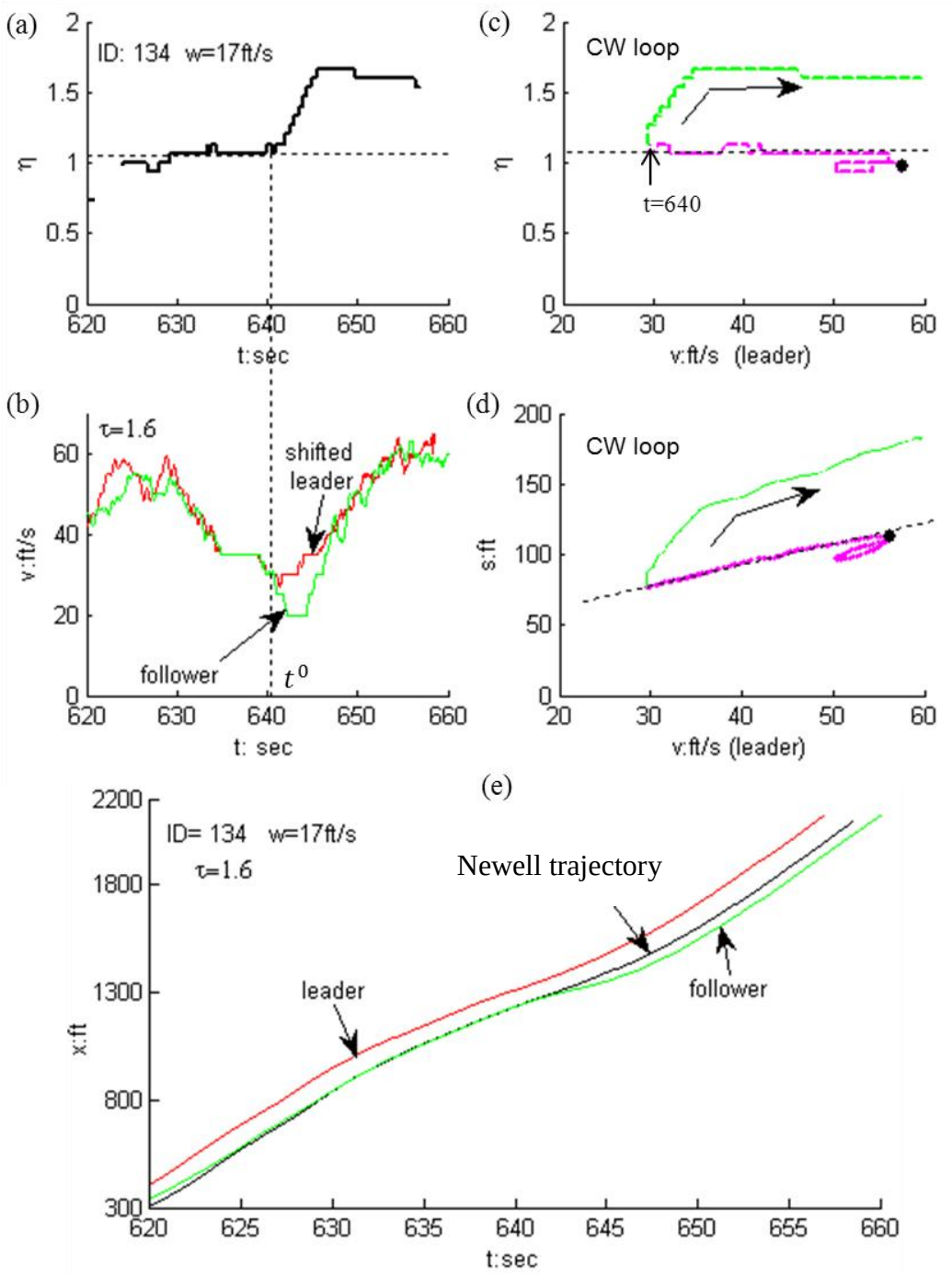

Figure 6:2 Non-decreasing Pattern

(a) $\eta_i(t)$ plot for the non-decreasing pattern; (b) corresponding speed plot throughout an oscillation (leader's trajectory is shifted to the right by τ) ; (c) η_i versus speed plot; (d) spacing versus speed; (e) trajectories (the Newell trajectory in black is obtained by shifting leader's trajectory by $(\tau, -\tau w)$).

6.1.2 Measurement of Traffic Hysteresis

Traffic hysteresis is analyzed on the v − η plane so that three key elements, driver category, reaction pattern, and traffic hysteresis can be captured simultaneously through a single variable, $\eta_i(t)$. Note that since $\eta_i(t)$ is the ratio of the actual steady spacing to the equilibrium spacing, the hysteresis orientation in the $v - \eta$ plot is the same as in the speed-density ($v - s$) plot, and the flow-density plot; see Figure 6:2 (c-d). Five hysteresis patterns are defined according to the orientation of the $v - \eta$ curves during an oscillation cycle (consisting of a deceleration and an acceleration process): clock-wise (CW) loop, counter clock-wise (CCW) loop, overlap, straight line, and multiple loops. This is illustrated in Figure 6:3 where the red dots denote the beginning of the $v - \eta$ plots and the arrows show the orientation. All the cases except for the overlap case are self-explanatory. In the overlap case, the $v - \eta$ relationship deviates from Newell's prediction but is identical in the deceleration and acceleration processes. Although hysteresis is not significant in the overlap and straight line cases, they are included to form a more comprehensive description. The CW and CCW loops in this study correspond to the hysteresis and reverse hysteresis loops respectively in the literature (Laval, 2010).

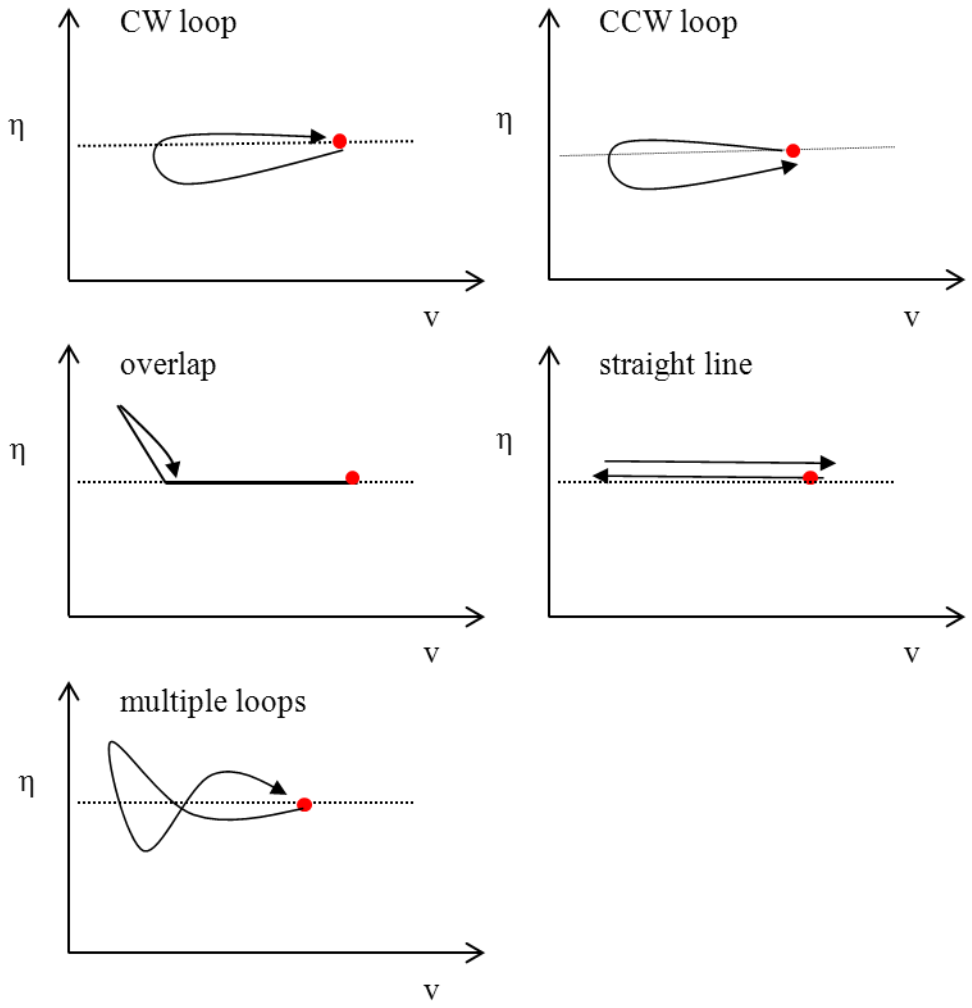

Figure 6:3 Hysteresis Cases

(red dot: beginning of hysteresis loop; dash lines are from Newell's car-following model)

6.1.3 Development Stage of Traffic Oscillations

When studying driver behavior, an oscillation is broken into two stages to capture the potential change of driver behavior and traffic hysteresis in different development stages of an oscillation.

In the growth stage, the minimum speed of drivers during an oscillation cycle *decreases* as the oscillation propagates upstream.

In the fully-developed stage the minimum speed of drivers during an oscillation cycle *stops decreasing*.

Figure 6:4 provides an illustration for the stage setting. The red solid line approximates the trend of minimum speed across vehicles in an oscillation. As one can see, the minimum speed tends to decrease until it becomes close to zero and then remains stable. Hence, the black point denotes the threshold and vehicles before (after) it fall into the growth (fully-developed) stage.

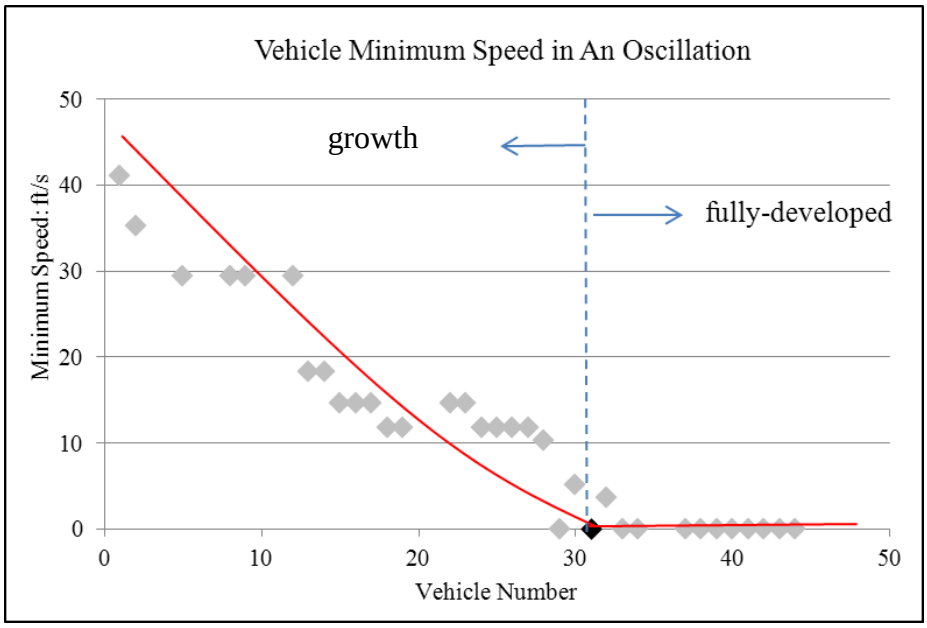

Figure 6:4 Minimum Speed of Vehicles along A Traffic Oscillation
(the red solid line approximates the trend

6.2 Statistical Results

This section presents statistical results of the three key elements, hysteresis pattern, driver category, and reaction pattern. Similar to Section 5.2, the chi-square test for homogeneity of proportions (Greenwood and Nikulin, 1996) is used to assess whether the distribution of a categorical variable from different populations are significantly different, at a 95% confidence level.

A total of 109 and 126 trajectory pairs are measured for the growth and fully-developed stages, respectively. Major remarks from the statistical results are summarized as follows:

R1: Drivers in the two stages come from the same distribution. The composition of driver category is not significantly different in the two stages (p-value =0.32).

R2: About 60~75% of drivers show CW or CCW loops in the two stages (see Figure 6:5), but the distribution of hysteresis types in the two stages differs significantly (p-value <0.001). CW loops are prevalent in the growth stage, while the proportions of CW and CCW loops are comparable in the fully-developed stage. The frequency of hysteresis types is shown in Table 1 in the Appendix A.2.

R3: Changes in reaction pattern preference between growth and fully-developed stages; see Figure 6:6 and the frequency distribution in Table 2a and Table 2b in Appendix A.2:

R3a: OA drivers have significantly different reaction pattern preference (p-value <0.001). In the growth stage, they tend to adopt both concave triangle and non-decreasing patterns but predominantly adopt the concave triangle pattern in the fully-developed stage.

R3b: ON drivers also have significantly different preferences (p-value =0.033). They have comparable probabilities to adopt any of the four reaction patterns in the growth stage but a marked preference for the concave triangle pattern in the fully-developed stage.

R3c: The preference of OT drivers has no significant change (p-value =0.972) in the two stages. They consistently prefer the convex triangle pattern.

R3d: For all driver categories combined, the distribution of reaction pattern is significantly different.

R3e: The distribution of reaction pattern for any two driver categories differs significantly; i.e., the number of driver category cannot be further reduced.

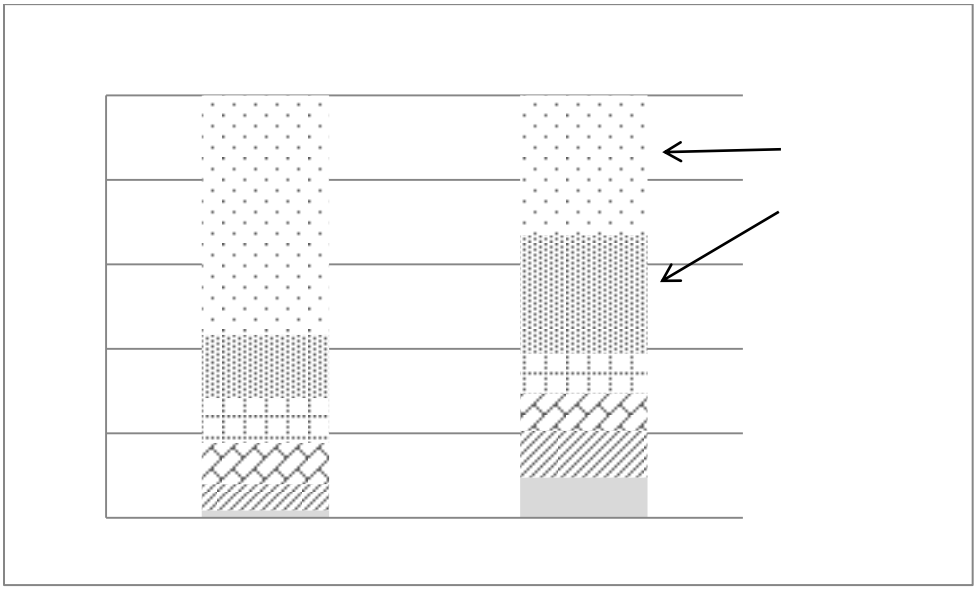

Figure 6:5 Composition Of Hysteresis Patterns

Remark R1 is intuitive because driver category is a driver characteristic and one does not expect it to vary with the development stage of traffic oscillations. This result eliminates potential variance caused by different driver samples in this study. In R2, the total proportion of CW and CCW loops is consistent with results of Ahn, et al. (Ahn et al., 2011)and Laval (Laval, 2010). However, the significant change of hysteresis type distribution across the two stages is surprising. Given R1, it is likely that this change is related to results in R3, which suggests that driver behavior may vary with the development stage of an oscillation. Examination on the relationship between the

composition of hysteresis types (CW and CCW loop), driver category, and reaction pattern indicates that statistical analysis is not sufficient to unveil the complex connections. Therefore, more thorough investigation on vehicle trajectories is conducted in the next section to explore the relationship.

(a)

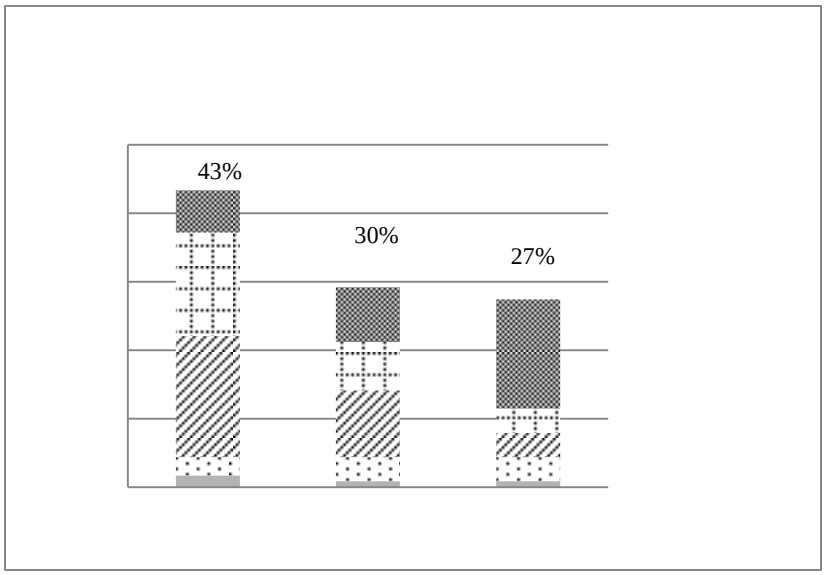

(b)

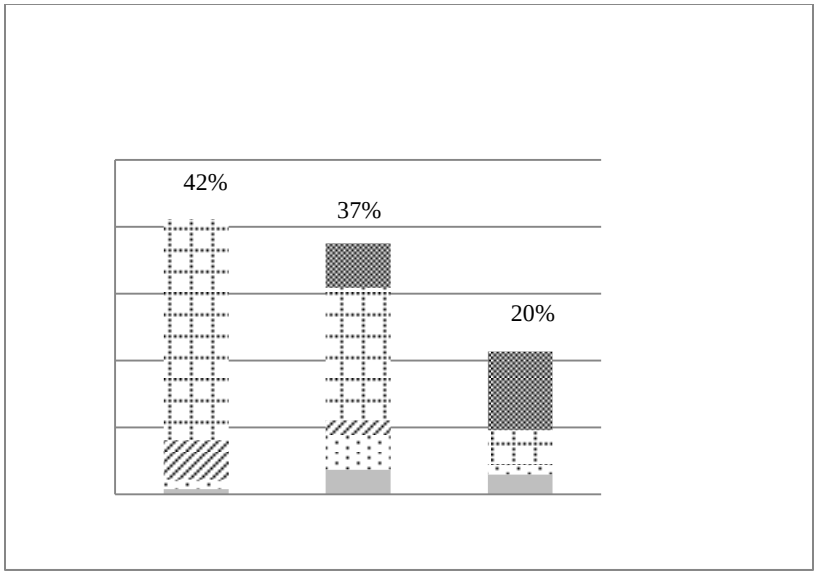

Figure 6:6 Driver Category vs. Reaction Pattern

(a) Growth stage; (b) Fully-developed stage.

6.3 Analyses

This section studies the formation mechanism of traffic hysteresis with the objective to explain the statistical results described in Section 6.2. First of all, Section 6.3.1 analyzes the potential cases that traffic hysteresis can be generated, and then Section 6.3.2 shows the major mechanisms suggested by the empirical results. Afterwards, Section 6.3.3 provides explanations for the distribution change of traffic hysteresis types in the growth and fully-developed stages.

6.3.1 Potential Traffic Hysteresis

It is found that the different reaction patterns are correlated with the different types of hysteresis loops. Illustrations of some common cases are shown in Figure 6:7 in which the red dots denote the starting point and the arrows show the orientation of $\eta(t)$. For a concave triangle pattern, if the increase-decrease change of $\eta(t)$ occurs and is completed within the deceleration process, a CCW loop is generated (see case "1" in Figure 6:7 (a)); if the change starts and ends within the acceleration process, the loop is CW; see "2" in the figure. If the change spreads across the whole cycle, multiple loops are possible (see case "3"). Apparently, if the changes in $\eta(t)$ are symmetric on the $v-\eta$ plane, the trajectory pair causes the overlap hysteresis type (see case "1" in Figure 6:7 (d)). Similar analysis applies to the convex triangle pattern (see Figure 6:7 (b) and case "2" in Figure 6:7 (d)). For the non-decreasing pattern, because $\eta(t)$ is non-decreasing in an oscillation cycle as speed decreases and increases, the acceleration branch of $v-\eta$ plot will always be above the deceleration branch, which consequently determines the CW orientation (see Figure 6:7 (c)). Of course, the hysteresis in this case is not a loop in a strict sense because the curve does not close. Since the primary concern of this study is the orientation, it is still referred to as the CW loop.

From the analysis above, one can see that as long as the change in $\eta(t)$ is not symmetric on the $v-\eta$ plane regardless of the dynamics of $\eta(t)$ (linear or non-linear), traffic hysteresis will be generated in the form of CW, CCW, or multiple loops. Empirical results suggest that the symmetry condition is not easy to satisfy and thus hysteresis loops (CW, CCW or multiple loops) are very commonly observed (see the histogram in Figure 6:5). While it seems that a reaction pattern could generate infinite hysteresis cases, empirical results reveal that only a handful are dominant as shown next.

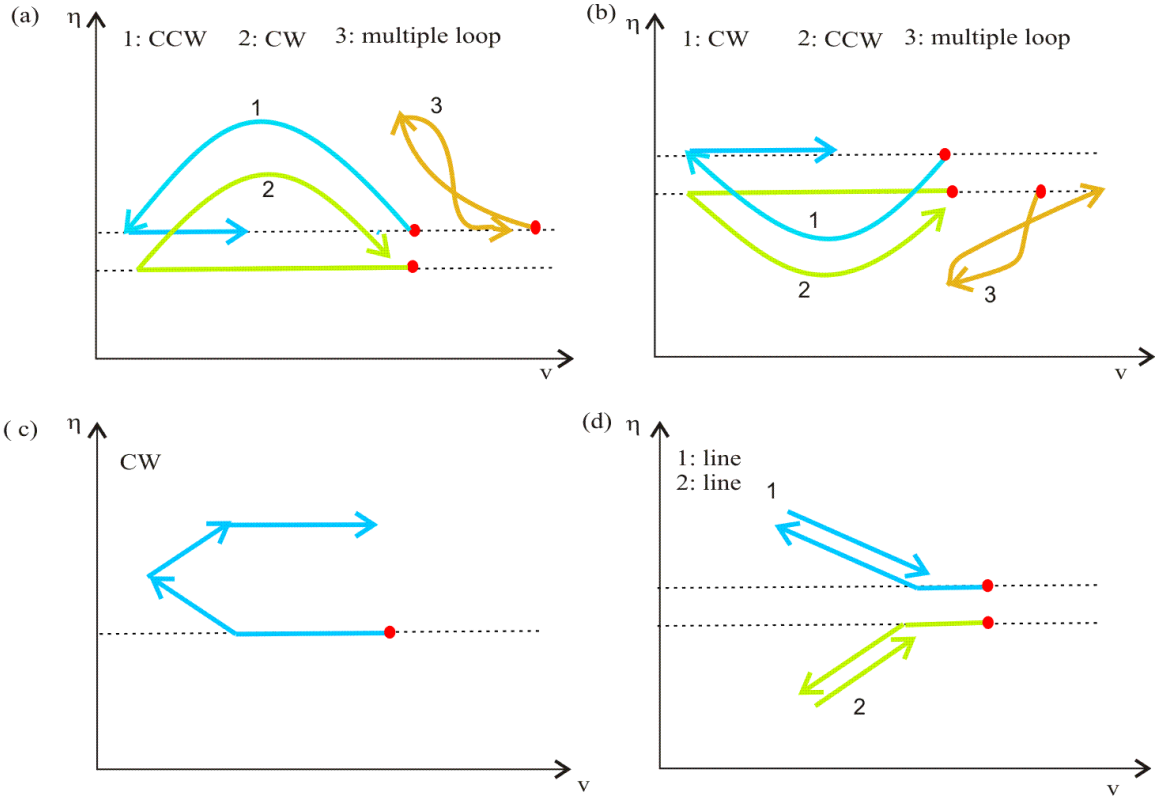

Figure 6:7 Reaction Pattern vs. Hysteresis Type During An Oscillation

(only some common cases are shown).

(a) concave pattern; (b) convex pattern; (c) non-decreasing pattern; (d) concave and convex pattern.

6.3.2 Major Formation Mechanisms of Traffic Hysteresis

Two response scenarios are defined for drivers that adopt reaction patterns in oscillations:

(i) *early* response: $\eta_i(t)$ starts to deviate from η_i^0 around the beginning of the deceleration process of an oscillation cycle and recovers to η_i^1 before (or near) the start of the acceleration process;

(ii) *late* response: $\eta_i(t)$ starts to deviate from η_i^0 at (or around) the end of the deceleration process of an oscillation cycle and continues the change in the acceleration process.

The response scenario is a critical factor when causing traffic hysteresis. Investigation of trajectories that exhibited CW or CCW loops reveals that when drivers use reaction patterns in oscillations, they mainly fall in two response scenarios defined above.

It is found that CW loops are mainly generated from the following two mechanisms: (1) generated from late-response concave triangle and non-decreasing patterns (see Figure 6:8 (a) and Figure 6:2, respectively); and (2) generated from early-response convex triangle pattern (Figure 6:8 (b)). Mechanism (1) is prevalent in both stages while a certain proportion (about 15%) of CW loops cases in the growth stage follow mechanism (2). Interestingly, the CW loops caused by the two mechanisms are different. As illustrated in Figure 6:8 (c), the region bounded by the loop can be above or below the driver's equilibrium level captured by η_i^0. In the former case the hysteresis is positive: the speed under hysteresis is greater than the equilibrium level. By contrast, the hysteresis is negative in the latter case. Thus, CW+ and CW- loop are used to distinguish the two cases.

The CCW loops are generated from two major mechanisms as well: (i) generated from early-response concave triangle pattern (Figure 6:9 (a)); and (ii) from late-response

convex triangle pattern (Figure 6:9 (b)). Interestingly, most of the CCW loop cases in the growth stage follow the second mechanism but accord well with the first one in the fully-developed stage. Similar to the CW loops, CCW loops caused by the two mechanisms are different and can be denoted by CCW+ and CCW- loop, respectively.

(a)

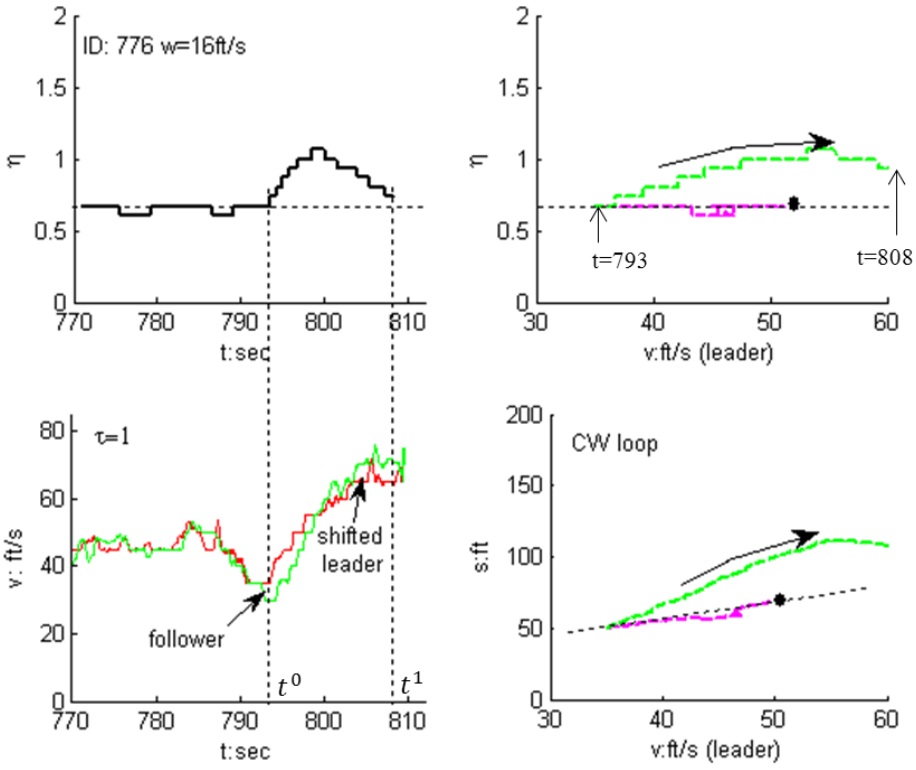

(b)

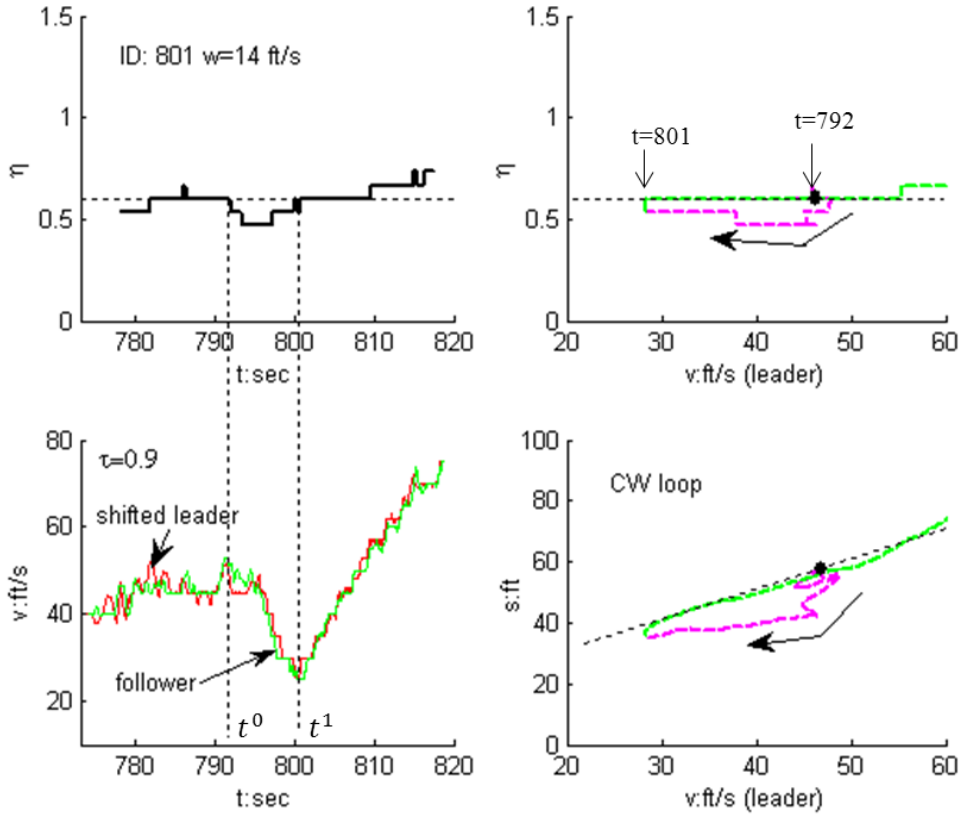

(c)

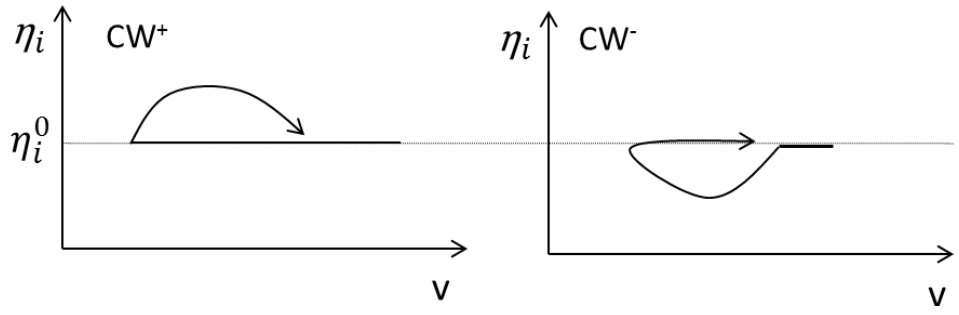

Figure 6:8 CW Loops

(a) Example of concave triangle pattern with CW loop; (b) Example of convex triangle pattern with CW loop; (c) Illustration of CW+ and CW- hysteresis loop

(a)

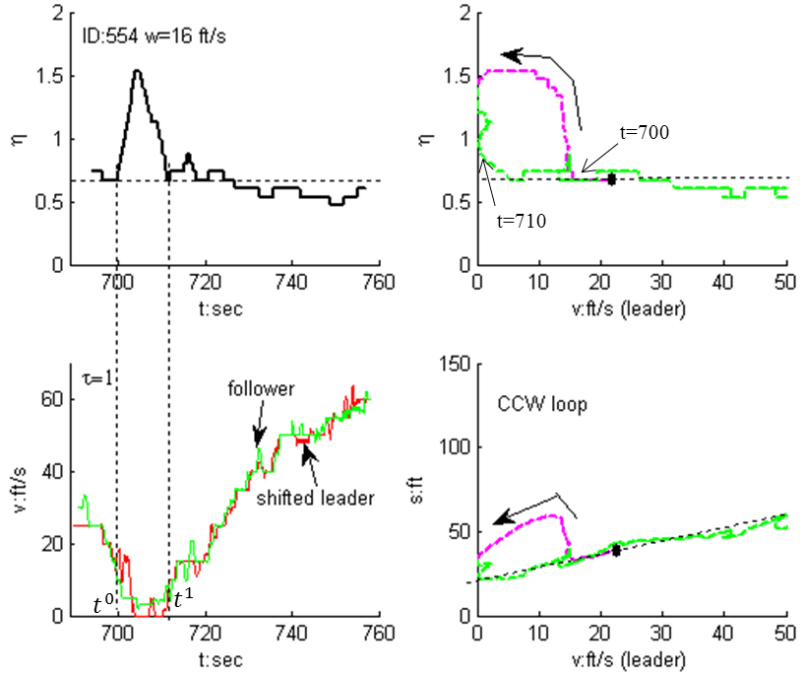

(b)

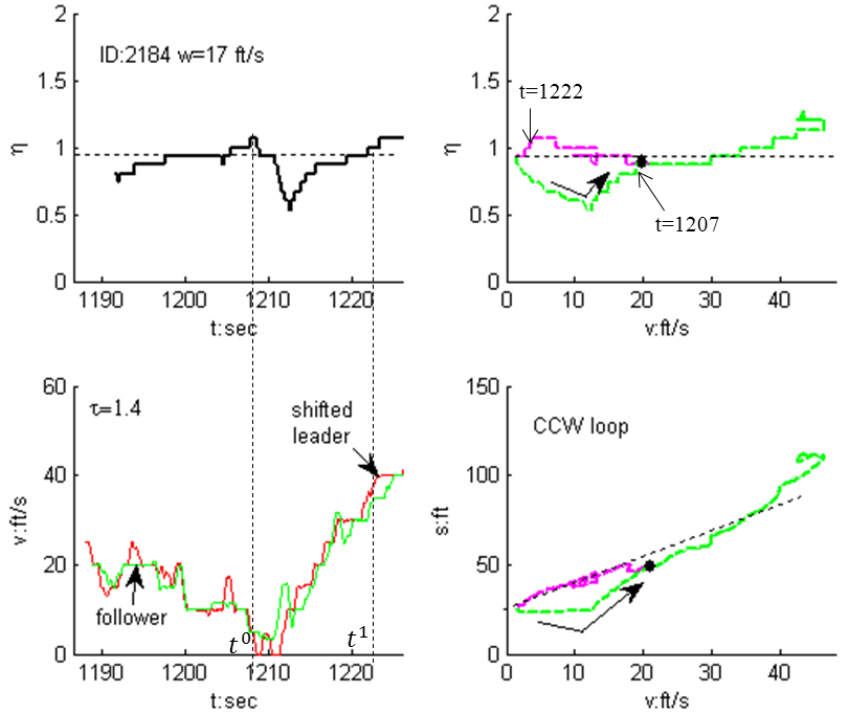

Figure 6:9 CCW Loops

(a) Illustration of concave triangle pattern with CCW loop; (b) Illustration of convex triangle pattern with CCW loop.

6.3.3 Distribution of Traffic Hysteresis

The mechanisms of generating traffic hysteresis in the two stages are introduced by the following remarks with the frequency histogram shown in Figure 6:10:

R5: In growth stage, OA drivers tend to have non-decreasing and concave triangle patterns in late response scenario, which both cause CW+ loops. In full-developed stage, when using concave triangle pattern, OA drivers have even probability to have early and late response, which results in CW+ and CCW+ loops, respectively.

R6: In both stages OT drivers tend to have convex triangle pattern in late response scenario and generate CCW- loops.

R7: In growth stage, ON drivers tend to have concave triangle and non-decreasing patterns in late response scenario but convex triangle pattern in early response scenario, which generates CW+ loops and CW- loops, respectively. In fully-developed stage, ON drivers have comparable probability to have concave triangle pattern in early and late response scenarios, which generates CW+ and CCW+ loops, respectively.

A summary of the results is provided in Table 6:1, in which the solid dots (circles) represent CW (CCW) loops and the size of the dots/circles qualitatively illustrates the frequency.

One can see that the distribution of hysteresis types is affected by three factors: (1) the distribution of driver category, (2) the preference of reaction pattern for each driver category, and (3) the response scenario used. Given that the distribution of driver categories is not significantly different (see R2), R4-7 suggest that (2) and (3) play a critical role in the hysteresis distribution change in the two stages. In particular, the increased proportion of CCW loops in the fully-developed stage is the result of the

increased number of concave triangle pattern that occurs in early response scenario, which is a compound effect of (i) the increased probability of OA and ON drivers to adopt concave triangle pattern (see R3a & R3b) and (ii) the increased probability to have early response when they use concave triangle pattern (see R5 and R7). Both (i) and (ii) suggest changes in driver behavior.

Table 6:1 Major Hysteresis Patterns for Two Stages

	OA					OT					ON				
	concave		n-d*	convex		concave		n-d	convex		concave		n-d	convex	
	early	late	Both	early	late	early	late	both	early	late	early	late	both	early	late
	CCW^+	CW^+	CW^+	CW^-	CCW^-	CCW^+	CW^+	CW^+	CW^-	CCW^-	CCW^+	CW^+	CW^+	CW^-	CCW^-
growth		●	●							○		●	●	●	
fully-developed	○	●								○	○	●			

○ : CCW
● : CW

*: n-d stands for non-decreasing pattern.

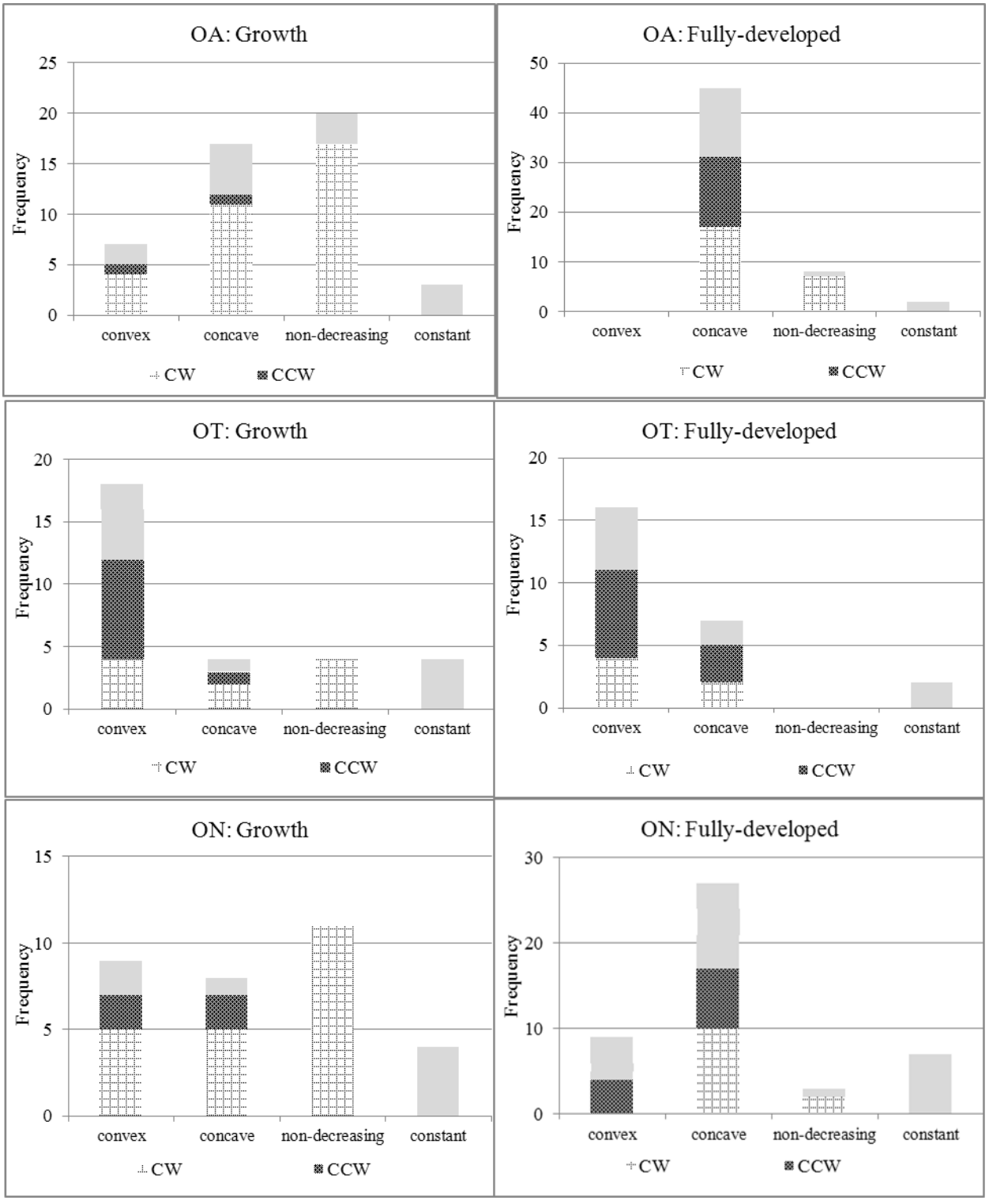

Figure 6:10 Driver Category, Behavior Pattern and Hysteresis Pattern

6.4 Discussions

This chapter has investigated the traffic hysteresis arising in traffic oscillations from a behavioral perspective based on the framework of the asymmetric behavioral model. Traffic hysteresis is connected to two key elements of the model, driver category and their reaction pattern to traffic oscillations, by a variable, $\eta_i(t)$. Empirical observations suggest that traffic hysteresis is generated when drivers' reaction to traffic oscillations is not symmetric on the $v-\eta$ plane. The major generation mechanisms are unveiled, and the different distribution of hysteresis patterns are explained as well.

Note that this traffic hysteresis study also confirmed the findings about the potential behavior change observed in chapter 5: (1) $\eta_i^1 \neq \eta_i^0$ in samples from period 1 and (2) the preferred reaction pattern of certain driver categories differs in period 1 and 2. It seems clear that both (1) & (2) are because some of the trajectories sampled for period 1 are from the growth stage of traffic oscillations while trajectories in period 2 are in the fully-developed stage, which is consistent with the conjectures in Section 5.2. Of course, it is still possible that (1) is because of the limited length of vehicle trajectories. This is to be explored once extensive trajectories are available.

From a modeling perspective, findings in this chapter indicate that the oscillation development stage should be taken into account when modeling driver's car-following behavior. The statistical results of this study suggest that driver behavior varies with the development stage of traffic oscillations (see R3); i.e., (a) the preference on reaction pattern and (b) when the reaction pattern undergoes in an oscillation cycle; i.e., response scenario. To do that, the minimum speed of vehicles experiencing traffic oscillations may be an indicator of the different states as in this study. For example, once the minimum speed is zero, the oscillation becomes fully-developed.

It is also found necessary to capture the response scenario when describing driver's car-following behavior because that will affect the traffic hysteresis generated. Fortunately, empirical results suggest that the reaction pattern tends to start early or late.

Therefore, one may assume that early response is initiated whenever the deceleration wave is triggered and the late response starts at the beginning of the acceleration process. This can be included in the behavioral model without adding additional parameters.

Notice that driver category, reaction pattern, and response scenario are all correlated and the relationship depends on the development stage of traffic oscillations. Therefore, driver behavior is determined in four layers: (1) stage of traffic oscillations, (2) driver category, (3) reaction pattern, and (4) response scenario. In the modeling of traffic oscillations in chapter 4 and 5, (2) and (3) are captured by the five parameters [$\eta_i^0, \eta_i^T, \eta_i^1, \varepsilon_i^0, \varepsilon_i^1$]. It is unclear whether the joint distribution of this parameter set is independent of (4). If not, another parameter capturing (4) needs to be added to the model, and one may estimate the joint distribution of the new parameter set.

Note that in this study the non-decreasing pattern is distinguished from the concave triangle pattern and is used to describe a reaction pattern. This pattern suggests that drivers increases their equilibrium spacing level but do not return to the preferred level before oscillations. This pattern contributes to the finding that driver characteristic has changed after experiencing growth-stage traffic oscillations. As mentioned in chapter5, this may be because the trajectories are not long enough to cover the recovery. Notice that this pattern is very common in the growth stage and plays an important role in producing CW loops. The hysteresis resulting from this pattern is quite significant, and the difference of spacing for a given speed may be up to 70 feet (see Figure 6:2 (d)). Interestingly, its mechanism in generating CW loops is very similar to the concave triangle pattern. Thorough investigation based on extensive trajectories is needed.

CHAPTER 7 SIMULATIONS FOR THE IMPROVED MODEL

This chapter has two major tasks: (1) introducing the improved asymmetric behavioral model formulated based on results of the traffic hysteresis study in chapter 6; and (2) conducting traffic simulations to test performance of the improved model.

7.1 Formulation of the Improved Asymmetric Behavioral Model

The original asymmetric behavioral model described in chapter 4 considers two elements when describing driver behavior through traffic oscillations: driver category and reaction pattern. Empirical results in chapter 6 suggest that another two elements should be considered as well: the development stage of traffic oscillations and the response scenario. Therefore, the improved asymmetric behavioral model is proposed to describe a driver's car-following behavior in congestion: (i) drivers enter the non-equilibrium mode either in early response or late response scenario; (ii) the ensuing dynamics of $\eta_i(t)$ in non-equilibrium, named "reaction pattern", follow one of four categories: concave triangle, convex triangle, constant, and non-decreasing; (iii) a driver's preference on reaction patterns may vary with the development stage of oscillations: growth or fully-developed; (4) before and after the non-equilibrium mode, drivers are in equilibrium, but (5) the before and after equilibrium levels (denoted by η_i^0 and η_i^1, respectively) may be different. This model is referred to as the Asymmetric Behavioral 2-stage model, abbreviated as AB2 model.

Apparently, the AB2 model is based on the AB1 model and the major difference between the two models is that the AB2 model has taken the response scenario and development stage of oscillations into the model. Note that the response scenario determines when drivers enter the non-equilibrium mode, and the development stage of traffic oscillations may affect driver behavior either in the reaction pattern used or response scenario or both. Hence, the measurement of these two new elements is critical.

To capture the response scenario, one may measure the response time as in relative to the starting time of the deceleration wave. To simplify the modeling process, it is assumed here that early response will occur when the deceleration wave of an oscillation starts. Similarly, late response occurs when the acceleration wave starts. To define the stage of traffic oscillations, the method used here is to track the minimum speed of drivers during the deceleration-acceleration process of an oscillation cycle as used in chapter 6. When the minimum speed stops decreasing, the fully-developed stage starts and the stage before is the growth stage.

Based on the statistical results in chapter 6, for simulation purpose, AB2 can be reduced to five parameters per driver $[\eta_i^0, \eta_i^T, \eta_i^1, \varepsilon_i]$, where $\varepsilon_i = \varepsilon_i^0 = \varepsilon_i^1$ since $\varepsilon_i^0$and ε_i^1 are not significantly, r denotes the response scenario, which is a binary variable, early or late. Notice that the effects of development stage on reaction pattern and response scenario are implicitly incorporated by the five parameters.

7.2 Model Comparison

In this section, three models, the L-L model, the original asymmetric behavioral model, and the AB2 model are tested on the rubbernecking experiment and uphill experiment. The original Asymmetrical Behavioral model is abbreviated as the AB1 model hereafter, where "1" indicates only one stage is used in the model. The basic characteristics of the three models are summarized in Table 7:1.

Table 7:1 Summary of Three Models

	L-L Model	AB1 Model	AB2 Model
Vehicles	Identical in equilibrium but different in non-equilibrium.	Unique. Each vehicle has its own set of parameters.	Unique. Each vehicle has its own set of parameters
$\eta_i^0, \eta_i^1, \eta_i^T, \varepsilon_i^0, \varepsilon_i^1$	$\eta_i^0 = \eta_i^1 = 1$ $\varepsilon_i^0 = \varepsilon_i^1 = \varepsilon$	$\eta_i^0 = \eta_i^1$ $\varepsilon_i^0 <> \varepsilon_i^1$	$\eta_i^0 <> \eta_i^1$ $\varepsilon_i^0 <> \varepsilon_i^1$
Driver categories in equilibrium	Homogenous $\eta_i^0 = 1$	$\eta_i^0 \ll 1$: originally aggressive $\eta_i^0 \gg 1$: originally timid $\eta_i^0 \sim 1$: originally Newell	$\eta_i^0 \ll 1$: originally aggressive $\eta_i^0 \gg 1$: originally timid $\eta_i^0 \sim 1$: originally Newell
Reaction patterns in non-equilibrium*	concave (aggressive) convex (timid) constant (Newell)	concave (OA, OT, or ON) convex (OA, OT, or ON) constant (OA, OT, or ON)	concave (OA, OT, or ON) convex (OA, OT, or ON) constant (OA, OT, or ON) non-decreasing (OA, OT, or ON)
Development stage of oscillations	All in one stage; i.e., no separation.	All in one stage; i.e., no separation.	Two stages: growth or fully-developed
Response scenario	No difference.	No difference.	Two scenarios: early or late

* With driver class in the parentheses.

7.2.1 Rubbernecking Experiment

7.2.1.1 Experiment

The rubbernecking model is the same as described in Section 5.3 except for that the simulated freeway is further extended to be 5.06km long and the rubbernecking zone is located at x $\in [4,4.06]$ km. For generation of model parameters, still the sample enumeration method (Ben-Akiva and Lerman, 1985) is used to preserve potential correlation between model parameters. Of course, each measurement contains four parameters $[\eta_i^0, \eta_i^T, \eta_i^1, \varepsilon_i]$. A growth sample is obtained by randomly sampling the growth stage of traffic oscillations in US 101 lane 1 from 7:50am-8:05am (see Figure 6:1). Similarly, a fully-developed sample is obtained in the same approach. Both samples have 56 trajectory pairs.

For the L-L model, since there is not separation of stages, the growth and fully-developed samples are mixed into one. Each time a vehicle is generated, a parameter set $[\eta_i^0, \eta_i^T, \eta_i^1, \varepsilon_i]$ is randomly selected from the mixed sample for this vehicle, but both η_i^0 and η_i^1 are set to equal to 1, α_i is set to be $\alpha_i = \eta_i^T - \eta_i^0$, and ε_i equal to the mean of ε_i^0 and ε_i^1. Obviously, according to the definition of L-L model, all drivers are assumed to enter non-equilibrium mode when the deceleration wave of a traffic oscillation starts (i.e., early response) regardless of the development stage of the oscillation.

For the AB1 model, the growth and fully-developed samples are mixed into one as well. When a vehicle is generated, a parameter set $[\eta_i^0, \eta_i^T, \varepsilon_i]$ is assigned for it; i.e., η_i^1 is assumed to be equal to η_i^0, and ε_i equal to the mean of ε_i^0 and ε_i^1. Similar to the L-L model, in the AB1 model, all drivers are assumed to enter non-equilibrium mode as long as the deceleration wave is perceived. Development stage of oscillation is not distinguished either.

For the AB2 model, each time a vehicle i is generated, a η_i^0 value will be selected from the mixed two samples. Meanwhile, all parameter sets in the growth sample that have close η_i^0 value ($\eta_i^0 \pm 0.05$) will form a corresponding subsample, which will offer a parameter set for the vehicle if it stands in the growth stage of an oscillation. A similar subsample for fully-developed stage is created in the same approach. In this way, a driver has consistent η_i^0 value across oscillations but the reaction pattern and response scenario depend on the development stage. Notice that before an oscillation starts, only η_i^0 matters and other parameters are not used. When the vehicle has perceived the deceleration wave of an oscillation, the development stage will be determined and a parameter set will be randomly selected from the subsample accordingly. Also note that a vehicle may experience multiple oscillation cycles and that driver characteristic (denoted by η_i^0) may change. In this case, the growth and fully-developed subsamples for a new cycle will be determined using the η_i^1value from the previous cycle, because the η_i^1value represents the new driver characteristic in equilibrium.

Notice that in the parameter generation process described above, how to determine the development stage that the vehicle stands is a challenging task in simulation. This is because in simulations the spatial positions of all vehicles are updated downstream towards upstream in every time step, and the time step is set to be as small as possible to reduce numerical errors (e.g., it is set as τ, equal to 1.71sec, in the following simulations). This suggests that, at each time step, the traffic state of the leading vehicle is only one time step in advance of the following vehicle. Hence, when a vehicle has perceived the deceleration wave of an oscillation, it is very likely that the leader has not finished the deceleration process. In this case, it is impossible to decide whether the leader will come to a complete stop during the oscillation and therefore determine the development stage.

In the following simulations, the development stage is determined by foreseeing n vehicles downstream: when a vehicle has perceived the deceleration wave of an oscillation at time t, the speed of n vehicles downstream are examined. If any of the leading vehicles has zero speed, the stage is set as fully-developed stage and growth stage otherwise. Observations show that the deceleration process is less than 20sec when a vehicle comes to a complete stop in the oscillation process, which suggests that if the wave trip time between vehicle i and $i-n$ (i.e., n vehicles downstream) is over 20sec, one (or more than one) vehicle downstream between vehicle i and $i-n$ will display complete stop at time t; see illustration in Figure 7:1(a) on which vehicle $i-n-1$ (in red) is at a complete stop. In this case, it is assumed that vehicle i stands in the fully-developed stage. The wave trip time between vehicle i and $i-n$ equals to $\sum_{i}^{i-n-1}\eta_i(t_i^*)*\tau$, which can be approximated as $n\tau$, where t_i^* is the time when the wave lunched from vehicle i at time t intersects the trajectory of vehicle $i-1$; see Figure 7:1 (a). Hence, n is set to assure that $n\tau \geq 20sec$. Meanwhile, apparently this method will bring in a delay of n vehicles in starting the fully-developed stage. Therefore, the selection of n value should aim to minimize the delay while still capture the complete stop of the proceeding vehicle(s). Examination of the empirical data suggests that when n is about 12, the complete stop can be well captured; see Figure 7:1(b) for an example. It is set $n=12$ in the simulations.

(a)

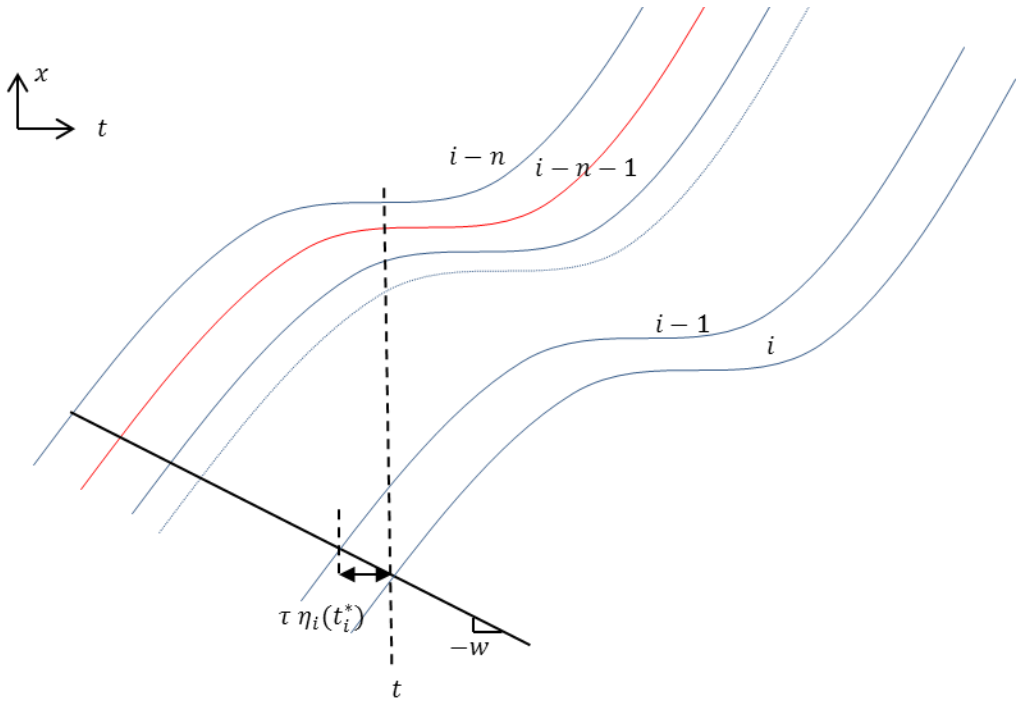

(b)

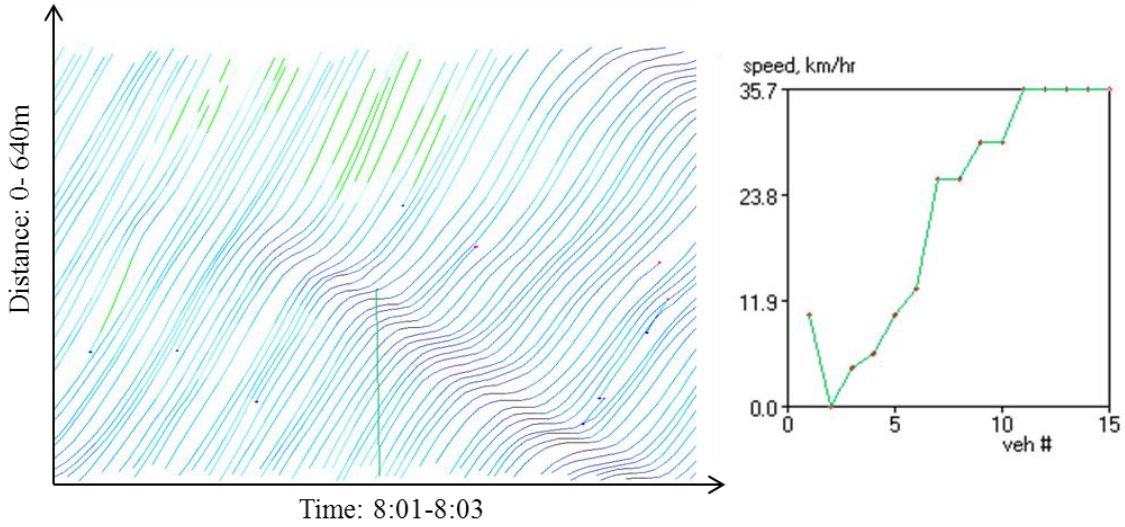

Figure 7:1 Illustration of Foreseeing Downstream Vehicles

(a) method illustration; (b) empirical example from US 101 lane 1 (left: trajectory, right: speed of vehicles intersecting the green line from downstream to upstream)

7.2.1.2 Traffic oscillations from simulations

7.2.1.2.1 Characteristics of traffic oscillations

Examples of simulated trajectories from the three models are shown in Figure 7:2. One can see that all three models have produced traffic oscillations and have the oscillations propagate far upstream. However, the AB2 model has better captured two important characteristics of traffic oscillations across different development stages:

(1) *It shows clear precursor region.*

A precursor region usually occurs in the very beginning of the growth stage and is characterized with zero (or close to zero) wave speed; i.e., oscillation propagates horizontally; see Figure 7:3 for empirical examples taken from Figure 4:1 (a). Trajectories from simulations are provided in Figure 7:4, on which the precursor region is circled by red dash curve. One can see that the precursor region in the AB2 model (see figure (a)) is well produced, consisting of about 10 vehicles, and the oscillation propagates almost horizontally. While in the AB1 model and L-L model (see figure (b) and (c)), the precursor period consists fewer vehicles (about 6) and the propagation of oscillation seems forward (i.e., positive wave speed).

(2) *It produces traffic hysteresis for different stages of traffic oscillations consistently with empirical results*.

Empirical observations suggest two basic features of oscillations in the development process: (i) the growth stage is characterized with open clockwise hysteresis loops when measured along a platoon; i.e., at the macroscopic level; and (ii) the fully-developed stage is characterized with negligible hysteresis loops, either clockwise or counter clockwise. Figure 7:5 shows one example taken from US 101 lane 1, on

which the flow-density ($q - k$) plots on the bottom are measured on the platoon displayed on the top using Edie's method (Edie, 1961) and the red dash line represents a fundamental diagram with parameters $u = 120km/h$, $w = -16.46km/h$, and $k_j = 160veh/km$. Note that the macroscopic traffic hysteresis here is shown on the $q - k$ plane, but it is consistent with the analysis on the $v - \eta$ plane and $v - s$ plane as in chapter 6. The same hysteresis measurement was conducted for the simulation results from the three models. One can see that the hysteresis produced from the AB2 model (Figure 7:6) is consistent with the feature (i) and (ii); while in the AB1 and L-L models (Figure 7:7 Figure 7:8) (i) is not well captured: the hysteresis magnitude (denoted by the flow difference at a given density) in the growth stage seems negligible and it has close loop.

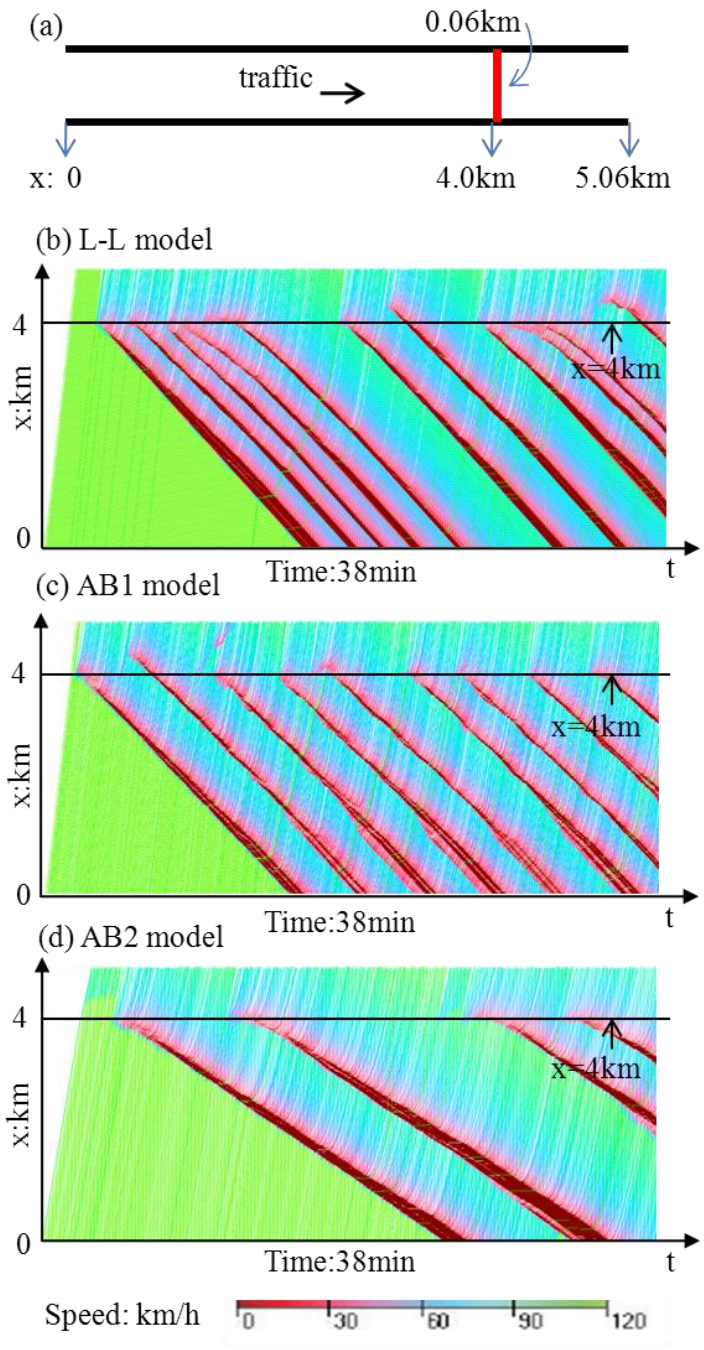

Figure 7:2 Simulated Trajectories from Three Models

(a_m=1m^2/s p=0.7 r =2%)

(a) Sketch for simulated segment; (b) result from L-L model; (c) result from AB1 model; (d) result from AB2 model;

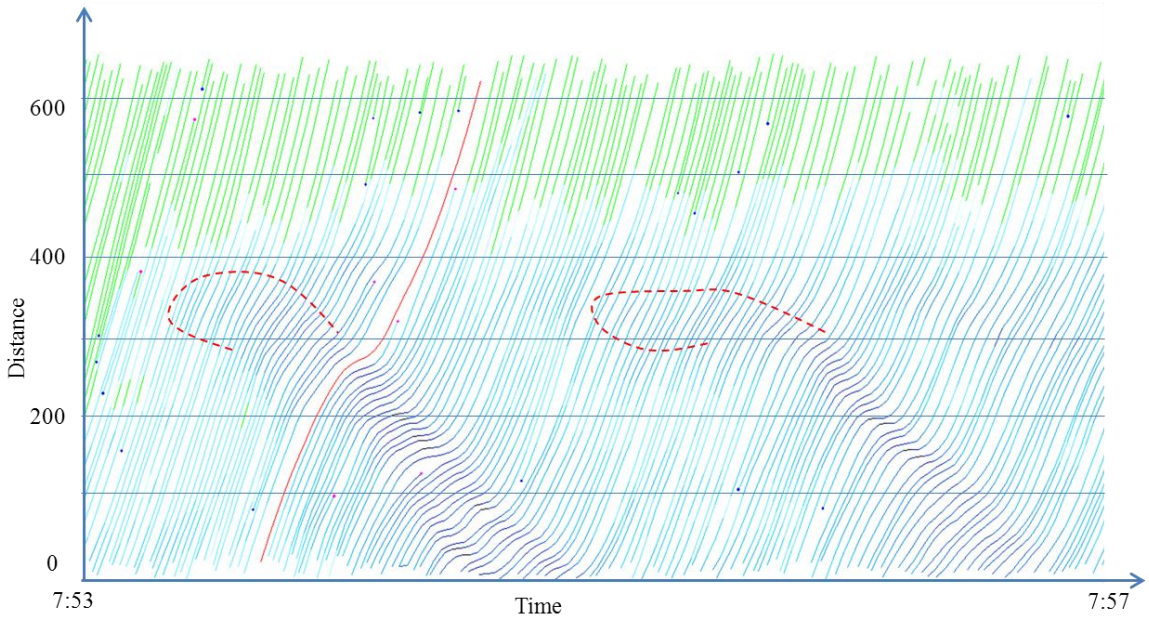

Figure 7:3 Detailed Traffic Oscillation Cycles

(zoom in from Figure 4:1 (a), NGSIM, US 101)

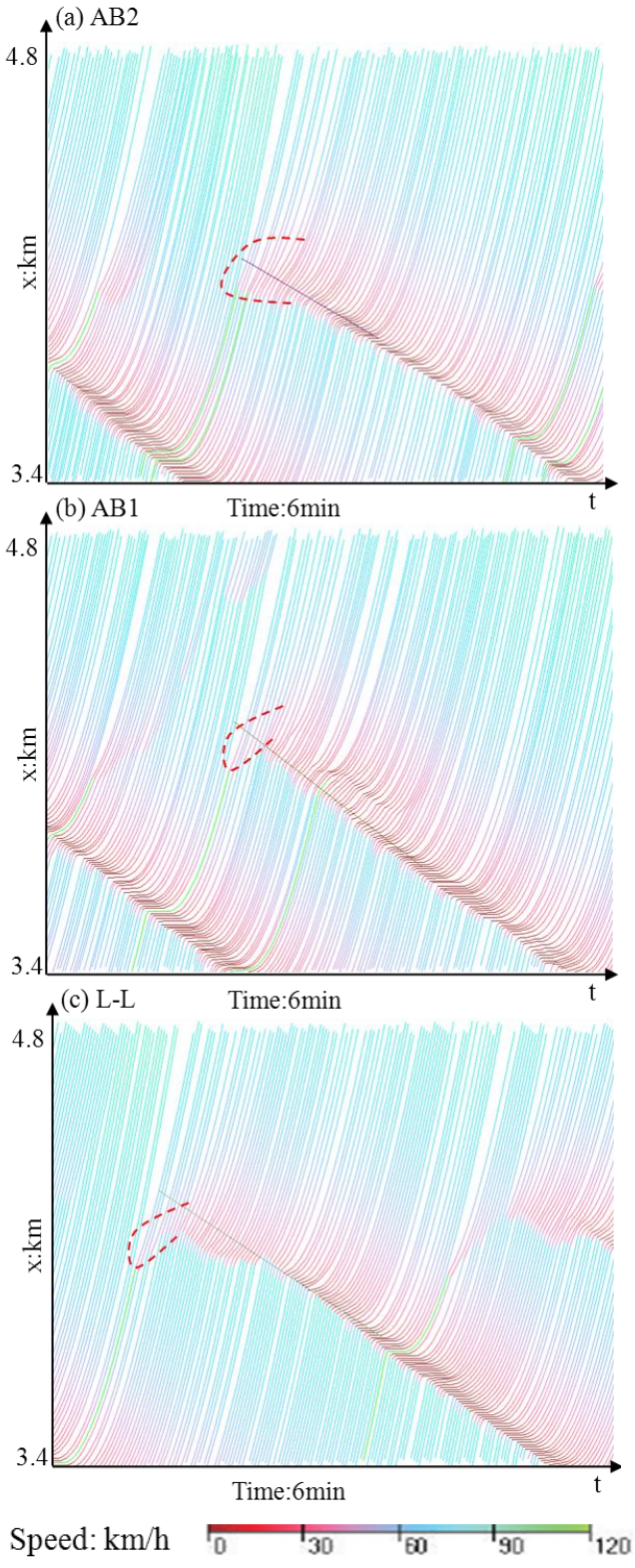

Figure 7:4 Development of Traffic Oscillations

(a_m=1.5m^2/s p=0.6 r =2%)

(a) (b)

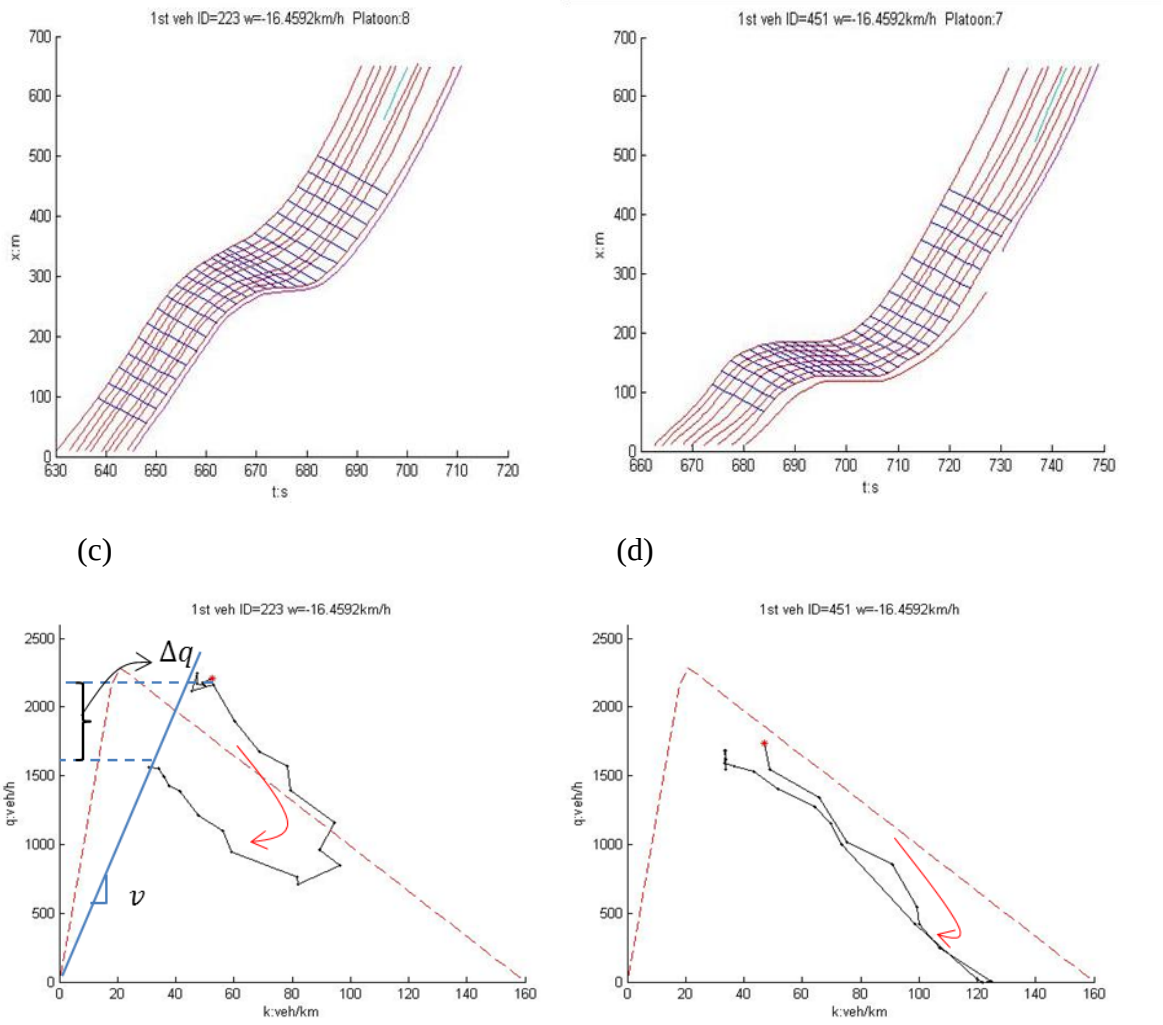

(c) (d)

Figure 7:5 Hysteresis Observed on Us 101 Lane 1

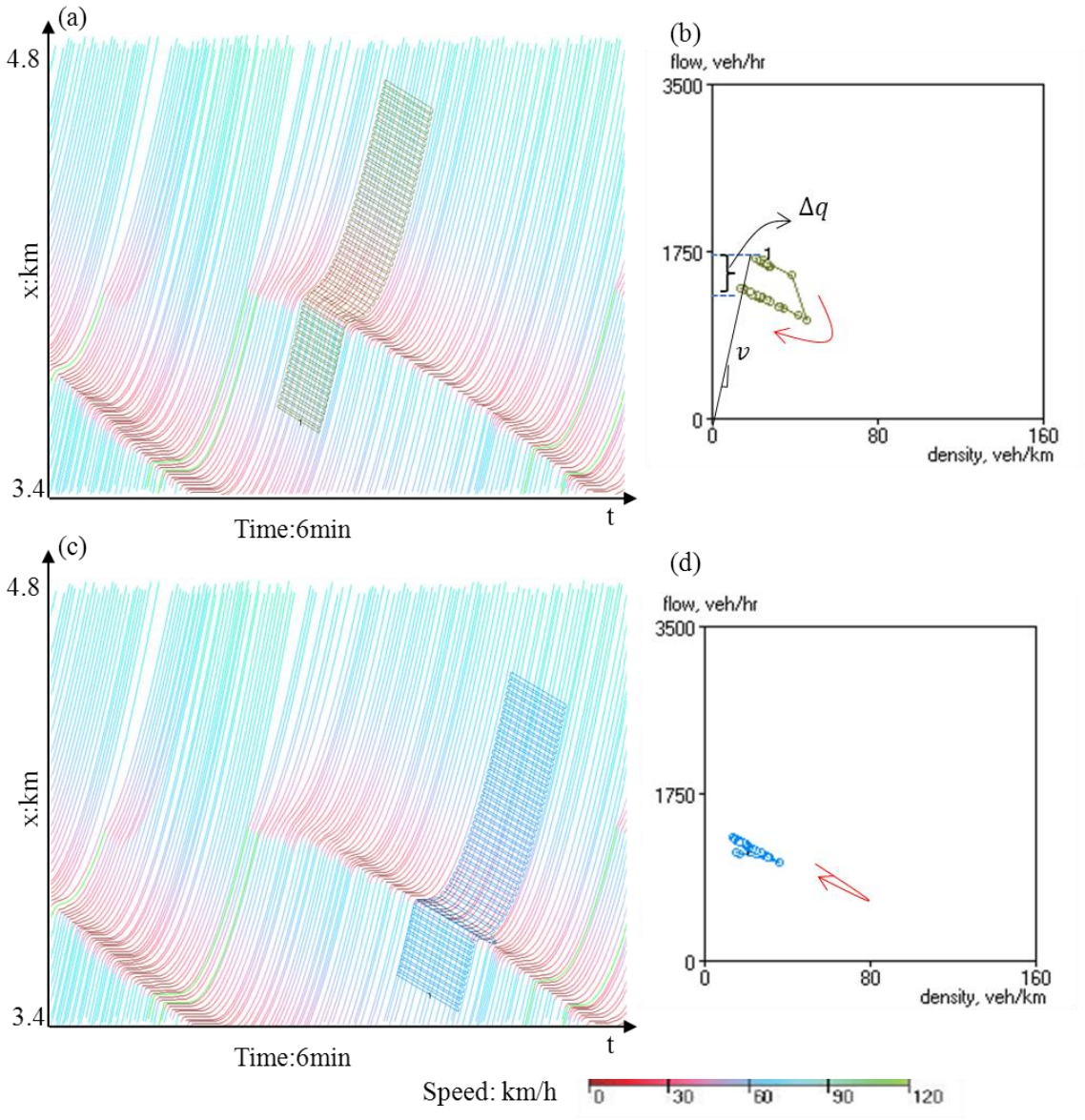

Figure 7:6 Hysteresis in AB2 Model

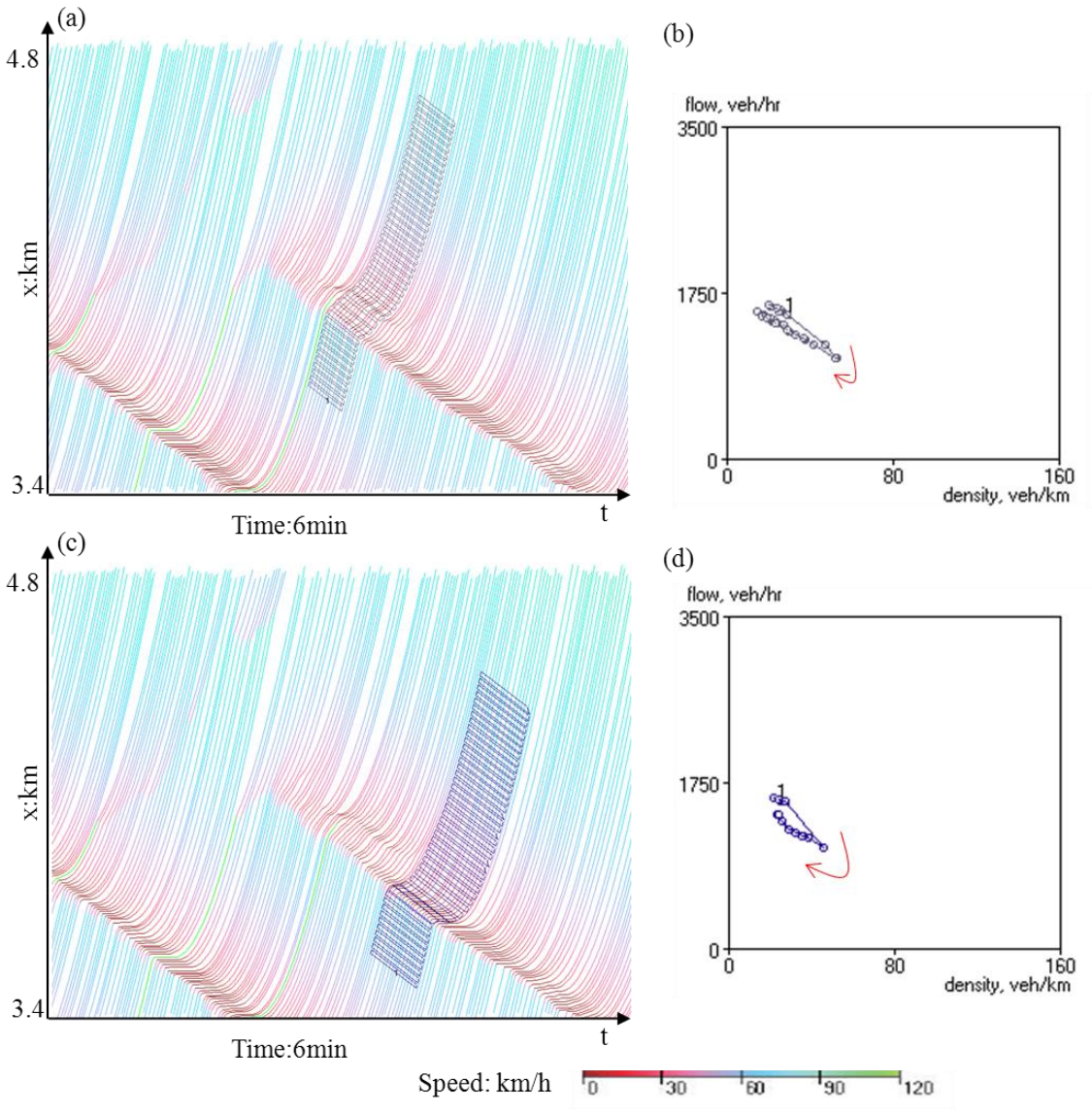

Figure 7:7 Hysteresis in AB1 Model

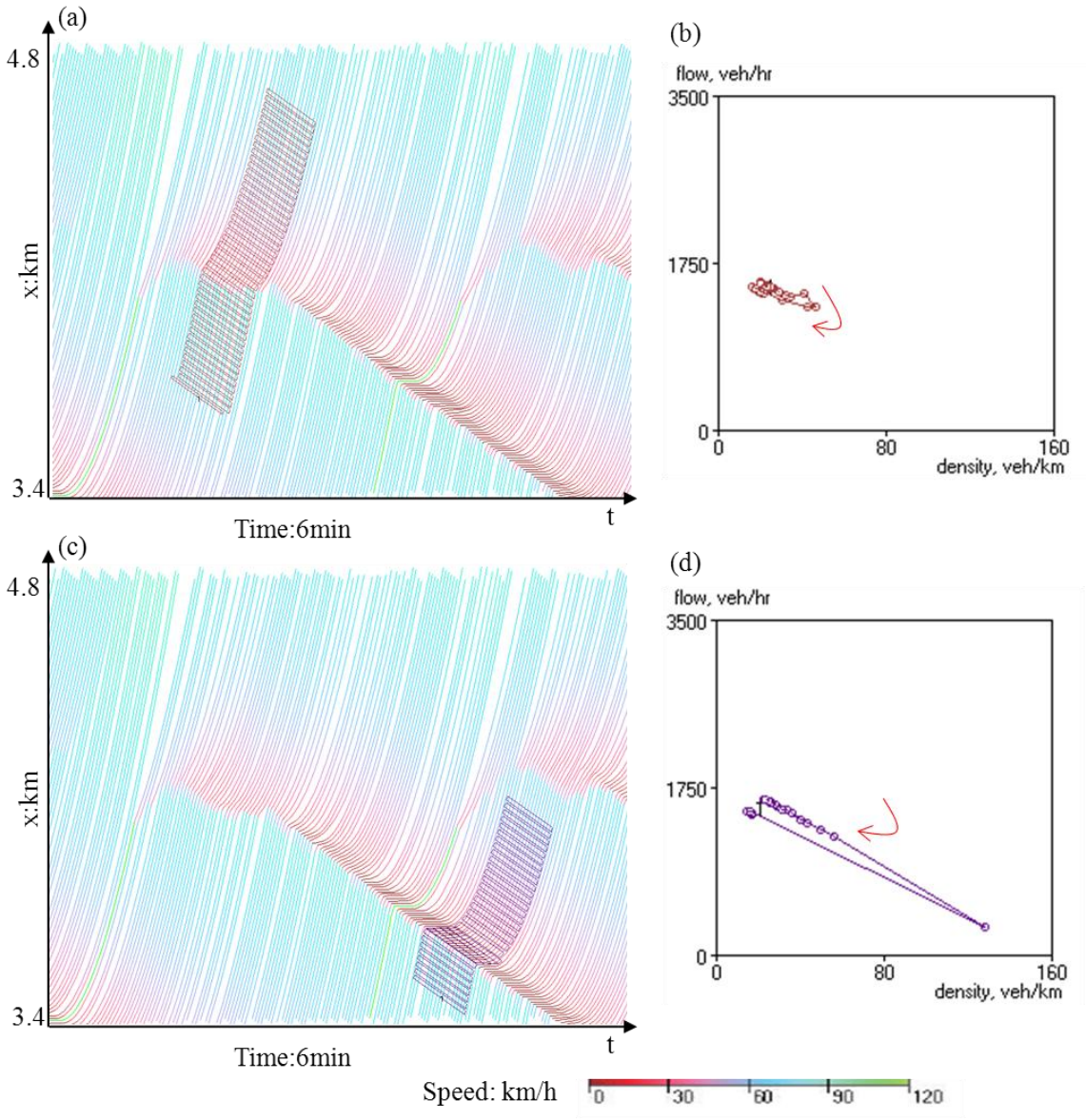

Figure 7:8 Hysteresis in L-L Model

Note that characteristic (2) is consistent with results from chapter 6 in which traffic hysteresis was measured at individual driver level. Recall that in the growth stage (a) CW hysteresis loops are dominating and (b) a significant proportion of vehicles adopt non-decreasing reaction pattern, which leads to open CW loops; while (c) in the fully-developed stage, the proportion of CW and CCW hysteresis loops are comparable and most of the loops are close. Hence, in the growth stage when vehicles are aggregated to obtain the macroscopic measurement, the effects of CW loops accumulate, which leads to

significant magnitude of hysteresis; i.e., it is the result of (a). Meanwhile, the effect of (b) persists at the macroscopic level. By contrast, because of (c) the effects of CW and CCW loops may offset, which leaves the magnitude of hysteresis negligible. Since the features (a-c) are well captured in the AB2 model by incorporating the development stages and response scenario, it is not surprising that the model has reproduced characteristic (2) while this characteristic is not obvious in the other two models.

Notably, characteristic (2) indicates that the overall driver population has changed their characteristics after experiencing growth-stage traffic oscillations. Recall that η_i^0 (η_i^1) represents a driver's characteristic in equilibrium before (after) oscillation and it corresponds to the position of the congestion branch on the fundamental diagram (see Figure 4:6). Hence, the macroscopic open clockwise loop suggests that the congestion branch shifts towards zero point, which indicates that on the average drivers maintain larger spacing level after oscillations; i.e., drivers become more conservative.

From the traffic flow perspective, the occurrence of open clockwise loop indicates that traffic oscillations may lead to discharge rate reduction or even capacity drop if oscillations arise near bottleneck. This effect can be easily seen on Figure 7:5 (c) and Figure 7:6 (b). When the speed before and after oscillation is the same, as the congestion branch shifts towards the zero point the flow decreases, which leads to discharge rate reduction, denoted by Δq on the figures. Obviously, when this occurs at bottlenecks, the discharge rate reduction is capacity drop. Of course, it is also possible that vehicles emerging from oscillations accelerate to higher speed and the discharge rate does not change.

The effect of discharge rate reduction resulting from open hysteresis loop is illustrated in Figure 7:9. Let (q_0,v_0) and (q_1,v_1) denote the traffic state before and after traffic oscillation. Assume that the wave speed remains unchanged and after the

oscillation the congestion branch shifts from κ_{j0} to κ_{j1}. Let $\alpha = 1 - \frac{\kappa_{j1}}{\kappa_{j0}}$ and $\beta = \frac{v_1}{v_0}$. Discharge rate reduction Δq is

$$\Delta q = q_0 - q_1 = \kappa_{j0} w v_0 \left(\frac{1}{v_0 + w} - \frac{1-\alpha}{1+\frac{w}{\beta}} \right).$$

Note that $\alpha = 1 - \frac{\kappa_{j1}}{\kappa_{j0}} = 1 - \frac{\eta_i^0}{\eta_i^1}$ if the measurement is at individual vehicle level. One can see that Δq is proportional to α and $-\beta$, indicating that the more the congestion branch shifts towards zero point, the higher reduction will be caused, and that smaller v_1 will lead to larger reduction. Notably, v_1 is bounded by the free-flow speed u. Therefore, there is a critical value for v_0:

$$v_c = \frac{(1-\alpha)w}{\alpha + \frac{w}{u}}.$$

When $v_0 > v_c$, Δq is always positive. This is the condition when the capacity of the new fundamental diagram equals to flow before oscillation, q_0. For a ratio $\frac{w}{u} = 6$, when $\alpha = 20\%$, v_c equals to $2.18w$. Note that $\alpha \sim 20\%$ has been observed in the empirical data (e.g., in Figure 7:5(c) α is about 27%). This suggests that it is not difficult to meet the condition $v_0 > v_c$. Consequently, it implies that discharge rate reduction may be common.

The analysis above suggests that the existence of open clockwise hysteresis loop in the growth stage is an important feature of traffic oscillations. It is particular important if one is interested in the impacts of traffic oscillations on traffic flow. From this perspective, the advantage of the AB2 model is very significant over the AB1 and L-L models. Of course, to quantify the overall impact on traffic flow, more factors should be investigated. For example, since open hysteresis loop is not common in the fully-developed stage, the time proportion of the growth stage in an oscillation cycle will affect the overall impacts. If the proportion varies with oscillation cycles, the period of oscillation may play a role as well. These problems are left for future research.

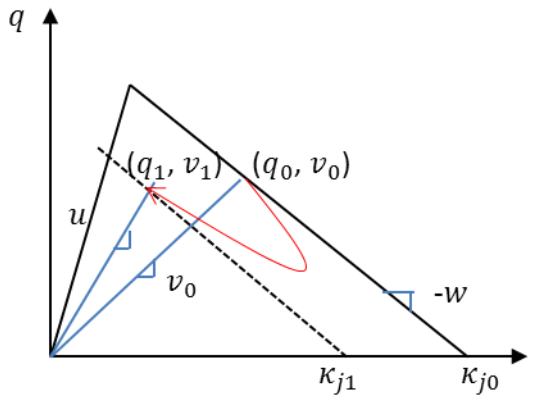

Figure 7:9 Illustration of Discharge Rate Reduction

7.2.1.2.2 Impacts of model parameters

Several combinations of the rubbernecking experiment parameters were tested to explore the impacts of model parameters on the period of traffic oscillations. The measurement of period is the same as in Section 5.3. The results are shown in Figure 7:10 with detailed output in Table 4-(A-C) in the Appendix C. Each combination has five runs with random seed. From the figure, one can see that all the three models have captured the general relationship between the period of oscillation and the parameters a_m, *r*, and *p*: (1) the period of traffic oscillation is negatively correlated with rubbernecker proportion, *r*, and speed reduction imposed by rubbernecking (denoted by 1-*p*); and (2) the period tends to converge to a lower bound as *r* increases. However, significant differences exist in the results of the three models:

R-(i): The relationship between oscillation period and *r* is much more concave in the AB2 model. Actually, the curve becomes more concave across L-L model, AB1 model, and AB2 model.

R-(ii): In AB2 model, the period of oscillation reaches the lower bound much later than the L-L model and the AB1 model. In the former case, the oscillation period becomes stable after $r \geq 8\%$ while in the latter two models convergences occurs after $r \geq 5\%$.

R-(iii): Overall all, the period of oscillation in AB2 model is significantly larger than the other two models for given parameters a_m, *r,* and *p,* while the period from the L-L model and the AB1 model does not differ significantly (see Table 5 in the Appendix).

R-(iv): The impact of speed reduction $(1 - p)$ is significant in the AB1 and AB2 model but not significant in the L-L model. With fixed a_m and varying r, the period of traffic oscillations when $p = 0.6$ and $p = 0.9$ was tested and found significantly different for any given a_m. However, it is not significant in the L-L model for most of a_m values; see Table 6 in the Appendix C.

R-(v): The impact of maximum acceleration rate a_m is not statistically significant in any of the three models. For each model, the period of all combinations of *r,* and *p* under a given a_m value was taken as a matrix and tested with the result from another a_m value. It is found that even result from $a_m = 2.5m/s^2$ does not differ significantly from result from $a_m = 0.5m/s^2$; see Table 7 in the Appendix C.

In the results above, significance of difference was from Mann-Whitney U test (Kvam and Vidakovic, 2007), which is a non-parametric statistical hypothesis test to determine whether the median of two samples from independent observations are different from each other. Similar to the student's t-test, whether the difference is significant is determined by the p statistic: if $p \leq 5\%$, the difference is significant at 95% confidence level. The details of this test are provided in the Appendix B. Apparently, the simulation

results are not necessarily following student-t distribution, the non-parametric test is more appropriate.

Results (i-iii) seem related to two factors, the duration of the precursor area, and the feature of growth stage. Recall from Section 7.2.1.2.1 that the precursor period in the AB2 model is longer than the other two models. It is found that when multiple rubberneckers occur in one precursor period, they usually lead to only one oscillation, which indicates that the longer the precursor period, the fewer oscillations will be created. Additionally, since the growth stage may impose discharge flow reduction, the flow approaching the rubbernecking zone might be lower in the AB2 model compared to the L-L model and the AB1 model, which consequently leaves smaller chances for the formation of traffic oscillations. These two factors explain why the period of traffic oscillations in the AB2 model is larger. In fact, it seems that the AB2 model has captured the upper bound of the period of traffic oscillations reported in the literature (Ahn, 2005; Ahn et al., 2004; Laval et al., 2009; Mauch and Cassidy, 2002), in which the period is about 2-15min.

Result (iv) suggests that the AB1 and AB2 models might have captured the connection between the period of traffic oscillations and traffic state right upstream of the location where traffic oscillations arise. Notice that, the larger p is, the higher is the speed and flow of traffic within the rubbernecking zone during the oscillation cycle. Results from AB1 and AB2 models indicate that the traffic speed right upstream of the oscillation formation zone is positively correlated with the period of traffic oscillations. This is consistent with the observation of (Treiber and Kesting, 2011), who examined traffic oscillations around bottlenecks and found a positive relationship between the period of traffic oscillation and the speed at bottleneck.

Result (v) seems surprising. However, it is risky to conclude that a_m has no effect in the models. Figure 7:11 to Figure 7:13 show examples of traffic oscillations with $a_m = 0.5m/s^2$ and $a_m = 1.5m/s^2$ for the three models. One can observe that (1)

generally more oscillations cycles were generated for the smaller a_m value (see (a) & (c) in the figures); and (2) more white voids were produced both downstream and upstream when a_m is smaller (see (b) & (d) in the figures for detailed look). Observations (1) and (2) seem reasonable because a_m describes the acceleration capability of vehicles. When a_m is small, vehicles around the rubbernecking zone have lower speed after emerging from oscillations, and the traffic flow is smaller too, which produces an effect similar to a larger speed reduction $(1 - p)$. Therefore, more oscillation cycles were produced. For (2), recall that white voids can be created either because (i) drivers prefer to maintain larger spacing level; i.e., they are OT drivers; or (ii) they cannot catch the leaders up because of limited acceleration capability. Hence, it is expected that when a_m is small, more white voids will be generated because of (ii). More empirical investigation is needed to understand the impact of a_m.

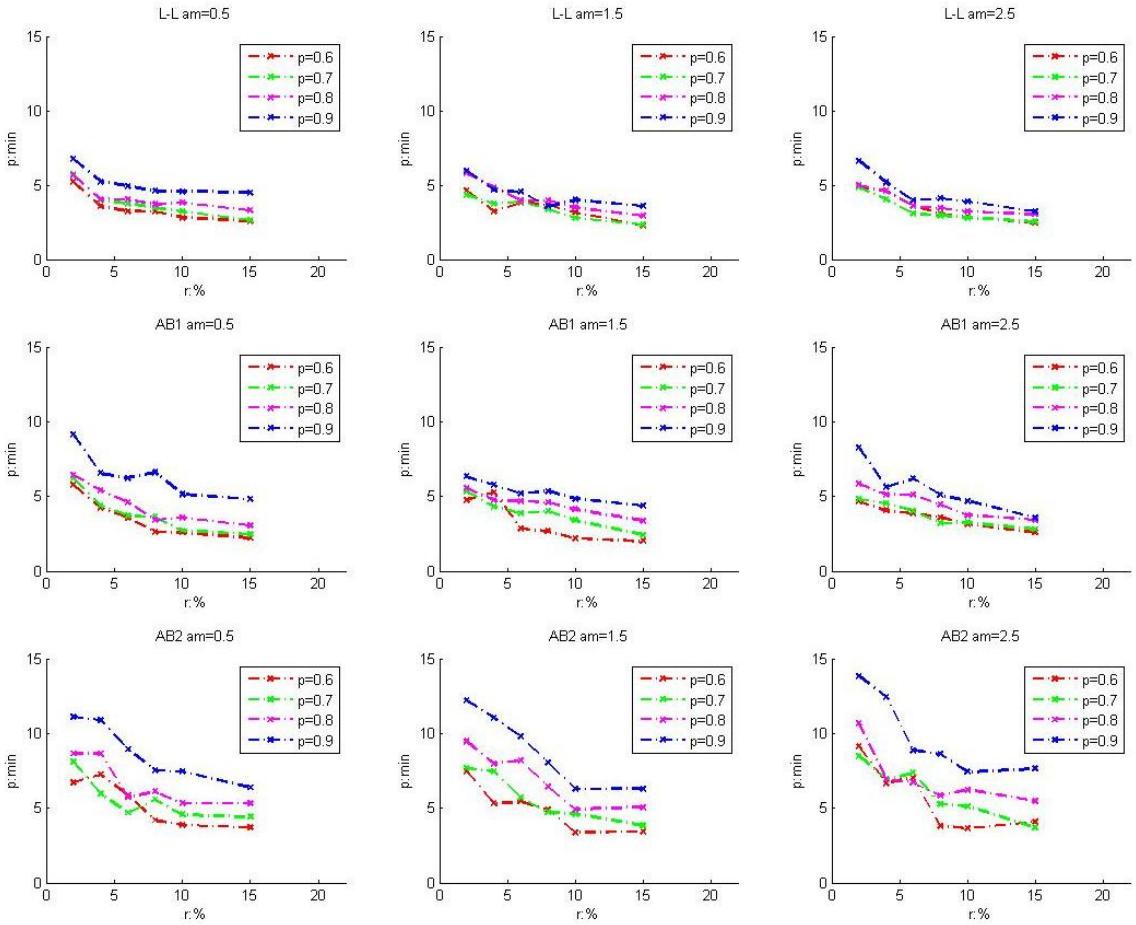

Figure 7:10 Impacts of Mode Parameters on the Period of Traffic Oscillation

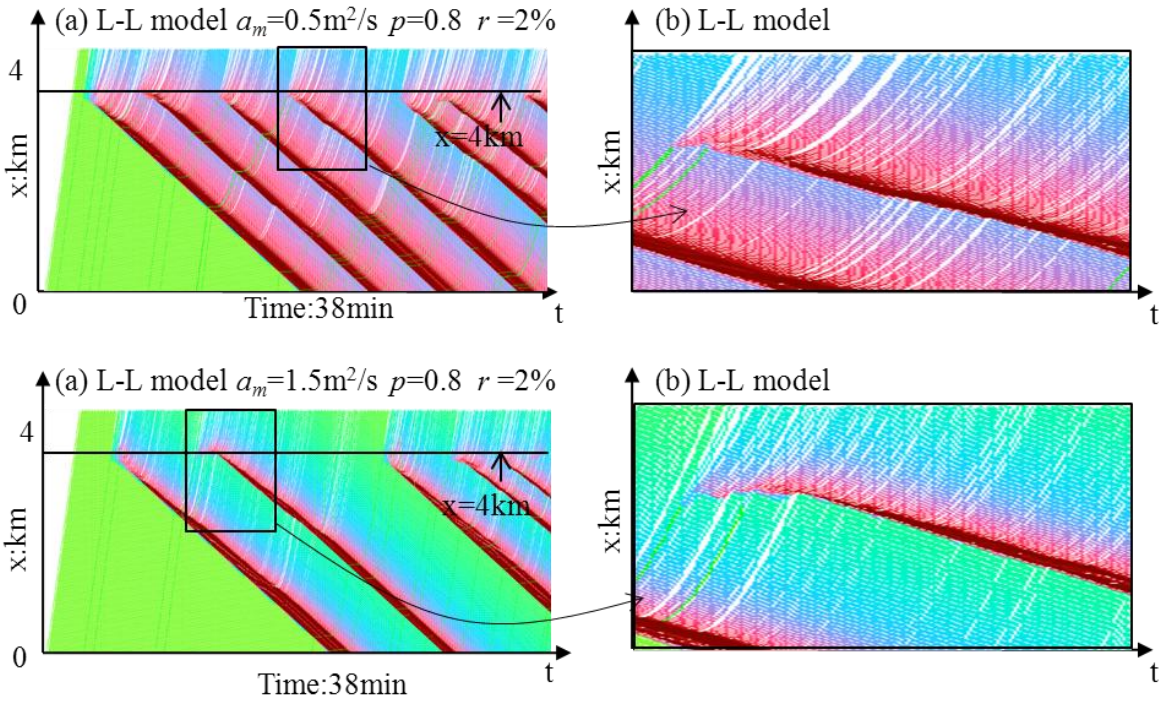

Figure 7:11 Impact of a_m in L-L model

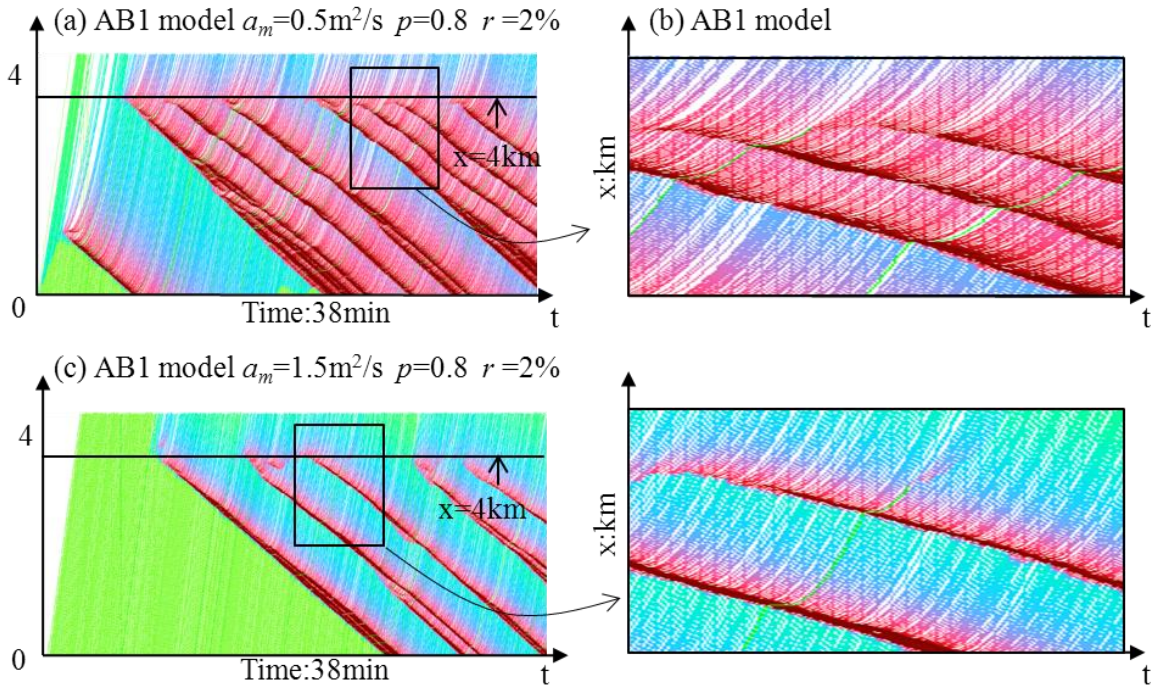

Figure 7:12 Impact of a_m AB1 model

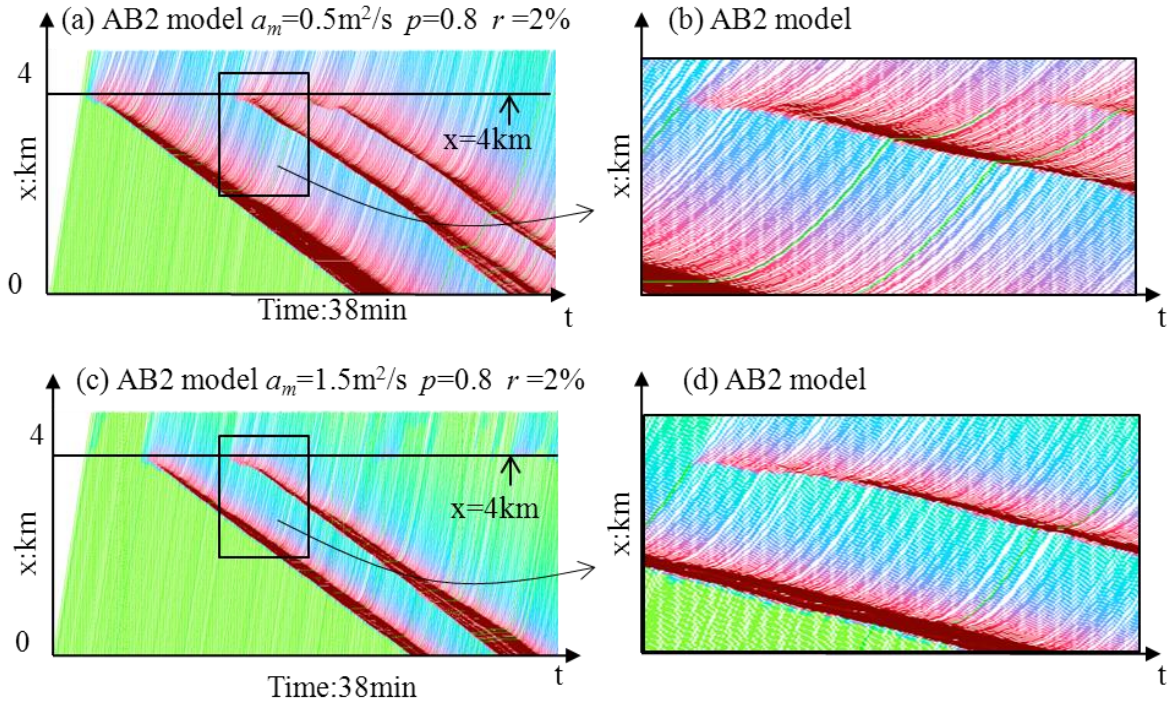

Figure 7:13 Impact of a_m in AB2 model

7.2.2 Uphill Experiment

7.2.2.1 Experiment

The setting of uphill experiment is similar to the experiment in (Laval and Leclercq, 2010): the simulated segment is a 5.06km long 1-lane road with an uphill segment located at x ∈ [4,4.3] km. The grade of the segment is 100G%, in which G is a parameter. Several combination of a_m and G were tested for the three models. Recall from equation (3-6) that $\tilde{x}_{i+1}(t)$, the desired distance travelled during τ, mainly depends on a dimensionless ratio $\frac{gG}{a_m}$, which describes the deceleration rate imposed by the grade. The value of a_m is between $0.5m/s^2$~$2.5\ m/s^2$, and the grade is between 1%~8%. Simulation time was 50 minutes.

7.2.2.2 Simulation Results

The macroscopic features of simulation results from uphill experiment seem similar to the rubbernecking experiment; see examples in Figure 7:14. One can see that traffic oscillations arise around the uphill segment and propagate upstream far away. At the microscopic level, when the value of $\frac{gG}{a_m}$ is small, oscillations from uphill model is similar to the rubbernecking experiment. For example, the right column of Figure 7:15 provides output examples from three models with $\frac{gG}{a_m} = 0.294$, which can be compared with outputs from the rubbernecking experiment on Figure 7:4. One can see that, still the precursor region has been well captured by the AB2 model but not very clear in the AB1 or L-L model, and the white voids associated with the growth stage of oscillations are more significant in the AB2 model. In other words, similar to the results of rubbernecking experiment, the AB2 model has better captured the features of the oscillation development in the uphill experiment. When the value of $\frac{gG}{a_m}$ is large, it seems that vehicles are crawling on the uphill and the whole uphill segment is in a homogeneous traffic state; see examples of trajectories on the left column of Figure 7:14. Interestingly, oscillations arise regularly upstream of the uphill segment. Of course, after drivers pass the uphill, they start to accelerate.

The relationship between the period of traffic oscillation and $\frac{gG}{a_m}$ is illustrated in Figure 7:16. It can be observed that (i) all three models show a well-defined negative relationship between oscillation period and the ratio $\frac{gG}{a_m}$; but (ii) the slope of the curve from the AB2 model is steeper than that from the AB1 model, and (iii) period from AB2 model is larger than the AB1 model. Observations (ii) &(iii) are supported by results the Mann-Whitney U test, which compared periods from the two models across different $\frac{gG}{a_m}$ values and found that the difference is significant ($p = 0.02$). The periods under each $\frac{gG}{a_m}$ value from the two models were tested using the student's t-test. It is found that the

periods are significantly different for half of the $\frac{gG}{a_m}$ values; see Table 9 in Appendix C. In the student's t-test, the difference is not found for some $\frac{gG}{a_m}$ values, which may be because of the large standard deviation; see Table 8-(B-C) in Appendix C.

Periods from the L-L model are also compared with the other models, but Mann Whitney U test suggests no significant difference at 95% confidence level. This result, however, is less conclusive because comparison was conducted only for $\frac{gG}{a_m} \geq 0.29$. Periods when $\frac{gG}{a_m} < 0.25$ were not available for the L-L model because traffic oscillations were not periodic.

Results on the relationship between oscillation period and $\frac{gG}{a_m}$ indicates that the period of oscillations seems to be related to the crawling speed on the uphill; i.e., the traffic state near the traffic oscillation formation zone. This is consistent with observations from the rubbernecking experiment.

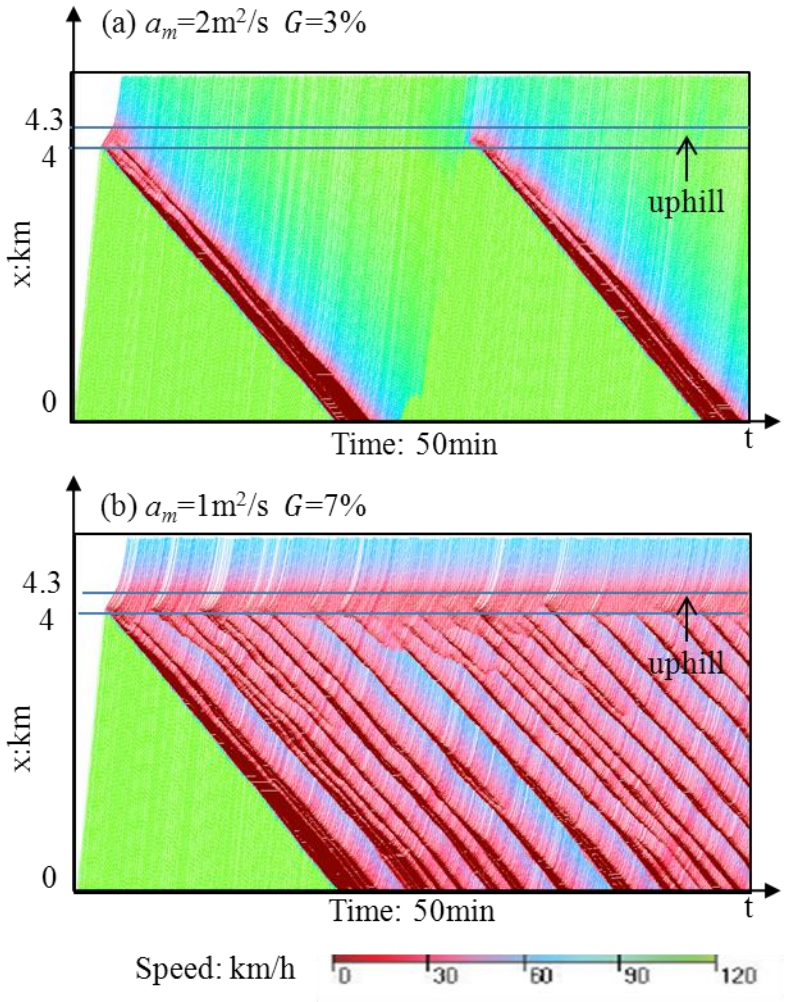

Figure 7:14 Traffic Oscillations from Uphill Experiment - AB2 Model

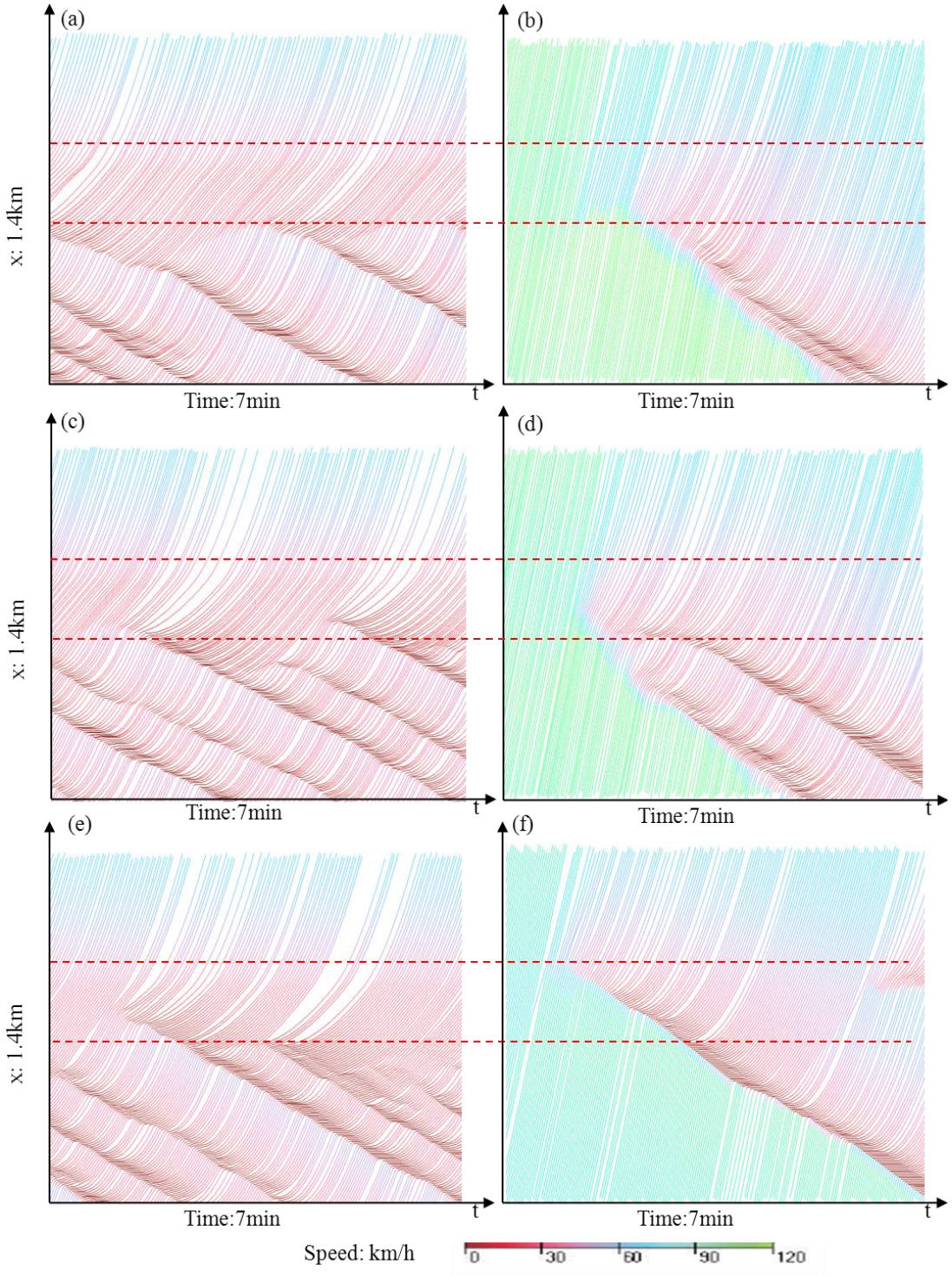

Figure 7:15 Trajectories for Uphill Experiment

(Left column: $a_m = 1m/s^2$, $G = 7\%$; right column: $a_m = 1m/s^2$, $G = 3\%$; dashed lines: bottom and top of uphill segment)

(a-b): AB2 model; (c-d): AB1 model; (e-f) L-L model.

(a) (b)

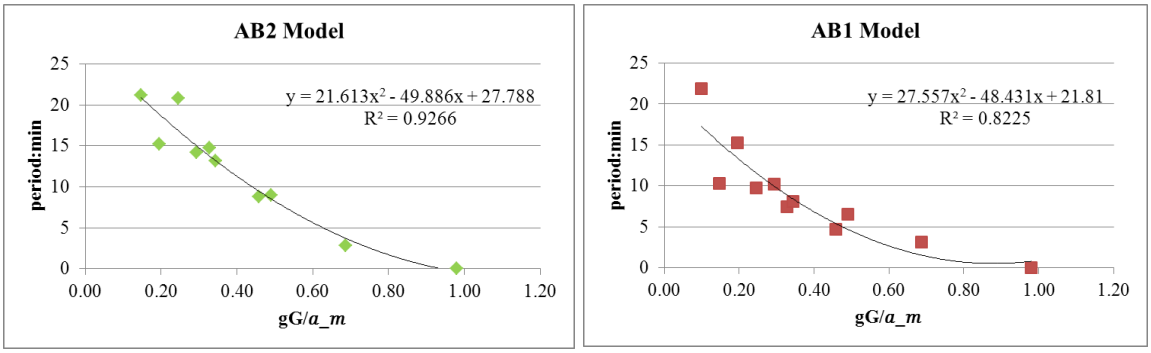

(c) (d)

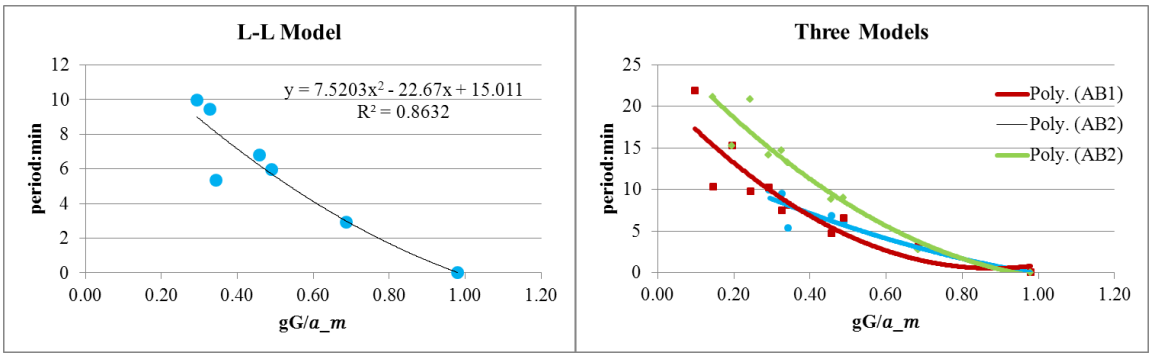

Figure 7:16 Impacts of $\frac{gG}{a_m}$ on Oscillation Period

7.2.3 Discussions

The rubbernecking experiment and uphill experiment show that rubbernecking or uphill can trigger traffic oscillations to form. All three models, the AB2, AB1, and L-L models, are able to capture the formation and propagation of traffic oscillations. Simulation results suggest that the AB2 model has significant advantages over the L-L model mainly in three aspects: it is able to (1) show clear precursor region, (2) produce the hysteresis patterns associated with different development stages of traffic oscillations; and (3) capture the connection between oscillation period and the traffic state near the traffic oscillations formation zone. The performance of the AB1 model turns out to be a

transition from the L-L model to the AB2 model. For example, it is able to capture (3), but not (1) and (2). Of course, the oscillation periods from the two models are significantly different too. It seems that the AB2 model has captured the upper bound of oscillation period. But more empirical observation is needed to validate the results and to determine whether the period is underestimated. Nevertheless, given that (1) & (2) are not only related to the period of traffic oscillations but also the impacts of traffic oscillations on traffic flow, the improvement of the AB2 model over the AB1 model is significant.

For application purpose, if general macroscopic features are desired, the L-L model, which is the most parsimonious, may be used. For example, it can be used to estimate the magnitude of the impacts of traffic oscillations on fuel efficiency. However, the AB2 model should be used for microscopic studies such as individual driver behavior and impact evaluation. Of course, the tradeoff is that the AB2 model is less parsimonious. The performance of the AB1 model is between the L-L model and the AB2 model. Hence, it could be used if model parsimoniousness is the priority, but one should be aware that the AB1 model may miss some important features, especially for those features associated with the growth stage of traffic oscillations.

Simulation results from the AB2 model provide some insights on understanding how oscillation period is related to other factors. However, the mechanism is complicated and has not been fully investigated in the literature. To the best knowledge of the author, the study of Treiber and Kesting (Treiber and Kesting, 2011) is the only one, but it only shows that the period of traffic oscillation is related to the strength of bottleneck, which is represented by the speed. Simulation results from the AB2 model seem to confirm the role of speed as per (Treiber and Kesting, 2011) but also reveal more insights on the mechanism. For example, simulations suggest that not only the magnitude of speed reduction but also the acceleration capability may play a role. More research is needed to understand the mechanism.

Once the mechanism of determining period of oscillation is clear, the parameters of the rubbernecking experiment, r and p, can be calibrated. To this end, a massive data collection plan is needed, which should include not only vehicle trajectory data but also video footage capturing driver head/eye movement to identify the rubberneckers and their speed reduction. Note that the Strategic Highway Research Program 2 (SHRP2) naturalistic driving study (2011) is collecting data on in-vehicle driving behavior, including continuous video of driver and vehicle movement, which can be used to examine driver's behavior and/or errors. Once these data become available, r and p can be estimated. Similar situation applies to the uphill experiment. As the grade of uphill can be easily measured, the results from the uphill experiment can be validated. Of course, one should be cautious in transferring our results to different driver population, because the model parameters are correlated and may vary with driver populations. In applications, one may use the sample enumeration to generate the parameters as in this study if a large sample is not available or assume a joint distribution estimated from a large sample size.

In the simulations of the AB2 model, there was a delay in starting the fully-developed stage. This problem can be eliminated if trajectories are updated spatially vehicle by vehicle; i.e., each time the position of a vehicle is updated in the whole spatial frame. In this case, when the follower enters the simulated segment, the dynamics of the leading vehicle within the simulated segment is all known. Of course, whether the leader has come to a complete stop can be easily told. The potential tradeoff of this method is the extra memory required in the simulation process because all the temporal-spatial information of the leading vehicle is needed to update the following vehicle. Future research is needed to evaluate the tradeoff and the impact of the delay in fully-developed stage.

The result that the AB2 model is able to capture the potential discharge rate reduction (or capacity drop at bottlenecks) imposed by growth-stage oscillations suggests

that the AB2 model could be used to study the capacity drop phenomenon at active merge bottleneck. Active merge bottlenecks refer to bottlenecks caused by merging traffic and the bottleneck capacity is not predetermined. It was thought that capacity drop at such bottlenecks was attributed to voids created by lane-changes with finite acceleration (Cassidy and Rudjanakanoknad, 2005; Laval and Daganzo, 2006; Laval and Leclercq, 2008). However, in a recent study Leclercq and Laval (Leclercq et al., 2011) proposed a model for the capacity drop at active merge bottleneck based on the impacts created by lane-changing voids and found that the model performed well when congestion is light but poorly in stop-and-go traffic. This finding suggests that lane-changing voids are not sufficient to explain the capacity drop and traffic oscillations in stop-and-go traffic may play an important role. The latter is consistent with the empirical and simulation results in this study. Hence, the AB2 model can be used to explore the mechanism of capacity drop at active merge bottleneck and quantify the effect of traffic oscillations. Note that the overall effect may be related to the period of oscillations since discharge rate reduction is only observed in the growth stage of traffic oscillations. It is likely that the discharge ration reduction in the long term will depend on the magnitude of reduction in the growth stage and the time proportion of the growth stage in an oscillation cycle.

The rubbernecking model has great potential to be used to explore the relationship between traffic oscillations and lane-changing maneuver. Essentially, the behavior of a lane-changer on the target lane is very similar to a rubbernecker after rubbernecking occurs: he/she starts with a speed lower than the traffic stream right downstream and accelerates thereafter. The insertion with lower driving speed creates a deceleration wave and it forces following drivers to react. Similarly, the acceleration of the lane-changer after insertion creates an acceleration wave. These deceleration-acceleration process forms an oscillation cycle. In this sense, the rubbernecking experiment seems to be similar to a highway section where lane-insertion occurs within a short segment such as a merging section. Of course, if the rubbernecking zone is relaxed

to vary with each rubbernecker, the experiment can model lane-insertion on regular highway segment. In this case, the AB2 model is expanded to include both car-following and lane-changing behavior, which will yield a more comprehensive representation of the highway traffic. The expanded model will have broad application potentials. For example, it can be used to fully estimate capacity drop at active merge bottlenecks or quantify the environmental and economic impacts of traffic oscillations.

CHAPTER 8 CONCLUSIONS AND FUTURE RESEARCH

8.1 Conclusions

This study has developed an asymmetric behavioral model that describes the complete dynamic behavior profile of drivers experiencing traffic oscillations based on empirical trajectory data. The model is able to produce traffic oscillations with consistent macroscopic and macroscopic features as observed empirically.

The main conclusions drawn from this study are as follows:

(1) Driver's aggressive/timid behaviors cause traffic oscillations to grow and propagate.

(2) Driver's aggressive/timid behaviors during traffic oscillations are highly correlated with their characteristic before oscillations (i.e., in equilibrium).

(3) Driver's behavior in the growth stage of traffic oscillations is different than in the fully-developed stage.

(4) The triggers for non-equilibrium behavior are mainly the deceleration or acceleration waves.

The major contribution of this study is that it improves the understanding of the formation and propagation mechanism of traffic oscillations and that it proposes an asymmetric behavioral model that is able to capture the mechanism. Particularly, the behaviors of drivers when experiencing traffic oscillations become clear and their connection with the formation and propagation of traffic oscillations is explicit. The model proposed has great potential to be used to investigate other features of traffic oscillations and study the impacts of the traffic oscillation phenomenon.

Another contribution is that this study has uncovered the main generation mechanisms of traffic hysteresis using the asymmetric behavioral model proposed. The mechanisms unveiled help to better understand the nature of driving dynamics, which

allows for investigations on other characteristics of traffic hysteresis and the corresponding impacts such as the connection with capacity drop.

A third contribution is that simulations of a rubbernecking experiment using the asymmetric behavior model suggest that rubbernecking may be the trigger of the traffic oscillations observed on US101 in the NGSIM data. Traffic oscillations produced from simulations are very consistent with the empirical data in terms of the oscillation period and the traffic hysteresis patterns associated with different development stages of oscillations. These results suggest that the asymmetric behavioral model can be used to study the trigger of traffic oscillations.

8.2 Limitations

The limitation of this study includes the following aspects:

(1) Limited trajectory length. It is possible that the driver behavior change after experiencing growing traffic oscillations is because the trajectories are too short to capture the recovery. Due to the limited length of the trajectories studied, this possibility not examined. This is to be explored once extensive trajectories are available.

(2) Lack of comparison across different study sites. In this study, measurement is conducted on only one site, the US101 segment. Although NGSIM (NGSIM, 2006) has trajectory data for another site, I-80, very few traffic oscillations from this site have the complete growth-fully-developed process. Thus, this site was not included. Except for NGSIM, no other complete dataset is available. However, it should be aware that driver behavior may vary with study site. Comparison across different sites is needed before generalizing the model. It is conjectured that the correlation between driver characteristic and driver behavior during oscillations holds generally but the value of the model parameters will vary

such as the proportion of aggressive/timid drivers and the probability to adopt a certain reaction to oscillations.

(3) Lack of validation and calibration of experiment parameters. In the rubbernecking experiment and uphill experiments conducted, the parameters (e.g., proportion of rubbernecker) are not validated or calibrated. This was not conducted in this study because for the rubbernecking experiment massive data is needed to estimate the parameters but that is not available currently; while for the uphill case, and no empirical trajectory data on uphill is available for validation or calibration. More data is needed for this purpose.

8.3 Future Research

Future research can be conducted in several directions.

(1) Improvement. Future research should be conducted to address the limitations described above to improve the model proposed. Additionally, some features of oscillations observed need further exploration such as the regular period exhibited, which is particularly important if quantitative outcome is desired.

(2) Extension. One important extension is to incorporate lane-changing activity, which requires a microscopic model that describes how drivers behave in the lane-changing process and a macroscopic model that describes how lane-changing is distributed across lanes. For example, the hybrid lane-changing model proposed by Laval (Laval and Daganzo, 2006) can be used. With that extension, the model can be used to predict traffic oscillations for multiple lanes on homogeneous or inhomogeneous (with exit or entrance) highway segments. Of course, it also can be used to explore the capacity drop phenomenon at bottlenecks such as the active merge bottleneck discussed in chapter 7.

(3) Application. Since the model proposed is able to produce traffic oscillations consistently with empirical observations, the impact evaluation of traffic oscillations can be conducted. For example, to quantify the increase of greenhouse emission and also the decrease of fuel efficiency. This can be conducted by using the model to produce vehicle trajectories with and without traffic oscillations and then evaluating the emission level respectively. Besides, the safety impacts of oscillations can be studied. Zheng et al. (Zheng et al., 2010) found that accident rate could increase by 5% in oscillatory traffic. However, it is still unclear what behavior is responsible for the safety risk increase. The behavioral model proposed could be used to explore this problem and predict the risk increase.

APPENDIX

A. Chi-square Test

In the chi-square test for homogeneity, the test-statistic is calculated as follows. For r samples with c categories of outcome in each sample, the value of the test-statistic is

$$X^2 = \sum_{i=1}^{r} \sum_{j=1}^{c} \frac{(O_{i,j} - E_{i,j})^2}{E_{i,j}},$$

where $o_{i,j}$ is the observation frequency for sample i category j, and $E_{i,j}$ is the corresponding expected value given by

$$E_{i,j} = \frac{(\sum_{k=1}^{c} O_{i,k})(\sum_{k=1}^{r} O_{k,j})}{\sum_{i=1}^{r} \sum_{j=1}^{c} O_{i,j}}.$$

The test-statistic is used to calculate the significance level (p-value) with degree of freedom $df = (c - 1) * (r - 1)$. Note that this test requires the frequency of each category in each sample to be equal or greater than 5 when $df \geq 2$ and equal or greater than 10 if $df = 1$. In our study, some categories were combined to meet this requirement.

B. Mann-Whitney U test

The Mann-Whitney U test (Kvam and Vidakovic, 2007) is used to assess whether two samples of independent observations are different from each other in respect of the center. This test requires the sample to be ordinal. Let $X_1, \ldots, X_{n1}$ and $Y_1, \ldots, Y_{n2}$ be two independent samples. The statistic is called U, which can be calculated in the following way:

$$U = \sum_{i=1}^{n1} \sum_{j=1}^{n2} D_{ij},$$

where D_{ij} is defined as $D_{ij} = I\ (Y_j < Y_j)$.

When the sample size is large, the distribution of U is approximately normal. In this case, the standardized value

$$z = \frac{U - m_U}{\sigma_U},$$

where m_U and σ_U are the mean and standard deviation of U, is approximately a standard normal deviate whose significance follows the tables of normal distribution. These two values are given by

$$m_U = \frac{n_1 n_2}{2},$$

$$\sigma_U = \sqrt{\frac{n_1 n_2 (n_1 + n_2 + 1)}{12}}.$$

The significance level can be obtained with the z value.

C. Tables

Table 1 Distribution of Hysteresis Pattern

	CCW loop	straight line	CW loop	multiple loop & others	overlap
Growth	17	12	64	9	11
Fully-developed	38	13	45	28	12

Table 2 Driver Category vs. Reaction Pattern

OT	Stage	convex	others	
p-value	Growth Stage	18	13	
0.972	Fully-developed Stage	16	13	
ON		convex	concave	others

p-value	Growth Stage	9	8	16
0.033	Fully-developed Stage	9	27	15
OA		concave	others	
p-value	Growth Stage	17	32	
0.000	Fully-developed Stage	45	11	

Table 3 Hysteresis Patterns for Different Driver Categories

OT		CCW	CW	Others
p-value	Growth Stage	11	10	9
0.8	Fully-developed Stage	10	6	8
ON		CCW	CW	Others
p-value	Growth Stage	5	19	7
0.055	Fully-developed Stage	13	15	17

OA		CW	Others	
p-value	Growth Stage	36	10	
0.003	Fully-developed Stage	23	26	

Table 4-A: Rubbernecking Experiment: L-L Model

r(%)	2	4	6	8	10	15
p(%)	a_m=0.5					
0.6	5.2	3.6	3.3	3.2	2.8	2.6
	0.4	0.2	0.1	0.1	0.2	0.2
0.7	5.7	3.9	3.8	3.5	3.2	2.6
	0.3	0.2	0.1	0.3	0.1	0.2
0.8	5.6	4.1	4.0	3.7	3.8	3.3
	0.1	0.1	0.1	0.1	0.1	0.2
0.9	6.8	5.2	4.9	4.6	4.6	4.5
	0.2	0.1	0.1	0.1	0.0	0.0
std(p)/mean	0.1	0.2	0.2	0.2	0.2	0.3
p(%)	a_m=1.5					
0.6	4.6	3.2	3.8	3.6	3.1	2.3
	0.2	0.1	0.1	0.1	0.1	0.2
0.7	4.3	3.7	3.9	3.4	2.8	2.3
	0.1	0.2	0.1	0.2	0.2	0.2
0.8	5.8	4.8	4.0	4.0	3.5	2.9
	0.2	0.2	0.1	0.3	0.2	0.2
0.9	6.0	4.7	4.6	3.6	4.0	3.6

	0.2	0.1	0.1	0.1	0.2	0.1
std(p)/mean	0.2	0.2	0.1	0.1	0.2	0.2
p(%)	a_m=2.5					
0.6	4.9	4.6	3.6	3.1	2.9	2.4
	0.2	0.0	0.2	0.2	0.0	0.1
0.7	4.9	4.0	3.1	3.0	2.8	2.5
	0.3	0.0	0.1	0.1	0.2	0.1
0.8	5.0	4.6	3.6	3.4	3.2	3.0
	0.2	0.1	0.2	0.3	0.2	0.1
0.9	6.6	5.2	4.0	4.1	3.9	3.2
	0.1	0.3	0.2	0.2	0.1	0.1
std(ps)/mean	0.2	0.1	0.1	0.2	0.2	0.1

Table 4-B: Rubbernecking Experiment: AB1 Model

r(%)	**2**	**4**	**6**	**8**	**10**	**15**
p(%)	a_m=0.5					
0.6	5.8	4.2	3.6	2.6	2.6	2.2
	0.2	0.2	0.2	0.1	0.1	0.1
0.7	6.2	4.4	3.7	3.6	2.7	2.5
	0.2	0.1	0.2	0.1	0.1	0.2
0.8	6.4	5.4	4.6	3.4	3.6	3.1
	0.2	0.1	0.3	0.1	0.1	0.0
0.9	9.1	6.5	6.2	6.6	5.1	4.8
	0.2	0.1	0.1	0.1	0.1	0.1
std(p)/mean	0.2	0.2	0.3	0.4	0.3	0.4

p(%)	a_m=1.5					
0.6	4.8	5.2	2.8	2.7	2.2	2.0
	0.2	0.2	0.2	0.1	0.2	0.1
0.7	5.4	4.3	3.9	4.0	3.4	2.4
	0.1	0.1	0.1	0.1	0.2	0.1
0.8	5.5	4.7	4.7	4.6	4.1	3.4
	0.3	0.1	0.2	0.1	0.1	0.1
0.9	6.3	5.7	5.2	5.4	4.8	4.4
	0.1	0.1	0.2	0.1	0.1	0.1
std(p)/mean	0.1	0.1	0.2	0.3	0.3	0.3
p(%)	a_m=2.5					
0.6	4.6	4.1	3.9	3.6	3.1	2.6
	0.1	0.2	0.1	0.2	0.1	0.2
0.7	4.8	4.5	4.0	3.2	3.2	2.8
	0.1	0.1	0.2	0.1	0.0	0.2
0.8	5.9	5.1	5.1	4.5	3.7	3.4
	0.2	0.2	0.1	0.2	0.1	0.1
0.9	8.2	5.6	6.2	5.1	4.7	3.6
	0.1	0.2	0.1	0.1	0.1	0.3
std(p)/mean	0.3	0.1	0.2	0.2	0.2	0.2

Table 4-C: Rubbernecking Experiment: AB2 Model

r(%)	2	4	6	8	10	15
p(%)	a_m=0.5					
0.6	6.7	7.2	5.9	4.2	3.9	3.7

	0.2	0.3	0.4	0.1	0.2	0.3
0.7	8.1	6.0	4.7	5.6	4.6	4.4
	0.6	0.2	0.4	0.2	0.2	0.2
0.8	8.6	8.6	5.7	6.1	5.3	5.3
	0.3	0.3	0.2	0.2	0.1	0.4
0.9	11.1	10.9	8.9	7.5	7.5	6.4
	0.5	0.3	0.1	0.2	0.4	0.2
std(p)/mean	0.2	0.3	0.3	0.2	0.3	0.2
p(%)	a_m=1.5					
0.6	7.5	5.3	5.4	4.9	3.4	3.4
	0.1	0.2	0.3	0.2	0.3	0.2
0.7	7.7	7.5	5.7	4.7	4.6	3.8
	0.2	0.1	0.1	0.3	0.2	0.2
0.8	9.5	8.0	8.2	6.4	4.9	5.1
	0.3	0.3	0.2	0.4	0.2	0.1
0.9	12.2	11.0	9.8	8.0	6.3	6.3
	0.4	0.3	0.1	0.3	0.2	0.2
std(p)/mean	0.2	0.3	0.3	0.3	0.2	0.3
p(%)	a_m=2.5					
0.6	9.1	6.7	7.0	3.8	3.6	4.1
	0.2	0.3	0.2	0.2	0.4	0.3
0.7	8.5	6.9	7.3	5.2	5.1	3.7
	0.1	0.2	0.2	0.2	0.1	0.3
0.8	10.7	6.9	6.7	5.9	6.2	5.5
	0.1	0.3	0.2	0.3	0.2	0.3
0.9	13.8	12.5	8.9	8.6	7.4	7.6

	0.1	0.2	0.5	0.1	0.2	0.3
std(p)/mean	0.2	0.3	0.1	0.3	0.3	0.3

Table 5: p-value from Mann-Whitney U test on period (grey cells: $\boldsymbol{p \leq 0.05}$)

p (%)	0.6	0.7	0.8	0.9	0.6	0.7	0.8	0.9	0.6	0.7	0.8	0.9
$\boldsymbol{a_m}$ (m/s^2)	0.50				1.50				2.50			
L-L vs. AB1	0.81	1.00	1.00	0.11	0.59	0.30	0.52	0.08	0.81	0.33	0.09	0.31
AB2 vs. L-L	0.02	0.03	0.01	0.01	0.05	0.01	0.01	0.00	0.07	0.01	0.00	0.00
AB2 vs. AB1	0.04	0.04	0.05	0.05	0.04	0.06	0.01	0.01	0.11	0.02	0.01	0.01

Table 6: p-value from Mann-Whitney U test on period when $p = 0.6$ vs $p = 0.9$ (grey cells: $\boldsymbol{p \leq 0.05}$)

$\boldsymbol{a_m}$ (m/s^2)	L-L	AB1	AB2
0.5	0.03	0.01	0.01
1.5	0.06	0.02	0.01
2.5	0.18	0.02	0.03

Table 7: p-value from Mann-Whitney U test on $\boldsymbol{a_m}$

a_m (m/s^2)	L-L	AB1	AB2
0.5 vs. 1.5	0.52	0.73	0.95
1.5 vs. 2.5	0.79	0.94	0.50
0.5 vs. 2.5	0.29	0.93	0.46

Table 8-A: Uphill Measurement: L-L Model

gG/a	0.29	0.33	0.34	0.46	0.49	0.69	0.98
Period (min)	10.0	9.5	5.4	6.8	6.0	2.9	0.0
CV	0.49	0.33	0.16	0.51	0.28	0.26	NA

Table 8-B: Uphill Measurement: AB1 Model

gG/a	0.10	0.15	0.20	0.25	0.29	0.33	0.34	0.46	0.49	0.69	0.98
Period (min)	21.9	10.3	15.3	9.8	10.2	7.4	8.1	4.7	6.6	3.2	0.0
CV	0	0.38	0.52	0.21	0.25	0.22	0.13	0.41	0.15	0.26	NA

Table 8-C: Uphill Measurement: AB2 Model

gG/a	0.15	0.20	0.25	0.29	0.33	0.34	0.46	0.49	0.69	0.98
Period (min)	21.2	15.3	20.8	14.2	14.7	13.2	8.8	9.0	2.8	0.0
CV	0.31	0.06	0.21	0.08	0.41	0.42	0.31	0.40	0.11	NA

Table 9: Period from Three models in uphill Measurement (grey cells: $\boldsymbol{p \leq 0.05}$)

gG/a_m	0.15	0.20	0.25	0.29	0.33	0.34	0.46	0.49	0.69	0.98
***p*-value**	0.0866	NA	0.00	0.02	0.05	0.11	0.03	0.21	0.37	0.00

REFERENCES

Ahn, S., 2005. Growth of oscillations in queued traffic. *Ph.D. thesis, Depart. of Civil Engineering, University of California, Berkeley*.

Ahn, S., Cassidy, M.J., 2006. Freway traffic oscillations and vehicle lane-changing manuevers. *The 17th International Symposium on Transportation and Traffic flow Theory. Elseview, New York.*

Ahn, S., Cassidy, M.J., Laval, J., 2004. Verification of a simplified car-following theory. *Transportation Research Part B* 38, 431-440.

Ahn, S., Laval, J.A., Cassidy, M., 2010. Merging and Diverging Effects on Freeway Traffic Oscillations: Theory and Observation. *Transportation Research Record* Forthcoming.

Ahn, S., Vadlamani, S., Laval, J.A., 2011. A method to account for non-steady conditions in measuring traffic hysteresis. *Transportation Research Part C* (In Press).

Bando, M., Hasebe, K., Nakayama, A., Shibata, A., Sugiyama, Y., 1995. Dynamical model of traffic congestion and numerical simulation. *Physical Review E* 51, 1035.

Banks, J.H., 1989. Freeway speed-flow-concentration relationships: more vidence and interpretations (with discussion and closure). *Transportation Research Record*, 53-60.

Barlovic, R., Huisinga, T., Schadschneider, A., Schreckenberg, M., 2002. Open boundaries in a cellular automaton model for traffic flow with metastable states. *Physical Review E* 66, 046113.

Barlovic, R., Santen, L., Schadschneider, A., Schreckenberg, M., 1998. Metastable states in cellular automata for traffic flow. *The European Physical Journal B - Condensed Matter and Complex Systems* 5, 793-800.

Bilbao-Ubillos, J., 2008. The costs of urban congestion: estimation of welfare losses arising from congestion on cross-town link roads. *Transportation Research Part A* 42, 1098-1108.

Cassidy, M.J., 1998a. Bivariate relations in nearly stationary highway traffic. *Transportation Research Part B* 32, 49-59.

Cassidy, M.J., 1998b. Bivariate relations in nearly stationary highway traffic. *Transportation Research Part B: Methodological* 32, 49-59.

Cassidy, M.J., Rudjanakanoknad, J., 2005. Increasing the capacity of an isolated merge by metering its on-ramp. *Transportation Research Part B: Methodological* 39, 896-913.

Cassidy, M.J., Windover, J.R., 1995. Methodology for assessing dynamics of freeway traffic flow. *Transportation Research Record*, 73-79.

Chandler, R.E., Herman, R., Montroll, E.W., 1958. Traffic dynamics: studies in car following, *Operations Research*. INFORMS: Institute for Operations Research, p. 165.

Chen, D., Laval, J.A., Zheng, Z., Ahn, S., 2012. Traffic oscillations: a behavioral car-following model. *Transportation Research Part B* (In press).

Chiabaut, N., Buisson, C., Leclercq, L., 2009a. Fundamental Diagram Estimation Through Passing Rate Measurements in Congestion. *Intelligent Transportation Systems, IEEE Transactions on* 10, 355-359.

Chiabaut, N., Leclercq, L., Buisson, C., 2009b. From heterogeneous drivers to macroscopic patterns in congestion. *Transportation Research Part B* 44, 299-308.

Daganzo, C.F., 2002. A behavioral theory of multi-lane traffic flow. Part I: Long homogeneous freeway sections. *Transportation Research Part B* 36, 131-158.

del Castillo, J.M., 2001. Propagation of perturbations in dense traffic flow: a model and its implications. *Transportation Research Part B* 35, 367-389.

Durent, A., Ahn, S., Buisson, C., 2011. Passing rates to measure relaxation and impact of lane-changing in queue. *Computeraided engineering and infrastructure engineering* 26, 285-297.

Edie, L.C., 1961. Car-following and steady-state theory for noncongested traffic, *Operations Research*. INFORMS: Institute for Operations Research, pp. 66-76.

Edie, L.C., Foote, R.S., 1958. Traffic flow in tunnels. *Highway Research Board Proceedings* 37.

Edie, L.C., Foote, R.S., 1960. Effect of shock waves on tunnel traffic flow. *Proc. Highw. Rec. Bd* 39, 492-505.

Edie, L.C., Foote, R.S., 1961. Experiments on single-lane flow in tunnels. *Theory of traffic flow, Amsterdam*, 193-206.

FHWA, 2000. The capability and enhancement of vdanl and twopas for analyzing vehicular performance on upgrades and downgrades within ihsdm. *Technical Report. 00-078, Federal Highway Administration*.

Forbes, T.W., Zagorski, M.J., holshouser, E.L., Deterline, W.A., 1958. Measurement of driver reactions to tunnel condition *Proc. Highw. Rec. Bd* 37, 345-357.

Foster, J., 1962. An investigation of the hydrodynamic model for traffic flow with particular reference to the effect of various speed-density relationships. *In: 1st Conference of the Australian Road Research Board*.

Gasser, I., Sirito, G., Werner, B., 2004. Bifurcation analysis of a class of car following traffic models. *Physica D: Nonlinear Phenomena* 197, 222-241.

Gazis, D.C., Herman, R., Rothery, R.W., 1961. Nonlinear follow-the-leader models of traffic flow, *Operations Research*. INFORMS: Institute for Operations Research, pp. 545-567.

Gipps, P.G., 1981. A behavioural car-following model for computer simulation. *Transportation Research Part B* 15, 105-111.

Greenberg, H., Daou, A., 1960. The control of traffic flow to increase the flow. *Operations Research* 8, 524-532.

Greenwood, P.E., Nikulin, M.S., 1996. A guide to chi-squared testing. *Wiley-Interscience (1 edition)*.

Hall, F.L., Allen, B.L., Gunter, M.A., 1986. Empirical analysis of freeway flow-density relationships. *Transportation Research Part A* 20, 197-210.

Helbing, D., Hennecke, A., Shvetsov, V., Treiber, M., 2001. MASTER: macroscopic traffic simulation based on a gas-kinetic, non-local traffic model. *Transportation Research Part B* 35, 183-211.

Helbing, D., Moussaid, M., 2009. Analytical calculation of critical perturbation amplitudes and critical densities by non-linear stability analysis of a simple traffic flow model. *The European Physical Journal B - Condensed Matter and Complex Systems* 69, 571-581.

Helbing, D., Treiber, M., 1998. Gas-Kinetic-Based Traffic Model Explaining Observed Hysteretic Phase Transition. *Physical Review Letters* 81, 3042.

Herman, R., Montroll, E.W., Potts, R.B., Rothery, R.W., 1959. Traffic dynamics: analysis of stability in car following, *Operations Research*. INFORMS: Institute for Operations Research, p. 86.

Hillegas, B.B., Houghton, D.G., Athol, P.J., 1974. Investigation of flow-density discontinuity and dual-mode traffic behavior. *Transportation Research Record*, 53-63.

Hoogendoorn, S., Van Zuylen, H., Schreuder, M., Gorte, B., Vosselman, G., 2003. Microscopic Traffic Data Collection by Remote Sensing. *Transportation Research Record* 1855, 121-128.

Igarashi, Y., Itoh, K., Nakanishi, K., Ogura, K., Yokokawa, K., 2001. Bifurcation phenomena in the optimal velocity model for traffic flow. *Physical Review E* 64, 047102.

Kerner, B.S., Rehborn, H., 1996. Experimental features and characteristics of traffic jams. *Physical Review E* 53, R1297.

Kim, T., Zhang, H.M., 2008. A stochastic wave propagation model. *Transportation Research Part B* 42, 619-634.

Kometani, E., Sasaki, T., 1958. On the stability of traffic flow. *Journal of the Operations Research Society of Japan* 2, 11-26.

Koshi, M., Iwasaki, M., Ohkuru, I., 1983. Some findings and and overview on vehicular flow characteristics. *The 8th International Symposium on Transportation and Traffic flow Theory. In: Hurdle, V., Hauer, E., Stuart, G. (Eds.)*, 403-426.

Koshi, M., Kuwahara, M., Akahane, H., 1992. Capacity of sags and tunnels in Japanese motorways. *ITE Journal* 2, 17-22.

Krauss, S., Wagner, P., Gawron, C., 1997. Metastable states in a microscopic model of traffic flow. *Physical Review E* 55, 5597-5602.

Kvam, P.H., Vidakovic, B., 2007. Nonparametric Statistics with Applications to Science and Engineering. *Wiley Series in Probability and Statistics*.

Laval, J., 2006. Stochastic Processes of Moving Bottlenecks: Approximate Formulas for Highway Capacity. *Transportation Research Record* 1988, 86-91.

Laval, J., Chen, D., Amer, K., Guin, A., Ahn, S., 2009. Evolution of Oscillations in Congested Traffic. *Transportation Research Record* 2124, 194-202.

Laval, J.A., 2004. Hybrid models of traffic flow: impacts of bounded vehicle acceleratins. *Ph.D. thesis, Depart. of Civil Engineering, University of California, Berkeley*.

Laval, J.A., 2010. Hysteresis in traffic flow revisited: An improved measurement method. *Transportation Research Part B* 45, 385-391.

Laval, J.A., Daganzo, C.F., 2006. Lane-changing in traffic streams. *Transportation Research Part B* 40, 251-264.

Laval, J.A., Leclercq, L., 2008. Microscopic modeling of the relaxation phenomenon using a macroscopic lane-changing model. *Transportation Research Part B* 42, 511-522.

Laval, J.A., Leclercq, L., 2010. A mechanism to describe the formation and propagation of stop-and-go waves in congested freeway traffic. *Philosophical Transactions of the Royal Society A: Mathematical, Physical and Engineering Sciences* 368, 4519-4541.

Leclercq, L., Laval, J.A., Chiabaut, N., 2011. Capacity drops at merges: An endogenous model. *Transportation Research Part B: Methodological* 45, 1302-1313.

Lee, H.Y., Lee, H.W., Kim, D., 1998. Origin of Synchronized Traffic Flow on Highways and Its Dynamic Phase Transitions. *Physical Review Letters* 81, 1130-1133.

Li, X., Ouyang, Y., 2011. Characterization of traffic oscillation propagation under nonlinear car-following laws. *Transportation Research Part B: Methodological* 45, 1346-1361.

Li, X., Peng, F., Ouyang, Y., 2009. Measurement and estimation of traffic oscillation properties. *Transportation Research Part B* 44, 1-14.

Lighthill, M.J., Whitham, G.B., 1955. On Kinematic Waves. I. Flood Movement in Long Rivers. *Proceedings of the Royal Society of London. Series A. Mathematical and Physical Sciences* 229, 281-316.

Maes, W., 1979. Traffic data collection system for the Belgian motorway network-measures of effectiveness aspects. *Proceedings of the International Symposium on Traffic Control Systems. 2D-Analysis and Evaluation*, 45-73.

Mauch, M., Cassidy, M.J., 2002. Freeway traffic oscillations: observation and predictions. *The 15th International Symposium on Transportation and Traffic flow Theory. (ed. by M.P. Taylor)*

Munoz, J., Daganzo, C.F., 2000a. Experimental characterization of multi-lane freeway traffic upstream of an off-ramp bottleenck. *Technical Report. UCB-ITS-PWP-2000-13, Institute of Transportation Studies, University of California, Berkeley, CA.*

Munoz, J., Daganzo, C.F., 2000b. Structure of the transition zone behind freeway queues. *Transportation Science* 37, 312.

Nagel, K., Schreckenberg, M., 1992. A cellular automaton model for freeway traffic. *J. Phys. I France* 2, 2221-2229.

Newell, G.F., 1961. Nonlinear effects in the dynamics of car following, *Operations Research*. INFORMS: Institute for Operations Research, pp. 209-229.

Newell, G.F., 1965. Instability in dense highway traffic, a review. *The 2nd International Symposium on Transportation and Traffic flow Theory (ed J. Almond)*, 73-83.

Newell, G.F., 1993. A simplified theory of kinematic waves in highway traffic, part I: general theory; part II: queuing at freeway bottlenecks; part III: multi-destination flows. *Transportation Research Part B* 27, 281-313.

Newell, G.F., 2002. A simplified car-following theory: a lower order model. *Transportation Research Part B* 36, 195-205.

Ngoduy, D., 2008. Operational effects of acceleration lane on main traffic flow at discontinuities. *Transportmetrica* 4, 195 - 207.

Ngoduy, D., Hoogendoorn, S., Van Zuylen, H., 2006. Part 2: Car-Following Models: Continuum Traffic Model for Freeway with On- and Off-Ramp to Explain Different Traffic-Congested States. *Transportation Research Record* 1965, 91-102.

NGSIM, 2006. Next generation simulation. *http://ops.fhwa.dot.gov/trafficanalysistools/ngsim.htm*.

Orosz, G., Stepan, G., 2006. Subcritical hopf bifurcations in a car-following model with reaction time delay. *Proceedings of the Royal Society A* 462, 2643-2670.

Orosz, G., Wilson, R.E., Krauskopf, B., 2004. Global bifurcation investigation of an optimal velocity traffic model with driver reaction time. *Physical Review E* 70, 026207.

Orosz, G.b., Wilson, R.E., Szalai, R.b., StÃ©pÃ¡n, G.b., 2009. Exciting traffic jams: Nonlinear phenomena behind traffic jam formation on highways. *Physical Review E* 80, 046205.

Richards, P.I., 1956. Shock Waves on the Highway. *Operations research* 4, 42-51.

Safonov, L.A., Tomer, E., Strygin, V.V., Ashkenazy, Y., Havlin, S., 2002. Multifractal chaotic attractors in a system of delay-differential equations modeling road traffic. *Chaos* 12, 42–51.

Scho¨nhof, M., Helbing, D., 2007. Empirical features of congested traffic states and their implications for traffic modelling. *Transportation Science* 41.

Schrank, D., T., Lomax, and B., Eisele, 2011. TTI's 2011 Urban Mobility Report.

Shvetsov, V., Helbing, D., 1999. Macroscopic dynamics of multilane traffic. *Physical Review E* 59, 6328.

Treiber, M., Hennecke, A., Helbing, D., 2000. Congested traffic states in empirical observations and microscopic simulations. *Physical Review E* 62, 1805.

Treiber, M., Kesting, A., 2011. Evidence of Convective Instability in Congested Traffic Flow: A Systematic Empirical and Theoretical Investigation. *The 19th International Symposium on Transportation and Traffic flow Theory. (ed. by M. Cassidy, and A. Skabardonis)*, 698-716.

Treiterer, J., Myers, J.A., 1974. The hysteresis phenomenon in traffic flow. *The 6th International Symposium on Transportation and Traffic flow Theory*, 13-38.

Ward, J.A., Wilson, R.E., 2011. Criteria for convective versus absolute string instability in car-following models. *Proceedings of the Royal Society of London. Series A. Mathematical and Physical Sciences* 467, 2185-2208.

Wilson, R.E., 2001. An analysis of Gipps's car-following model of highway traffic. *IMA Journal of Applied Mathematics* 66, 509-537.

Wilson, R.E., 2008. Mechanisms for spatio-temporal pattern formation in highway traffic models. *Philosophical Transactions of the Royal Society A: Mathematical, Physical and Engineering Sciences* 366, 2017-2032.

Wilson, R.E., Ward, J.A., 2011. Car-following models: fifty years of linear stability analysis - a mathematical perspective *Transportation Planning and Technology* 34, 3-18.

Windover, J.R., 1998. Empirical studies of the dynamics features of freeway traffic. *Ph.D. thesis, Institute of Transportation Studies, University of California, Berkeley*.

Windover, J.R., Cassidy, M.J., 2001. Some observed details of freeway traffic evolution. *Transportation Research Part A* 35, 881-894.

Yeo, H., 2008. Asymmetric Microscopic Driving Behavior Theory. *Doctoral dissertation. Dept. of Civil and Environmental Engineering, University of California, Berkeley, U.S.A.*

Yeo, H., Skabardonis, A., 2009. Understanding stop-and-go traffic in view of asymmetric traffic theory. *The 18th International Symposium on Transportation and Traffic flow Theory. (ed. by W. Lam, S.C. Wong & H. Lo)* 1, 99-116.

Zhang, H.M., 1999. A mathematical theory of traffic hysteresis. *Transportation Research Part B* 33, 1-23.

Zhang, H.M., Kim, T., 2005. A car-following theory for multiphase vehicular traffic flow. *Transportation Research Part B* 39, 385-399.

Zheng, Z., Ahn, S., Chen, D., Laval, J., 2011a. Applications of wavelet transform for analysis of freeway traffic: Bottlenecks, transient traffic, and traffic oscillations. *Transportation Research Part B* 45, 372-384.

Zheng, Z., Ahn, S., Chen, D., Laval, J.A., 2011b. Freeway traffic oscillations: microscopic analysis of formations and propagations using wavelet transform. *Transportation Research Part B* 45, 1378-1388.

Zheng, Z., Ahn, S., Monsere, C.M., 2010. Impact of traffic oscillations on freeway crash occurrences. *Accident analysis and prevention* 42, 626-636.